THE UNIVERSITY OF ALBERTA

"A STUDY OF CHARGED PARTICLES AND SCATTERED PHOTONS IN MEGAVOLTAGE X-RAY BEAMS"

by

THOMAS ROCKWELL MACKIE

A THESIS

SUBMITTED TO THE FACULTY OF GRADUATE STUDIES AND RESEARCH

IN PARTIAL FULFILMENT OF THE REQUIREMENTS FOR THE DEGREE

OF DOCTOR OF PHILOSOPHY

DEPARTMENT OF PHYSICS

EDMONTON, ALBERTA

FALL 1984

Preface

Volume 1 entitled, "Contamination of Megavoltage X-Ray Beams By Electrons And Scattered Photons", was originally written as a thesis for the partial fulfilment of a Master of Science degree. At the defense of the thesis in September of 1982, it was felt by the examining committee that Volume 1 should be used towards a Doctor of Philosophy degree.

Section 3, in Volume 1, addressed the problem of the transport of charged particles in the build-up region of a unit-density phantom. The committee felt that this Section provided a good foundation for a more complete study of the transport of charged particles generated by photon beams in an inhomogeneous medium. A decision was made to undertake this investigation to complete the thesis. Volume 2 contains the results of this study as well as a method to calculate the primary and scattered dose in heterogeneous media.

It was decided to break the thesis into two Volumes because Volume 1 is a self-contained study of photon beam contamination. The contents of Volume 2 are not referenced in Volume 1. For this reason, the Discussion, Conclusions and Appendices concerning contamination are left in Volume 1. However, in a number of instances, the reader of Volume 2 is referred to Volume 1, therefore, the pagination in Volume 2 is a continuation of Volume 1.

TABLE OF CONTENTS FOR VOLUME 2

LIST OF TABLES FOR VOLUME 2

LIST OF FIGURES FOR VOLUME 2

LIST OF FIGURES FOR VOLUME 2 (CONT'D)

LIST OF FIGURES FOR VOLUME 2 (CONT'D)

LIST OF FIGURES FOR VOLUME 2 (CONT'D)

VOLUME 2

A CONVOLUTION METHOD OF CALCULATING RADIATION DOSE FOR MEGAVOLTAGE X-RAY BEAMS

5. Introduction To Radiotherapy Dose Computation

We need 3-D CT for CA RT.

(3-Dimensional Computer Tomography for Cancer Radiotherapy)

L.E. Reinstein (62)

5.1 Statement of Purpose

The goal of radiotherapy planning is to obtain a high therapeutic ratio, defined as:

$$\text{Therapeutic Ratio} = \frac{\text{Tumor Control}}{\text{Normal Tissue Complication}} \tag{5.1.1}$$

This can be achieved by giving a sufficiently high and uniform radiation dose to the target volume and a lower dose to the surrounding normal tissue. This implies localizing the tissues to be irradiated accurately and optimizing the dose distribution.

X-ray images have traditionally been the main technique for the localization of tumor tissue. They are obtained by passing an x-ray beam through a patient and detecting the transmitted x-rays in a 2-dimensional plane perpendicular to the beam. The x-ray image represents the transmission through all the tissues where the x-rays are passing. As a result, the tissue volume through which the diagnostic x-ray beam is passing is "compressed onto a 2-dimensional view.

A radiotherapy "simulator" is a specialized radiographic device which produces radiological images and also has the same degrees of freedom of movement as radiotherapy units. It is primarily used to localize the tumor site with respect to the radiotherapy beam. Even when the tumor volume is accurately localized from several such views, the 3-dimensional information is rarely used directly in treatment planning. Instead a "contour" of a

2-dimensional cross-sectional slice through the region of interest is usually obtained. This is usually done using a mechanical or optical distance indicator attached to the simulator gantry which can rotate about the patient. Section 5.3 investigates existing methods of correcting dose distributions for patient-specific surface contours.

Internal outines of heterogeneous regions can be included by noting the maximum extent of the region in lateral and anterior transverse views. The cross-sectional view of the heterogeneity is then interpolated by using a standard anatomy atlas. The density of such internal structures is noted when they are greatly different from that of water (e.g. lung or bone). The correction for tissue heterogeneity correctly takes into account only the primary fluence, estimates are made of the effects on the scattered radiation dose. Because of the uncertainties in their location, there was often no correction at all for internal heterogeneous tissue contours. Therefore, until the recent advances in imaging, there has been little incentive to improve the accuracy of the calculations of dose deposited in heterogeneous tissue.

Imaging techniques such as computed tomography (CT scanning) (55,56), nuclear medicine tomographic imaging and nuclear magnetic resonance (NMR) imaging have improved the localization of tumor volumes. This alone is expected to improved the success of radiotherapy. This information can also be used to simplify three aspects of treatment planning.

1) The patient-specific anatomy can replace estimates based on cross-sectional anatomy atlases.

2) It can eliminate the need for measuring and modifying the external contour.

3) It can eliminate the need to assume the density of internal tissues. X-ray CT provides "pixel-by-pixel" (a pixel is a "picture element") information on tissue density. The problem of extracting the density information from CT scans has been studied by a great number of authors (57-61)

Tomography also provides information in 3-dimensions. Therefore there has been an incentive to use this 3-dimensional information more fully in treatment planning (62). In the discussion of dose calculation methods (Section 5.4), this aspect will be emphasized.

Another important advance in radiotherapy, which can improve the therapeutic ratio, is the increased availability of reliable high energy linear accelerators. A greater amount of dose from these sources is deposited at greater depths in the patient. Therefore, deep-seated tumors will receive a greater dose. At the same time, the build-up region extends to a greater depth reducing the dose near the patient surface. At higher energies, the range of charged particles set in motion can be several centimeters. The problem of charged particle transport will be introduced in Section 5.2 and investigated using the Monte Carlo method in Section 6. A dose computation procedure to take this into account will be proposed in Section 7. The effect of

charged particle transport is greater for 15 MV x-rays than for 6 MV x-rays, and therefore, this investigation has concentrated on 15 MV x-rays.

5.2 Electronic Equilibrium

The energy transport in an x-ray beam is a two-stage process. Photons must first interact to set in motion fast charged particles. The charged particles then interact continuously with matter and deposit their energy as dose. This process was investigated in Volume 1 to explain the increase in central axis dose in the build-up region. It was assumed that the charged particle transport was predominantly in the forward direction. The justification of the assumption was as follows: If the distance from the point of measurement to the field boundary is larger than the lateral range of charged particles set-in-motion, then for every charged particle leaving the region of the central axis there would be a charged particle arriving from lateral regions. When this condition is true, lateral electronic equilibrium exists (63). In Volume 1, the forward transport of charged particle fluence from the point of production was approximated by an exponential term. The constant in the exponential, $\mu_{e^{\pm}}$, describing forward transport, was many times larger then the coefficient, μ_{γ}, describing the primary photon attenuation.

Equation 1.5.8 can be used to estimate the state of longitudinal electronic equilibrium in a heterogeneous region (illustrated in Figure 82). It will be assumed that all regions of the phantom are composed of material with the same atomic number. Therefore, there is only a difference in gravimetric density. The amount of primary energy

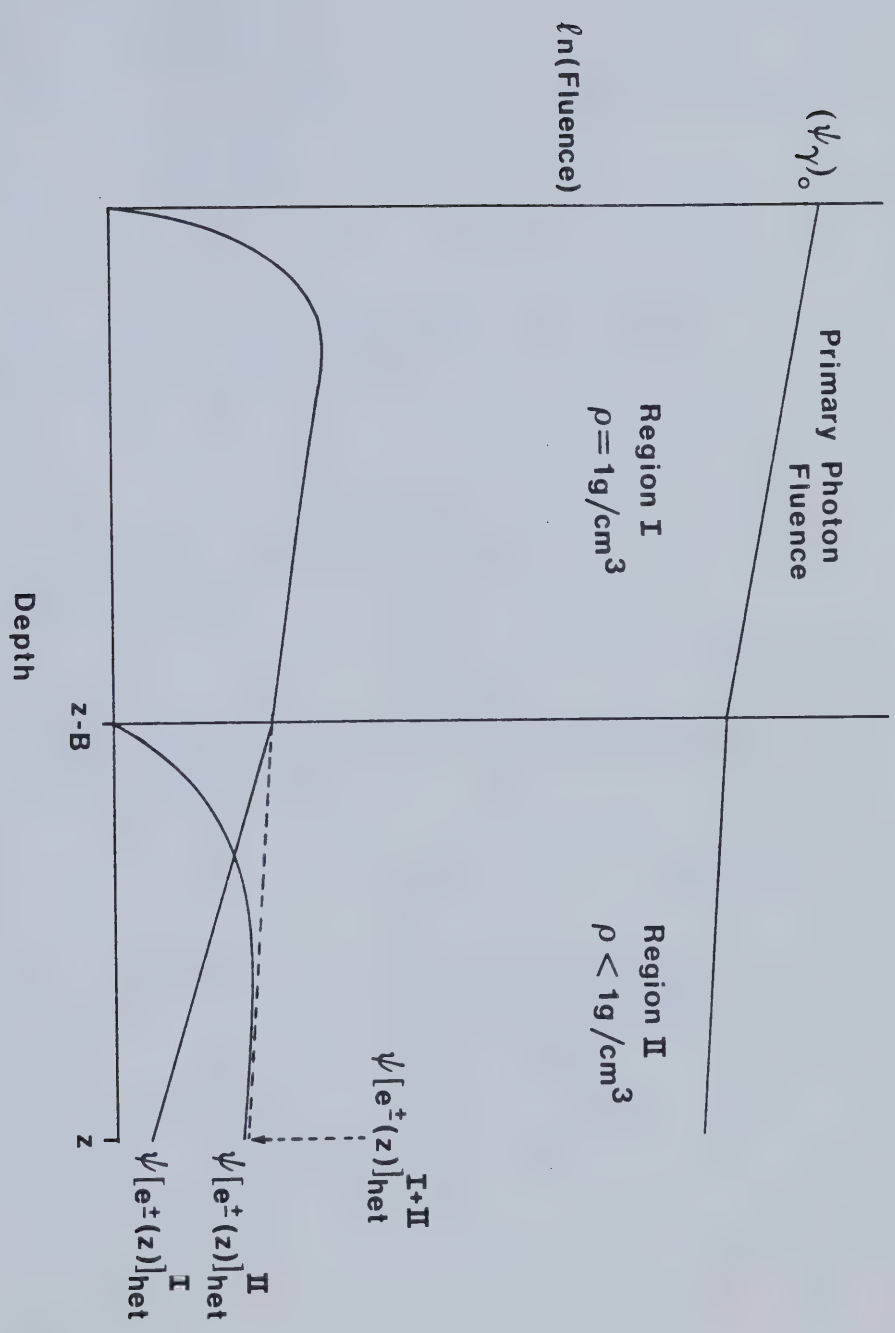

Figure 82. The state of longitudinal equilibrium in a heterogeneous phantom.

fluence at a depth, z, inside the heterogeneous phantom, is the sum of two contributions, one from a unit density region (Region I) of thickness z-B, $\Psi[e\pm(z)]^{I}_{het}$, and one from a region (Region II) of lower gravimetric density (compared to water), ρ, and thickness B, $\Psi[e\pm(z)]^{II}_{het}$:

$$\Psi[e^{\pm}(z)]^{I}_{het} = \frac{\mu_\gamma(\Psi_\gamma)_o}{\mu_{e^\pm} - \mu_\gamma}\left[e^{-\mu_\gamma(z-B)} - e^{-\mu_{e^\pm}(z-B)}\right] e^{-\mu_{e^\pm}(\rho B)} \tag{5.2.1}$$

$$\Psi[e^{\pm}(z)]^{II}_{het} = \frac{\mu_\gamma(\Psi_\gamma)_o}{\mu_{e^\pm} - \mu_\gamma}\left[e^{-\mu_\gamma\rho B} - e^{-\mu_{e^\pm}\rho B}\right] e^{-\mu_\gamma(z-B)} \tag{5.2.2}$$

$$\Psi[e^{\pm}(z)]^{I+II}_{het} = \frac{\mu_\gamma(\Psi_\gamma)_o}{\mu_{e^\pm} - \mu_\gamma}\left[e^{-\mu_\gamma[z+(\rho-1)B]} - e^{-\mu_{e^\pm}[z+(\rho-1)B]}\right] \tag{5.2.3}$$

The term, $e^{-\mu_{e^\pm}(\rho B)}$, in Equation 5.2.1 describes the attenuation in the low-density region of the charged particle fluence generated in the unit density region. The attenuation of the primary photon beam by the unit density region is accounted for by the term, $e^{-\mu_\gamma(z-B)}$ in Equation 5.2.2. If Region II is well beyond d_{max} i.e. z-B is large, then:

$$\Psi[e^{\pm}(z)]_{het}^{I+II} \cong \frac{\mu_\gamma (\Psi_\gamma)_o}{\mu_{e^\pm} - \mu_\gamma} e^{-\mu_\gamma z} e^{-\mu_\gamma (1-\rho)B} \qquad (5.2.4)$$

The correction factor CF is equal to the ratio of the charged particle fluence in a heterogeneous phantom to the charged paticle fluence in a homogeneous phantom:

$$CF(z) = \frac{\Psi[e^{\pm}(z)]_{het}^{I+II}}{\Psi[e^{\pm}(z)]_{hom}} = e^{\mu_\gamma (1-\rho)B} \qquad (5.2.5)$$

Equation 5.2.5 has no dependence on $\mu_{e^\pm}$. This means that if longitudinal equilibrium has been established, then longitudinal electronic equilibrium will not be perturbed in the low-density material. Equation 5.2.5 predicts that the inhomogeneity correction of the primary dose should always be greater than unity.

Perturbations in lateral equilibrium are not so easily described quantitatively. Analytic solutions of equations describing the transport of charged particles have yet to be achieved for generalized boundary conditions. Only Monte Carlo calculations provide a method to accurately quantify the role of lateral equilibrium. However, a qualitative description of the establishment of lateral equilibrium in a homogeneous phantom and its loss in a heterogeneous phantom is instructive.

Figure 83a) illustrates a homogeneous phantom irradiated by a non-divergent photon beam with a field size

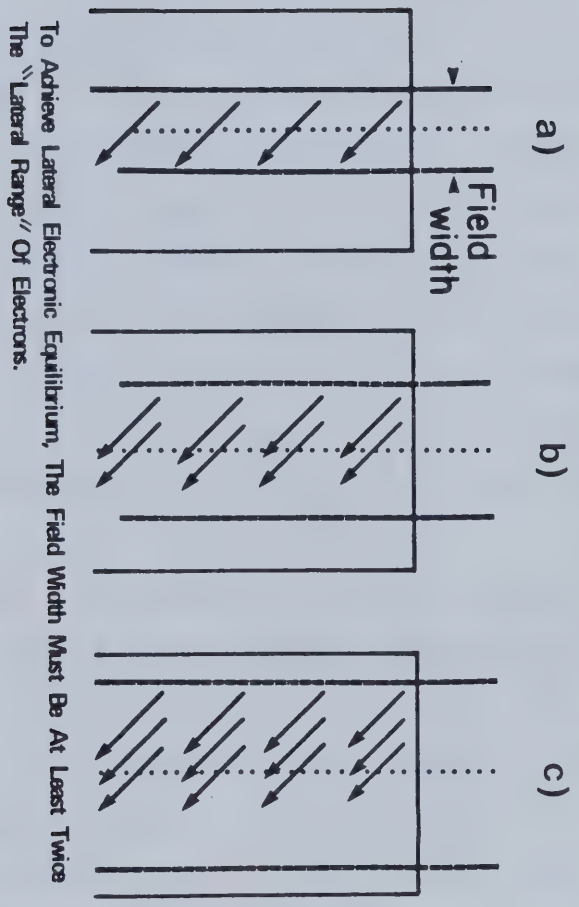

Figure 83. Lateral equilibrium does not exist at the central axis when the field size is less than twice the lateral range of electrons. Lateral equilibrium never exists near the field boundary.

smaller than the lateral charged particle range. The charged particles are assumed to be set in motion at a fixed angle with respect to the incident photon beam. For the sake of demonstration, it is assumed here that they do not deviate from their initial direction. The charged particles originating near the beam boundary deposit energy at the central axis and travel beyond (the dashed lines) to the end of their range. If the field size is increased (Figure 83b)) charged particles originating near the new boundary have enough range to reach the central axis increasing the dose deposited there. Lateral electronic equilibrium is established when a further increase in field size will not result in a further increase in dose because charged particles set in motion near the field boundary (Figure 83c)) do not have sufficient range to reach the central axis.

Figure 84a) illustrates the loss of lateral electronic equilibrium inside a heterogeneous region with a density of one half of the density in Figure 83. Since the range of particles in the low-density region will be double that in the unit density region, a field size sufficient to establish equilibrium in a unit density medium must be doubled in order to obtain equilibrium in the low-density region.

Even though this analysis of electronic equilibrium is heuristic it would be expected that the establishment and loss of lateral electronic equilibrium in heterogeneous phantoms may be a more important effect than that of

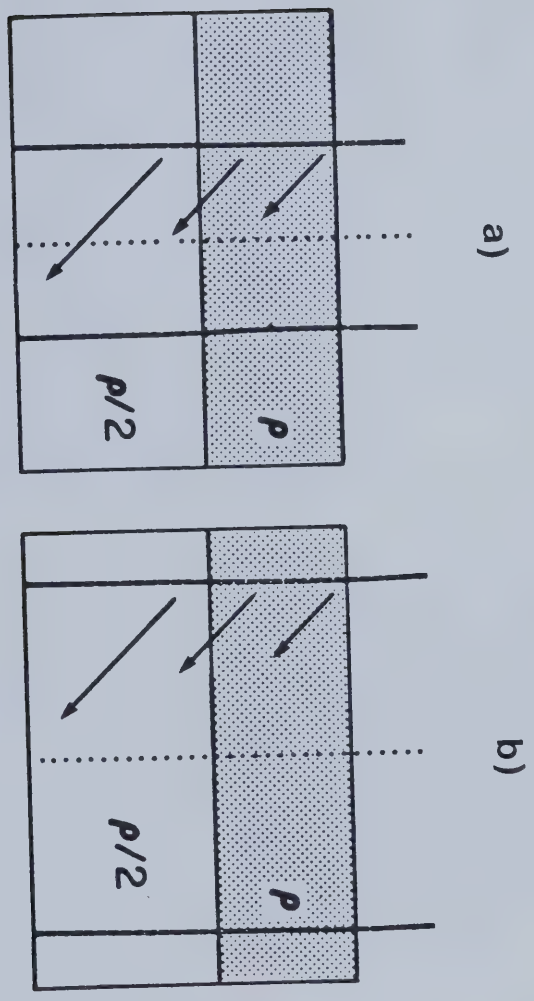

Figure 84. a) A field size large enough to establish lateral equilibrium at the central axis may not be large enough in a low-density region. b) If the heterogeneous region has a density of one-half, the field size must be doubled to re-establish lateral equilibrium.

longitudinal equilibrium.

A series of experiments was used to verify this hypothesis. Figure 85 illustrates the experimental set-up. An ion chamber (Capintec PR-06C) without a build-up cap was placed at the central axis a constant 100 cm from the source. The thickness of the cork region was also kept constant at 7.9 cm $\pm$ 0.2 cm. The total thickness of overlaying material was 15.6 cm $\pm$ 0.4 cm. The position of the cork was varied with respect to the ion chamber. The quantity, A, is the distance from the first interface to the probe. The correction factor, CF, was defined to be:

$$CF(z,A,W) = \frac{\text{Heterogeneous Phantom TMR}(z,A,W)}{\text{Homogeneous Phantom TMR}(z,W)} \qquad (5.2.6)$$

Figure 86 illustrates the correction factor as a function of A for various field sizes. At small field sizes inside cork, the correction factor is less than unity. This means that the dose in the low-density heterogeneous phantom is less than the dose in the homogeneous phantom even though the photon fluence in the low-density heterogeneous phantom is greater than in the homogeneous phantom. A small increase in the field size at field sizes less than 10 cm x 10 cm (for example from 5 cm x 5 cm to 6 cm x 6 cm) results in a relatively large increase in the correction factor. At a field size of 10 cm x 10 cm there is little further increase in the correction factor with field size. Both these effects are expected if lateral equilibrium did not exist for the smaller fields.

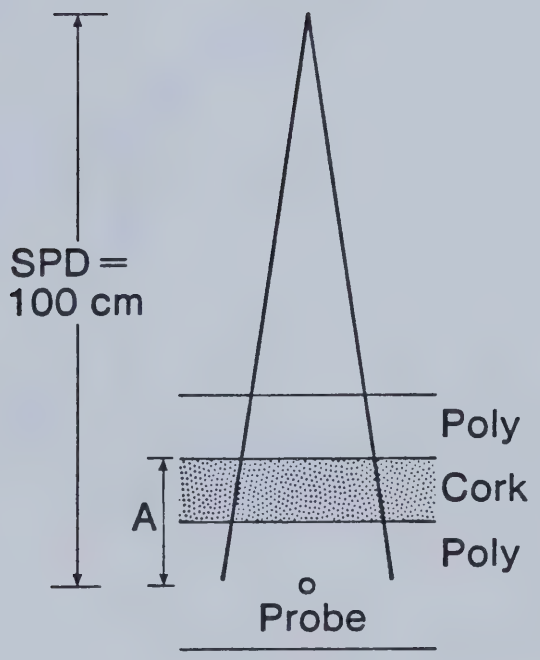

Figure 85. The experimental set-up to measure the inhomogeneity correction factor. The source-to-probe distance, the thickness of cork, and the depth of the probe from the surface was fixed. The position of the cork with respect to the probe is varied.

$$\text{Correction Factor} = \frac{\text{Heterogeneous Tissue Maximum Ratio}}{\text{Homogeneous Tissue Maximum Ratio}}$$

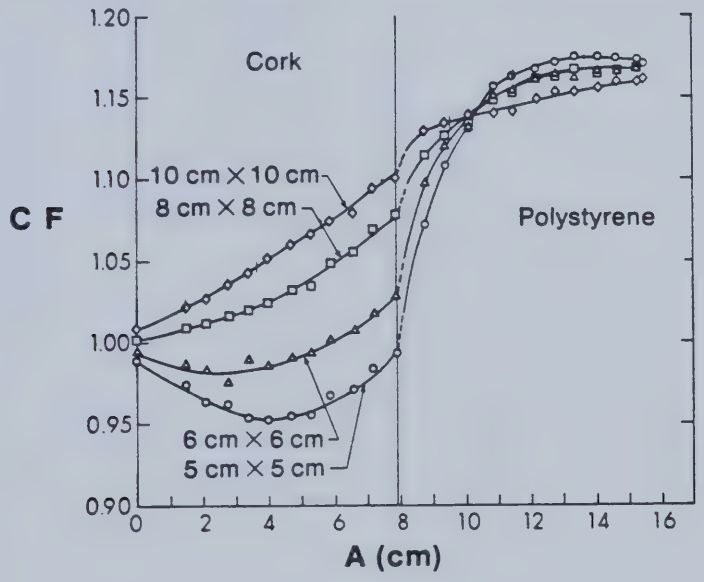

Figure 86. The correction factor, for the experimental set-up illustrated in Figure 85, for various field sizes.

Similar measurements have been performed by Young and Kornelsen for 10 MV x-rays (64). They also report a loss in lateral equilibrium in lung-equivalent materials when the field size is small.

5.3 Contour Corrections

Measurements of absorbed dose from a megavoltage x-ray beam are usually obtained in a water tank or phantom. The central axis of the beam is perpendicular to the water surface and the dimension of the tank is larger than any beam width to be measured. Figure 87a) illustrates the geometrical arrangement for the measurement of dose at point P. The surface of a patient is rarely flat, and thus the central axis, where the beam enters, is generally not perpendicular to the surface. The measured dose must be corrected to take patient surface contours into account. Figure 87b) shows the arrangement for the calculation of dose at point P which nows lies under a curved contour. A "ray" from the radiation source through P represents a pencil beam.

The "effective attenuation coefficient method" takes the surplus or deficit of tissue into account by the subtraction or addition of dose (63). The true depth, z', of a pencil beam through tissue with a contour is determined. The difference between the depth in the all-water situation from a reference surface, z, and the true distance, z', is multiplied by an empirically determined coefficient, k_{eff}, that depends on the photon energy to obtain the contour corrected dose:

$$DOSE(z') = DOSE(z)\, e^{k_{eff}(z-z')} \cong DOSE(z)[1 + k_{eff}(z-z')] \qquad (5.3.1)$$

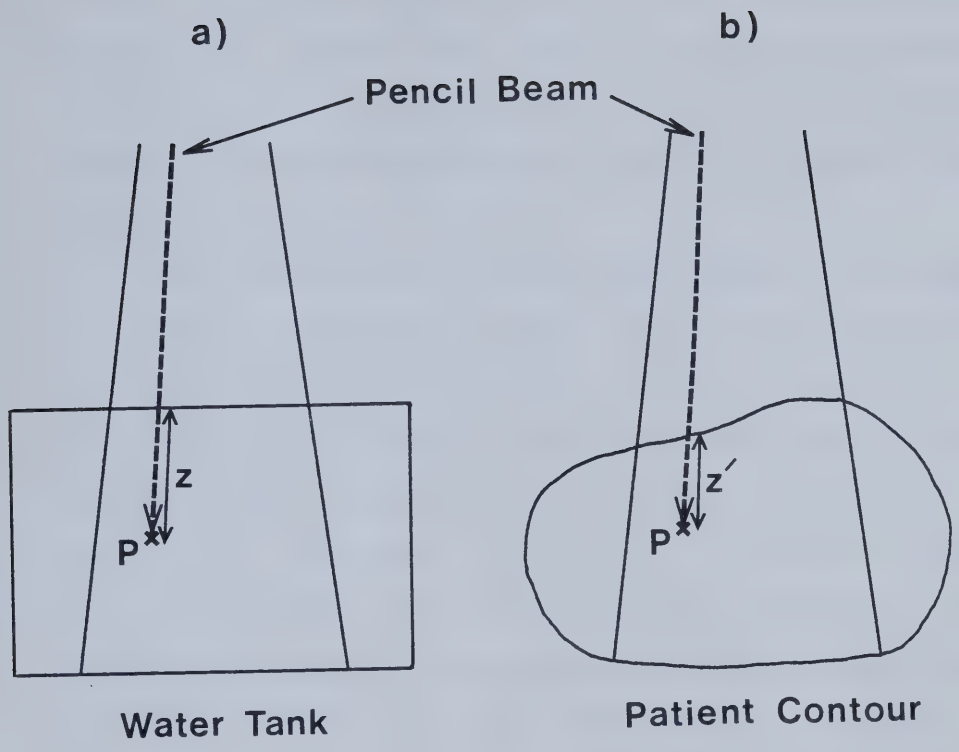

Figure 87. a) Measurement of the dose in a water tank. b) The dose must be modified to take into account the patient surface contour.

The coefficient, k_{eff}, for Co-60 beams is smaller than the linear attenuation coefficient so the effective attenuation coefficient method must take an unspecified amount of forward directed scatter as well as primary attenuation into account. The dose must be corrected at all depths for each pencil beam.

The "isodose shift method" (63), shifts the depth of all isodose lines by an amount directly proportional to the difference between the true and reference distance, z'-z. If the true thickness of tissue is less than the all-water thickness, the isodose lines are shifted towards the surface and in the opposite situation, the lines are shifted away from the surface. The method is computationally simpler than the effective attenuation coefficient method because the shift does not have to be applied at each depth. The constant of proportionality depends mainly on the beam quality and like the effective attenuation coefficient in the previous method it must be determined empirically. The isodose shift method is inaccurate very near the surface of the phantom.

The main disadvantage of the effective attenuation coefficient method and the isodose shift method is the determination of their empirically derived coefficients. In general, the coefficients depend not only on the energy of the beam but also to some extent on the beam size, depth of the calculation point, and the source-to-surface distance (SSD).

Two other methods, the "ratio of TAR" and "effective

SSD" methods, also employ the true length through tissue, z', but explicitly take into account the beam size, and therefore, account indirectly for some scattered radiation. The ratio of TAR method is based on measured tissue-air-ratio (TAR) data.* The tissue-air-ratio under a contour is found by interpolating in a look-up table, compiled as a function of depth and field size, using the true depth. Since TAR's are usually measured along the central axis, the method is, strictly-speaking, limited to correcting the dose there. However, in practice, this limitation is ignored and off-axis corrections are estimated using the central axis data.

The effective SSD method corrects the tabulated percent depth-dose data in a manner similar to the ratio of TAR correction method. The percentage depth-dose must also be corrected to "remove" the inverse square attenuation. The corrected percentage depth-dose P(z',W,SSD') is:

$$P(z',W,SSD') = P(z',W,SSD)\left(\frac{SSD + z}{SSD + z'}\right)^2 \qquad (5.3.2)$$

* TAR measurements are obtained in a similar manner as tissue-maximum-ratio (TMR) data (see Figure 11), except the normalization value is obtain with the probe in air surrounded by a build-up cap of sufficient thickness to establish electronic equilibrium. Like TMR measurements the measurements for TAR's are obtained at a fixed distance from the source.

This correction can be made to off-axis positions as well as positions on the central axis.

Since TAR's and percentage depth-dose data contain scatter as well as primary dose, these corrections may correct somewhat for perturbation in the scatter dose. The major drawback of these methods is a failure to consider explicitly the influence of the scatter contribution to the contour correction.

The "differential scatter-air-ratio (dSAR)" method takes the contour configuration into account (65). The differential scatter-air-ratios are produced from scatter-air-ratio (SAR) data which are in turn derived from tissue-air-ratio (TAR) data:

$$SAR(z,r) = TAR(z,r) - TAR(z,0) \qquad (5.3.3)$$

Where, r, is the field radius. TAR(z,0) is called the "zero-area" tissue-air-ratio. It cannot be measured directly but is extrapolated from TAR data as the field radius is decreased (see Figure 88). The zero-area TAR corresponds to the primary dose if the charged particle energy is locally deposited (i.e. if electronic equilibrium exists). The SAR values are then a measure of the dose contribution of scattered radiation in a beam.

The dSAR values at a specific depth, z, are equal to the difference in SAR values per unit change in the field size:

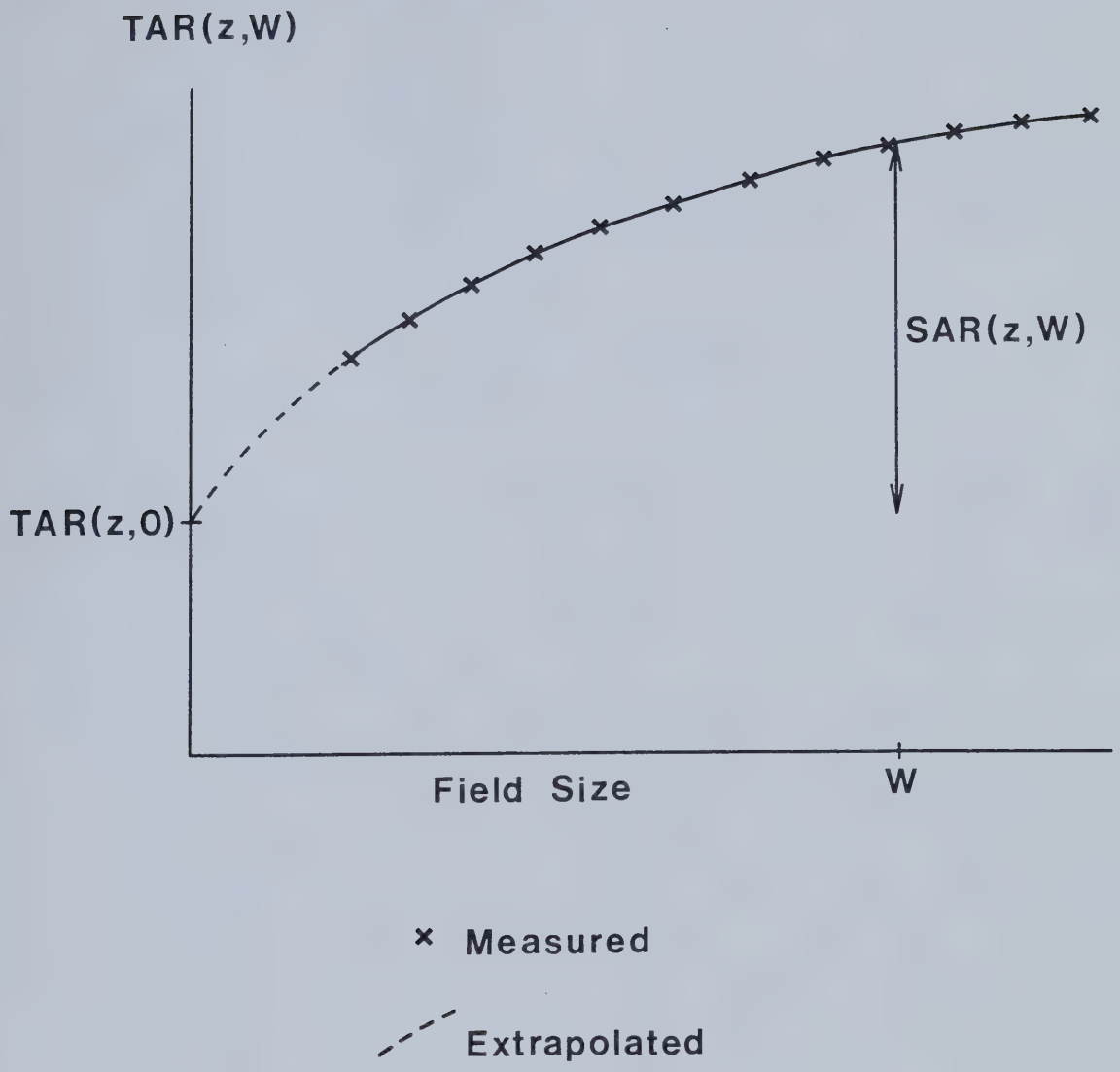

Figure 88. The definition of the zero-area TAR, TAR (z,0) and the scatter-air-ratio SAR (z,W). TAR (z,0) is found by extrapolated TAR measurements to a field size of zero.

$$\frac{d^2S(z,r)}{drd\theta} = \frac{1}{2\pi} \frac{[SAR(z,r+\delta r) - SAR(z,r-\delta r)]}{\delta r \delta\theta}$$

(5.3.4)

Equation 5.3.4 represents the scatter contribution for a pencil beam at radius, r, and angle, θ. The total scatter dose is found by summing the contributions as a function of radius and angular position:

$$D_{Scatter}(z,R) = D_A \sum_{ji}^{2\pi R} f(r_i,\theta_j) \frac{d^2S(z_i,r_i)}{drd\theta} \delta r_i \delta\theta_j$$

(5.3.5)

D_A is the dose in air at a distance from the source that corresponds to the depth, z. $f(r_i,\theta_j)$ is the relative primary fluence at the radius, r_i, and angular position, θ_j, incident on such pencil beams.

One of the main difficulties with the dSAR method is the extrapolation of TAR's to get the zero-area TAR values. The extrapolation takes place where the TAR values are changing rapidly in a non-linear fashion making the procedure technically difficult. There is a more fundamental problem. The TAR concept is defined only if electronic equilibrium exists, but this is impossible for a pencil beam of zero-area. Electronic equilibrium only exists in a lateral direction if the field size is larger than the lateral range of charged particles set in motion. The TAR's are extrapolated to field sizes where equilibrium does not exist. The dSAR method was first introduced for use with Co-60 beams such that the pencil beam is

sufficiently wide to establish equilibrium. The assumption of electronic equilibrium starts to break down for higher x-ray energies.

A second problem is that central axis data is applied to off-axis points. This may not be serious in practice, but the approximation has not been validated by modelling or experiment.

A final problem, is that the dSAR method does not take into account the contour where the beam exits the patient. Therefore, backscatter is not dealt with properly.

5.4 Correction For Tissue Heterogeneity

Contour corrections are simply a special case of corrections to account for heterogeneous tissue densities. The density outside the patient can be considered to be approximately zero. The only fundamental difference between contour corrections and other low-density heterogeneity corrections is that the dose in air outside the patient is irrelevant to the treatment and need not be calculated. For this reason, the effective attenuation coefficient, isodose shift, TAR ratio, and effective SSD methods have been applied to tissue inhomogeneity corrections. The true distance in the tissue, z',(discussed in Section 5.3) is now interpreted as the "radiological" or water-equivalent distance in the heterogeneous region. The major fault of these methods, when applied to heterogeneity corrections, is a failure to take into account the relative position of the heterogeneous region with respect to the calculation point.

The Batho or power-law method takes the depth of the heterogeneity, with respect to the depth of the point of measurement, into account. The original Batho method assumed that the heterogeneous region was a slab at right angles to the beam with an extent larger than the field boundary (66). Electronic equilibrium was assumed not to be perturbed and that only the dose beyond the heterogeneous region was required. The method was extended to include the dose inside, as well as distal to, the heterogeneous region by Sontag and Cunningham (67). Their formulation for the

correction factor, CF was:

$$CF(z_1,z_2,W) = \frac{TAR(z_2,W)^{\rho_2-\rho_1}}{TAR(z_1,W)^{1-\rho_1}} \qquad (5.4.1)$$

z_1 and z_2 are shown in Figure 89 and ρ_1 and ρ_2 are the relative electron densities (compared to water) of regions 1 and 2, respectively.

The Batho method has been subsequently modified by Cassell, Hobday and Parker (61) and Lulu and Bjärngaard (68) to take into account multiple slab geometries and estimate the correction factor when the lateral extent of the heterogeneity is less than the beam width. Limited success has been achieved by modifying the Batho method to take into account electronic disequilibrium (69).

The equivalent TAR method developed by Sontag and Cunningham (70) was inspired by O'Connors theorem. O'Connor (71) proposed that the dose at corresponding points in two media with different density, but the same atomic number, will be the same everywhere provided all distance measurements are scaled with the density (see Figure 90). The basis for the theorem is the linear dependence of the attenuation coefficient on density.

The premise on which Sontag and Cunningham based their method, was that an equivalent TAR could be found in tabulated TAR tables with the depth and field size suitably scaled:

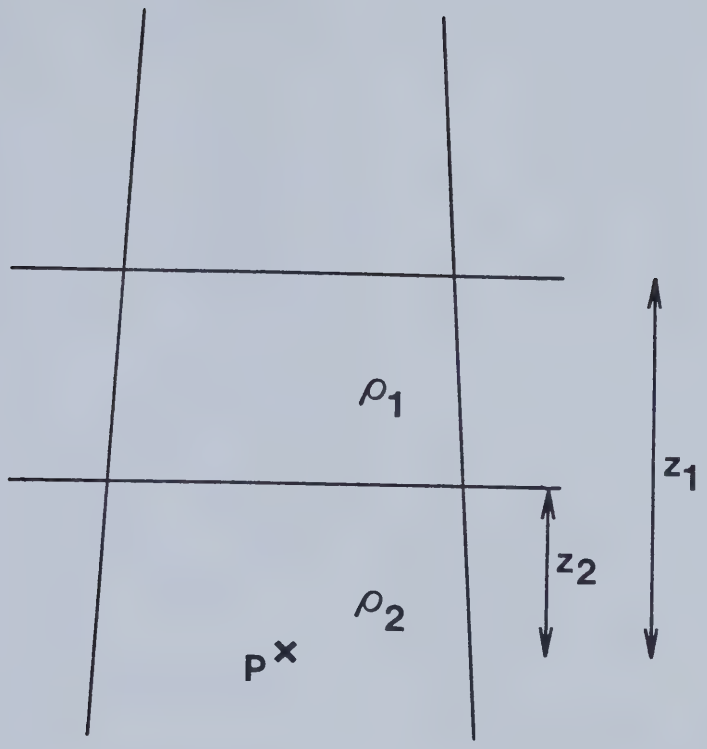

Figure 89. The geometrical parameters required for the Batho or power-law method.

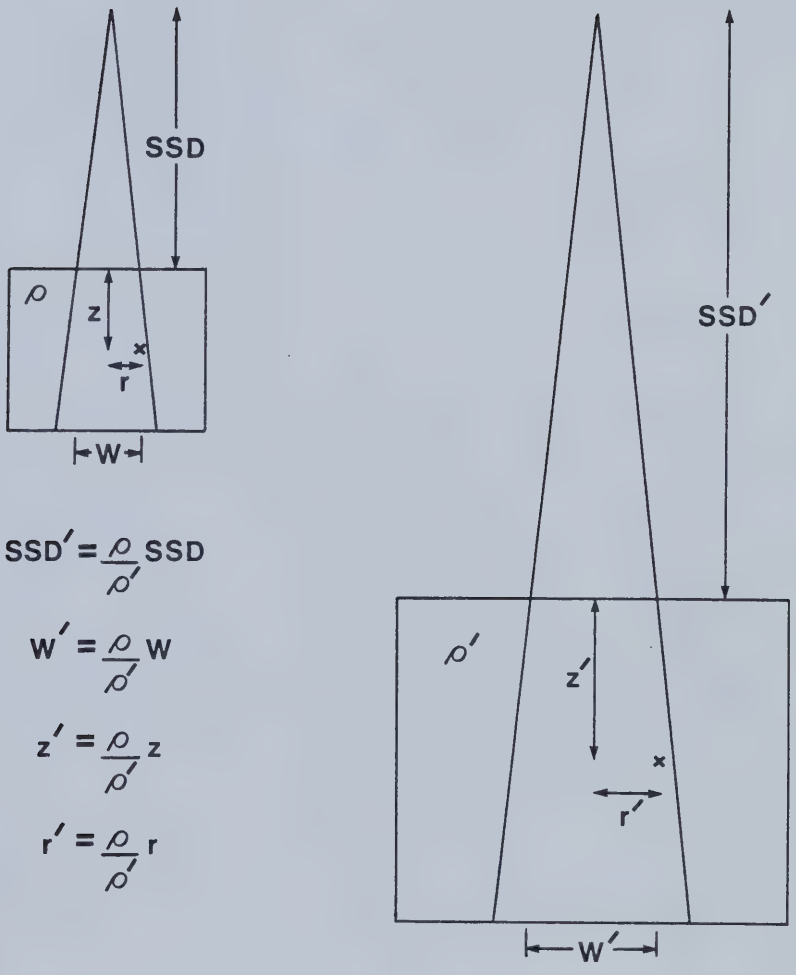

$$SSD' = \frac{\rho}{\rho'} SSD$$

$$W' = \frac{\rho}{\rho'} W$$

$$z' = \frac{\rho}{\rho'} z$$

$$r' = \frac{\rho}{\rho'} r$$

$$Dose(z',r',W',SSD') = Dose(z,r,W,SSD)$$

Figure 90. An illustration of O'Connor's theorem. All the distance measurements in this figure are inversely proportional to density.

$$CF(z',\hat{W}) = \frac{TAR(z',\hat{W})}{TAR(z,W)} \qquad (5.4.2)$$

The tissue-air-ratio was divided into primary (zero-area TAR) and scatter components:

$$TAR(z',\hat{W}) = TAR(z',0) + SAR(z',\hat{r}) \qquad (5.4.3)$$

$$\hat{r} = r \cdot \hat{\varepsilon} \qquad (5.4.4)$$

The term, r, is a circular field radius that produces the same dose at all depths along the central axis in a homogeneous phantom in a rectangular field. The term, $\hat{\varepsilon}$, is an effective relative electron density, weighted with respect to the scatter dose contributions from tissue elements surrounding the calculation point. The weighting procedure should be carried out over 3-dimensions:

$$\hat{\varepsilon} = \frac{\sum\sum\sum_{ijk} \varepsilon_{ijk} \cdot W_{ijk}}{\sum\sum\sum_{ijk} W_{ijk}} \qquad (5.4.5)$$

The weighting factors, W_{ijk}, is the contribution to the scatter dose from points surrounding the calculation point. The weighting factors are large in regions proximal to the calculation point and for points close to the calculation point.

Weighting in 3-dimensions, to arrive at an effective

electron density for each point, was felt to be too time consuming for computers available at the time. Since CT information is produced and stored in cross-sectional slices, the 3-dimensional dose was estimated using this plane-by-plane format. The electron density information, for all the slices neighboring the slice in which the dose calculation was being performed, was "coalesced" into a 2-dimensional effective relative electron density array (see Figure 91):

$$\hat{\varepsilon}_{ik} = \frac{\sum_j \varepsilon_{ijk} \cdot W_k}{\sum_j W_k} \qquad (5.4.6)$$

This 2-dimensional array is produced before the dose is calculated. It represents the scatter dose weighted electron density as if all the scatter dose was coming from one neighboring slice located at an effective location. A weighted relative electron density is determined for each calculation point in the slice:

$$\hat{\varepsilon} = \frac{\left(\sum_{ik} \left[\sum_j \varepsilon_{ijk} \cdot W_j \right] W_{ik} \right) \Big/ \sum_j W_j}{\sum_{ik} W_{ik}(Y_{eff})} \qquad (5.4.7)$$

The above procedure is repeated for each point in the calculation plane. It has been assumed that the weighting factor can be separated into space components:

$$W_{ijk} = W_j \cdot W_{ik}(Y_{eff})$$

(5.4.8)

The term W_j is given by:

$$W_j = SAR(z=10cm, r_2) - SAR(z=10cm, r_1)$$

(5.4.9)

The radius terms r_1 and r_2 are related to the equivalent circular field and the distance between neighboring slices in a non-linear fashion. The effective distance to the coalesced scatter slice, Y_{eff} is given by (see Figure 91):

$$Y_{eff} = \frac{\sum_j Y_j \cdot W_j}{\sum_j W_j}$$

(5.4.10)

The calculation is speeded up by the spatial separation of the weighting factor because the summation for each calculation point is carried out over two dimensions instead of three. However the assumption that the non-calculation planes can be replaced by one effective plane placed at an effective distance away was never validated by Monte Carlo modelling or experiment. The procedure could not be proved by a comparison of Equation 5.4.5 with 5.4.7 because the 3-dimensional weighting factors were never obtained. A simplification of the equivalent TAR method has been proposed by Tatcher and Palti (72). Equation 5.4.3 is maintained except, z', is the radiological length through the heterogeneous region and, $\hat{W}$, is replaced by:

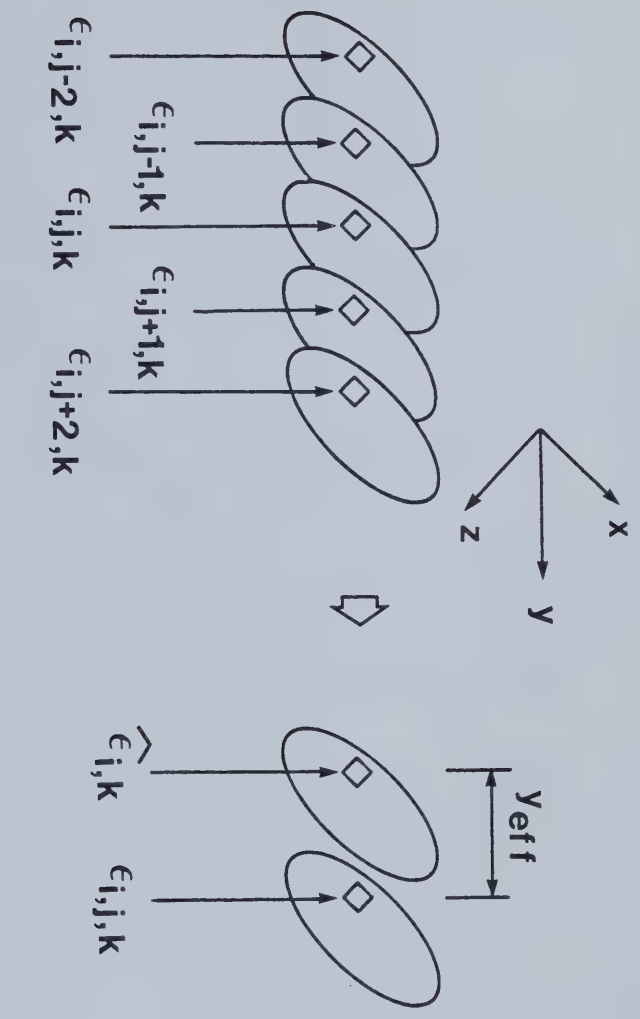

Figure 91. In the equivalent TAR method, the 3-dimensional electron density information is "coalesced" into one cross-sectional slice.

$$\hat{W} = W\tilde{\rho} \tag{5.4.11}$$

$$\tilde{\rho} = \frac{V_w + \sum\sum\sum_{ijk} V_{ijk}\,\rho_{ijk}\,f_{ijk}}{V_w + \sum\sum\sum_{ijk} V_{ijk}\,f_{ijk}} \tag{5.4.12}$$

Where $\tilde{\rho}$ and ρ_{ijk} refers to the relative density compared to water. V_w and V_{ijk} are the volumes of the water-equivalent and heterogeneous parts of the phantom, respectively. f_{ijk} is equal to 3 for cork and equal to ∞ (ie. $\tilde{\rho}$ =1) for teflon. It is later claimed that f_{ijk} is not sensitive to variations in density! It is also claimed that f_{ijk} is nearly independent of geometrical position although it is only applied when calculating the dose in heterogeneous phantoms!

The delta-volume method was originally suggested by Cunningham and Beudoin (73) and refined by Larson and Prasad (74) and Wong and Henkelman (75). The method, as formulated by Wong and Henkelman, divides the dose into primary, first scatter augmented by some second scatter, and residual multiple scatter dose. Mathematically, the expression is given by:

$$DOSE = PRIMARY + \sum_{ijk}\sum\sum \rho_{ijk}\, \Delta S^{*}_{1;ijk}\, f_{o;ijk}\, f_{1;ijk} + S_m \qquad (5.4.13)$$

$$S_m = \frac{SAR_m(\tilde{\rho}\cdot d, \tilde{\rho}\cdot r)}{SAR_m(d,r)} \left[S_m(med) + \sum_{ijk}\sum\sum \left(\frac{\tilde{\rho}-\rho_{ijk}}{\tilde{\rho}}\, \Delta H_{ijk}\right)\right] \qquad (5.4.14)$$

where ρ_{ijk} is the density of the volume element (voxel) which is the origin of the first or augmented second scatter dose at point i,j,k. $\Delta S^{*}_{1;ijk}$ is the contribution of first and augmented second scatter dose (second scatter dose contained within an angle of 45^{o} centered about the first scatter ray) to the calculation point i,j,k determined for a homogeneous water phantom. $f_{o;ijk}$ is the change in the primary attenuation along the primary ray to the point i,j,k. $f_{1;ijk}$ is the change in the first scatter attenuation along the path between the point i,j,k and the calculation point. The term $S_m(med)$ approximates the residual multiple scatter dose in a heterogeneous medium. ΔH_{ijk} is the perturbation in the multiple scatter dose from a small void at the point i,j,k. It is determined by the difference between the experimentally measured dose perturbation (see Figure 92) and the calculated value using $\Delta S^{*}_{1;kjk}$. $\tilde{\rho}$ is the overall mean density of the heterogeneous phantom. $SAR_m(d,r)$ is the residual multiple scatter-air-ratio for a homogeneous water phantom and is

obtained using SAR values and the augmented first scatter values. The determination of ΔH_{ijk} is worthy of note. It is obtained by displacing water by low-density polystyrene foam constructed in conical rings about the central axis (76). The small perturbation in dose due to the displacement of the ring is measured. The radius of the ring, the depth of the measurement point and the position of the ring with respect to the measurement point is varied. The experimental set-up is shown in Figure 92. The number of measurements involved requires automation of the procedure. The first and augmented second scatter dose are calculated and their contribution is subtracted from the total scatter perturbation measurements to arrive at the multiple scatter dose perturbation values.

The Δ-Volume method was the first "true" 3-dimensional dose calculation algorithm. It exactly corrects the first scatter dose due to the presence of heterogeneities (assuming electronic equilibrium of the scatter photons) and estimates the multiple scatter dose correction.

The delta-volume method has not been optimized for speed of calculation. As many operations are carried out to determine the dose corrections for first and augmented second scatter dose as for the residual multiple scatter dose, even though the contribution of the latter is much smaller. Calculation time should be appropriated on the basis of the importance of the contribution of the calculation to the overall result. However, the speed limitations may not be critical. The method is being

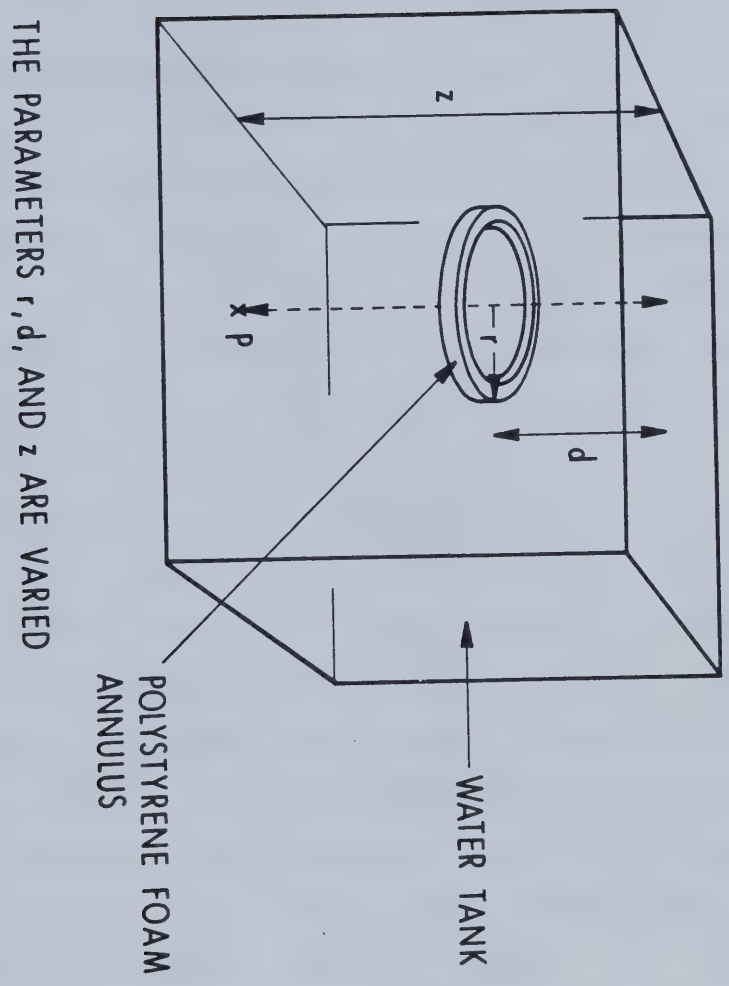

Figure 92. Polystyrene foam conical annuli were placed in a water tank. The perturbation in dose compared to the all-water saturation was measured.

implemented using a dedicated microcomputer. A group promoting the Δ-volume method (Mallinckrodt) is using Very Large Scale Integration (VLSI) microelectronic technology to develope a "chip" that will do the "ray-tracing" portion of the Δ-volume calculation rapidly (77).

A major criticism of all the above methods is that the inherent assumptions are not identified explicitly and they have not been validated directly by measurements or simulation (eg. the Monte Carlo method). Consequently, their scope of applicability is ill-defined, and the clinical situations in which they are limited are difficult to identify a priori.

The major fault of the equivalent TAR and delta-volume methods is an inability to handle situations of electronic disequilibrium. Most of the dose arriving at a point is due to primary dose which will be most perturbed by changes in the state of electronic equilibrium. A related problem with these methods is that they are based on the separation of primary and scatter dose using the zero-area TAR and SAR's obtained empirically. The concept becomes more and more untenable at higher photon energies as electronic equilibrium becomes more important and the extrapolation of TAR's to such fields is incompatible with the equilibrium requirement.

The need for considering non-local energy deposition has been documented by several authors (78-81). Some photon dose parametrization models have accounted for electronic "build-up" longitudinally along the central axis, but none

have rigorously treated the lateral spread of charged particles set-in-motion (40,82) (see Section 3 in Volume 1). Young and Kornelsen (64) have taken into account the dose reduction caused by a lack of charged particle lateral equilibrium using a semi-empirical "loss factor".

6. Modelling Dose Using The EGS Monte Carlo Code

The state-of-the-art of the Monte Carlo method in 1952:

"The electrons or photons were followed through successive intervals and their fate in passing through a given interval was decided by spinning a wheel of chance; the fate being read from one of a family of curves drawn on a cylinder"..."the [cylinder] motor was observed to stop at random ..."

R.R. Wilson (83)

It has been shown that lateral electronic equilibrium does not exist near field boundaries and along the central axis in low-density heterogeneities for small fields (see Figure 86). The EGS (Electron Gamma Shower) Monte Carlo code was used to investigate regions of lateral disequilibrium directly by simulating the transport of photons and charged particles set in motion.

EGS was originally developed at Stanford University for the study of the cascade of charged particles and photons produced by high energy (up to 1 GeV) cosmic rays or photons (83). Rogers, at the National Research Council of Canada, has corrected and modified the code to make it applicable to the energies encountered in medical physics and health physics problems (84-86).

EGS takes into account most of the radiation physics required for megavoltage energies. The interactions treated for photons are pair production, Compton, and the photoelectric effect, and for charged particles, multiple scattering (Moliere's theory as formulated by Bethe), "knock-on" collisions (Moller scattering for electrons and Bhabha scattering for positrons), continuous slowing down, bremsstrahlung and positron annhilation. The only present flaw is an inaccuracy (up to a factor of two) in calculating correct bremsstrahlung spectra (86). The charged particle "cut-off" energy, below which the residual energy can be deposited "on the spot", can be varied continuously upward from 10 keV.

The program was implemented to produce the dose

distribution in homogeneous and heterogeneous phantoms from primary pencil photon beams. The modelled beam was a 0.50 cm in radius, monoenergetic parallel beam. The phantom was composed of 20 cm of either "water" or a combination of "water" and "cork" (water-like in chemical composition but with a gravimetric density of 0.25) slabs totalling 20 cm in overall thickness.

The pencil beam dose distribution was also used to compose the central axis dose due to a broad photon beam. Figure 93 illustrates the procedure schematically for a pencil beam directed into the page. The small circle of area, A_{pencil}, represents the pencil beam. The dashed lines represent an annulus in which dose has been deposited from the pencil beam. DOSE CONTRIBUTION (P) is the dose contribution at point P from an annulus of area $A_{annulus}$ (shown by solid lines):

$$\text{DOSE CONTRIBUTION (P)} = \frac{A_{ANNULUS}}{A_{PENCIL}} [\text{DOSE}]_{ANNULUS} \qquad (6.1)$$

The ratio of the area of the annulus to the area of the pencil beam gives the relative amount of energy being released in the annulus compared to the pencil beam.

A widely used "rule of thumb" states that the mean energy of x-rays produced in an accelerator is approximately one-third of its nominal energy. Therefore, the mean energy of a 15 MV x-ray beam should be approximately 5 MeV. Figure 94 illustrates that the calculated tissue-maximum-ratio as a function of depth is within 5 % of the measured values for a

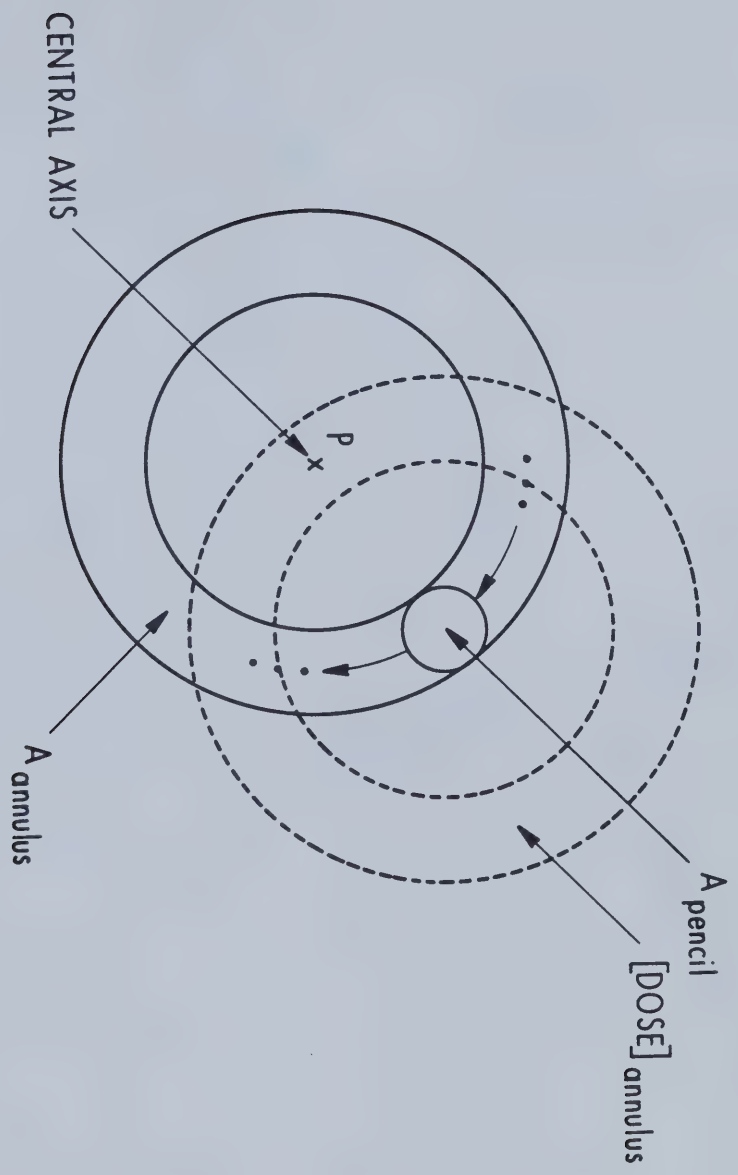

Figure 93. The dose at point P gets a dose contribution from an annulus by "revolving" a pencil dose distribution about point P. The value of the pencil dose distribution is $[DOSE]_{annulus}$.

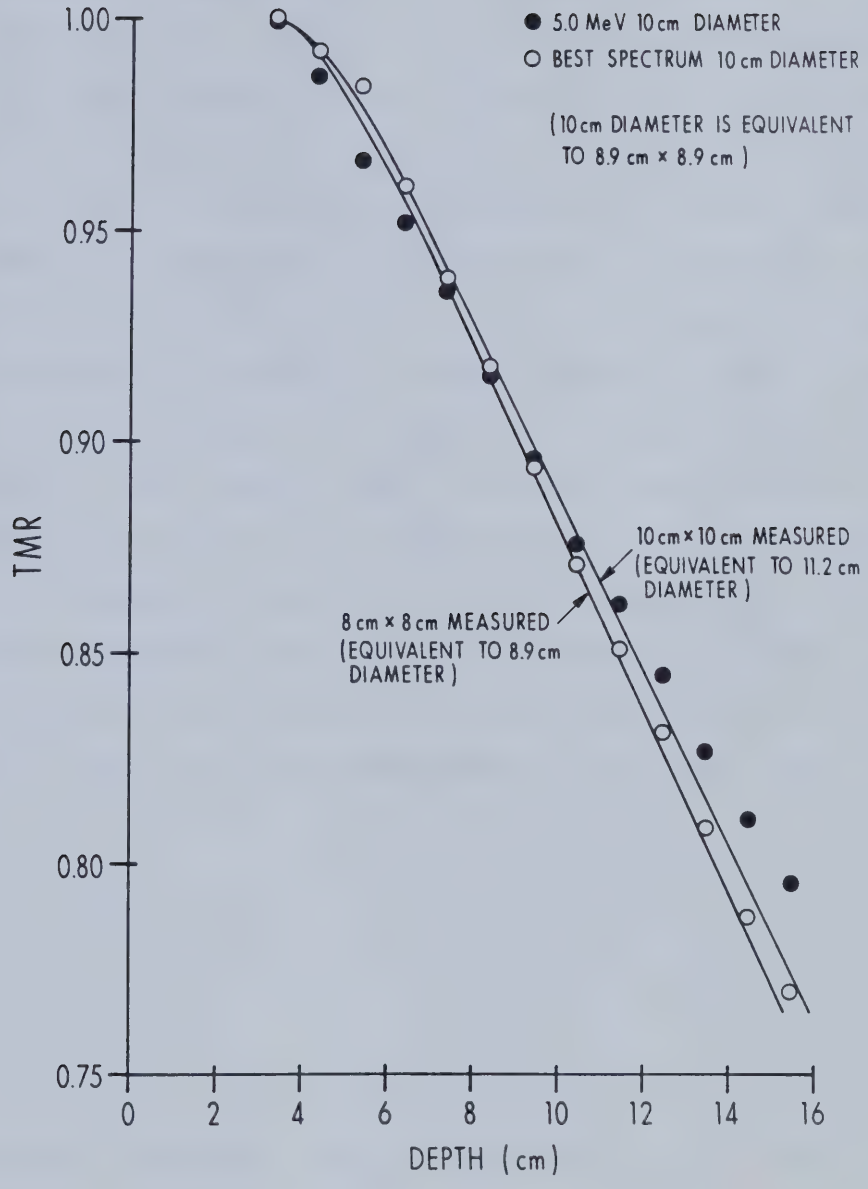

Figure 94. The measured TMR is compared to the EGS calculation of the TMR.

field size equivalent to a 10.0 cm diameter field.* The present version of the program accepts only a monoenergetic initial photon energy, so that each energy component in the spectrum requires a separate run of the program. The 15 MV spectrum used to model the dose in the build-up region (see Figure 70) had 36 energy components. Therefore, this would require 36 runs of the program to produce the dose results for the x-ray spectrum. It was felt that if the dose, as a function of depth (see Figure 94), could be modelled with good precision with only one energy component (5 MeV), then a spectrum containing six components would improve the agreement. The energy range between 0 and 15 MeV was, therefore, divided into six components and the mean energy of each component determined. The 36-component 15 MV spectrum (Figure 70) was used as a starting point. The mean energy of the six components were chosen with the mean energy of the bins of the 36-component spectrum, $(h\nu_o)_{nm}$, using:

$$(h\nu_o)_n = \frac{\sum_m (h\nu_o)_{nm} \cdot F_{nm}}{\sum_m F_{nm}} \qquad (6.2)$$

Where F_{nm} is the fluence of photons in each component of the 36-component spectrum. The photon energies that resulted

* The EGS program assumed cylindrical geometry so the equivalent circular field was used to model rectangular fields (54).

were 0.18 MeV, 0.67 MeV, 2.57 MeV, 6.61 MeV, 11.12 MeV and 13.78 MeV. A determination of the weighting of the spectral components, to give the best agreement with measured data, was made using the least-squares method. Figure 94 illustrates that the photon fluence, weighted in the proportions 0:11:11:11:5:0, improved the agreement of the calculated and measured dose to within 0.5 %.

The effect of a low-density water-like slab heterogeneity on pencil and broad beam geometries was investigated. The cut-off kinetic energy for the charged particle was chosen to be 189 keV (total energy of 700 keV). Figure 95 illustrates a comparison between pencil isodose curves in a homogeneous (on the right) and a heterogeneous phantom (on the left). The 50 % isodose line is not present inside the heterogeneous portion of the pencil beam. The 5 % and lesser isodose lines "bulge" outwards. This indicates that charged particles are "streaming" outward from the pencil beam into the surrounding low-density region. At first sight, the 0.1 % isodose line does not seem to be a very important contribution to the dose. However, $A_{annulus}$ increases with distance from the central axis. Therefore, Equation 6.1 suggests that a shift in isodose lines to greater radius will produce a greater contribution when summed for a broad beam.

The TMR inhomogeneity correction factor for a broad beam was determined by summing pencil beam contributions for a heterogeneous and homogeneous phantoms. The thickness and density of the heterogeneity was fixed at 8 cm and

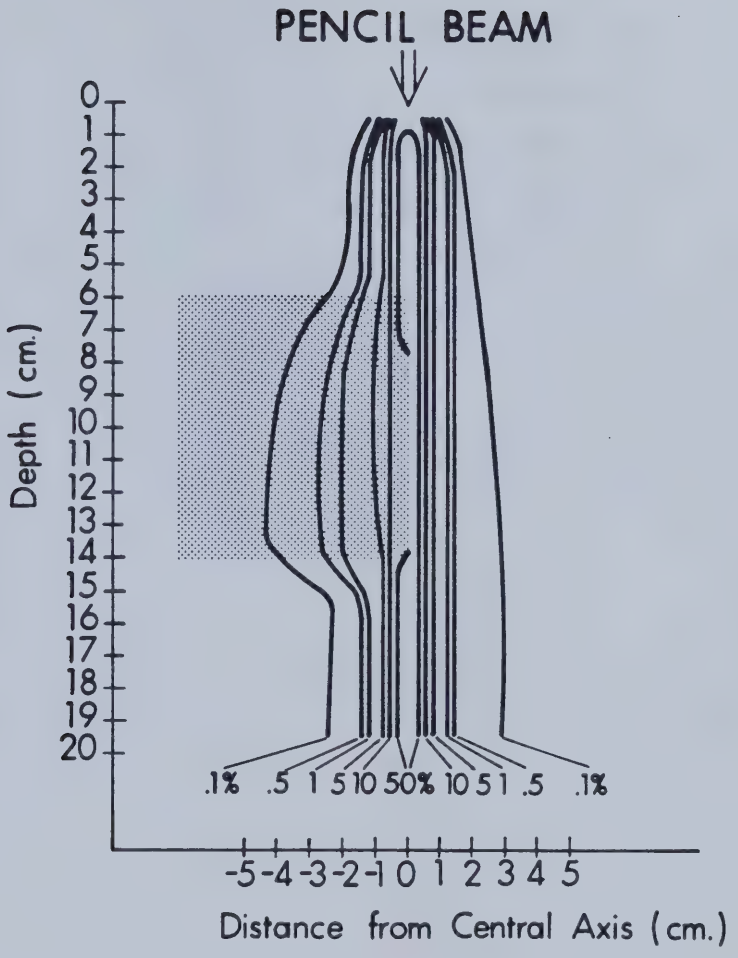

Figure 95. A comparison between pencil beam isodose curves in a homogeneous (right) and heterogeneous phantoms (left). The shaded region has a density of 0.25 g/cm^3.

0.25g/cm^3, respectively. The total thickness of overlying material was 15.5 cm (actually, the average dose between 15 and 16 cm was determined). Figure 96 illustrates the calculated correction factor. Also shown is the measured correction factor from Figure 86 obtained with cork as the low-density heterogeneity (with a density of 0.30 $\pm$ 0.02 g/cm^3). There is a 2 % discrepancy between the calculated and measured data. Most of the discrepancy is probably due to the difference between the actual cork density (0.30g/cm^3) used in the measurements and the density used in the Monte Carlo simulation (0.25g/cm^3). When determining the correction factor from measurement there was an underlying assumption that the mean stopping power of charged particles in a disequilibrium situation was equal to the mean stopping power in an equilibrium situation. This is equivalent to assuming that Equation 1.5.15 can be simplified to a simple ratio of ionization measurements. In contrast, the Monte Carlo correction factor implicitly takes into account the particle's changing stopping power as it loses energy. It is unlikely that this effect would produce a discrepancy of 2 % (53).

Lateral disequilibrium was investigated directly by setting the charged particle cut-off equal to the incident photon energy. This forced all of the charged particle energy to be deposited "on the spot". In this way, the KERMA, rather than the dose, is determined. Figure 97 illustrates a comparison between the profiles of KERMA and dose for a homogeneous and a heterogeneous phantom for a 5.0

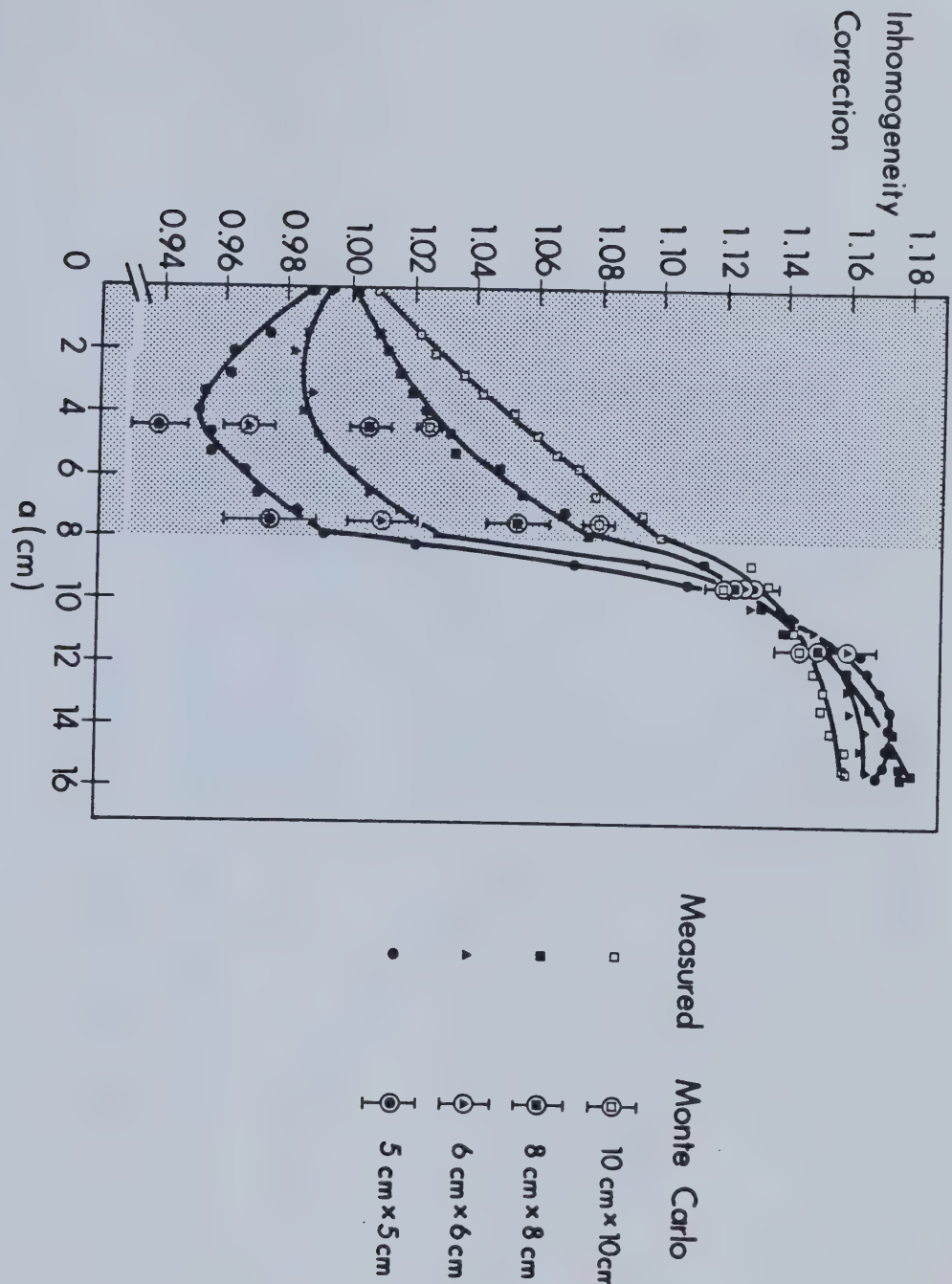

Figure 96. A comparison of measured inhomogeneity correction factors and ones calculated using the EGS Monte Carlo code.

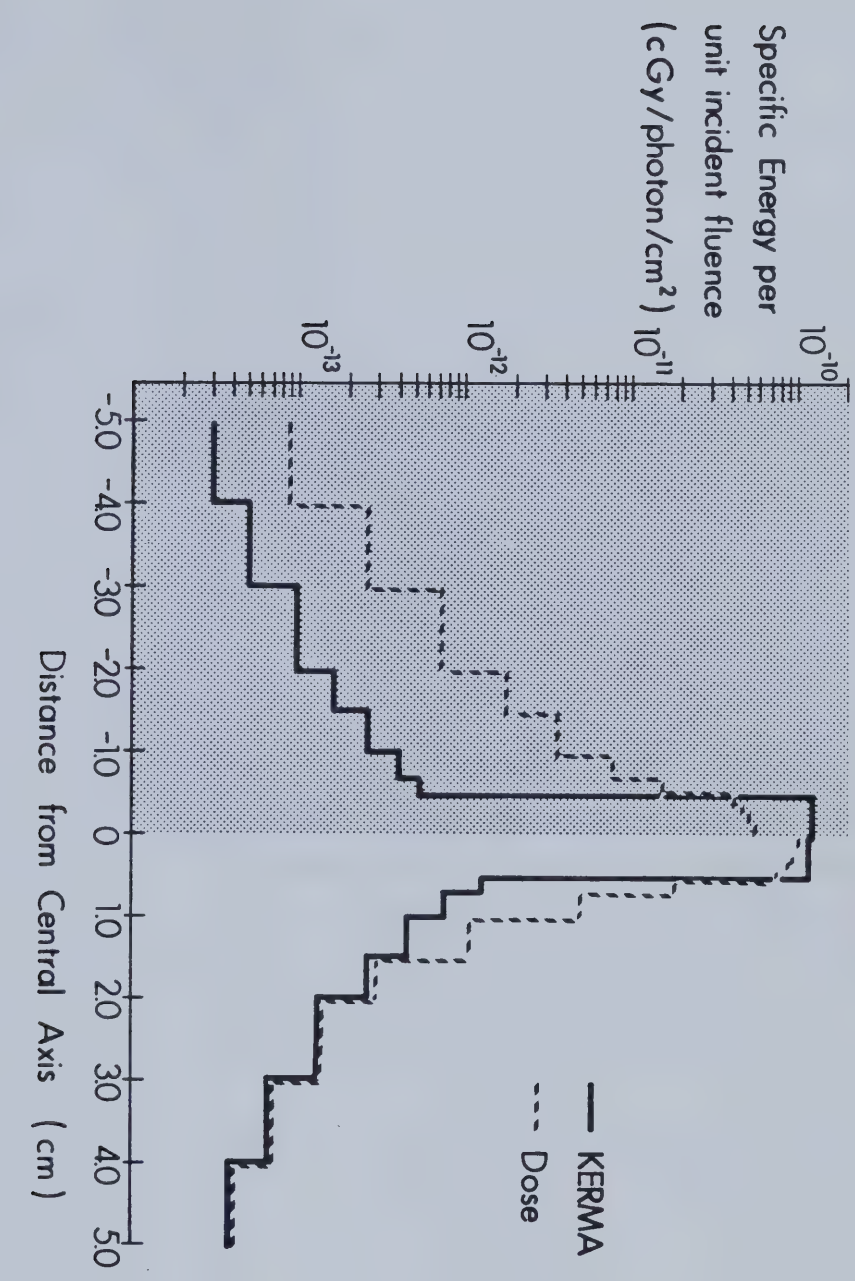

Figure 97. A comparison between the calculated profiles of KERMA and dose for a heterogeneous (left) and a homogeneous phantom (right).

MeV pencil beam. The profiles were taken at a depth of 10.5 cm. In the homogeneous case, the parameter, A, was 4.5 cm. It can be seen that in a homogeneous phantom, KERMA equals dose at a lateral distance of 1.5 to 2.0 cm from the central axis of the pencil beam. However, dose does not equal KERMA in a heterogeneous phantom even at a distance of 5.0 cm from the central axis of the pencil beam.

Broad beam KERMA distributions were produced from the pencil beam KERMA distributions. Figure 98 illustrates a comparison between the dose and KERMA correction factors for the 15 MV spectrum and its spectral components. The dose correction factor at first increases as a function of field radius and then decreases. The KERMA correction factor only decreases. At an energy of 0.67 MeV the dose and KERMA correction factors are in close agreement at field radii greater than 1 cm. At higher energies, the discrepancy between dose and KERMA correction facors becomes greater. Therefore, at lower energies KERMA is a good approximation to dose, but at higher energies, the KERMA equality with dose breaks down.

The measured correction factor is also shown in Figure 98. For higher energy beams the dose increases as a function of field size, whereas the KERMA always decreases as a function of field size. The increasing trend of the masured correction factor as a function of depth agrees best with the calculated correction factor using non-local energy deposition (the dose curves, rather than the KERMA curves).

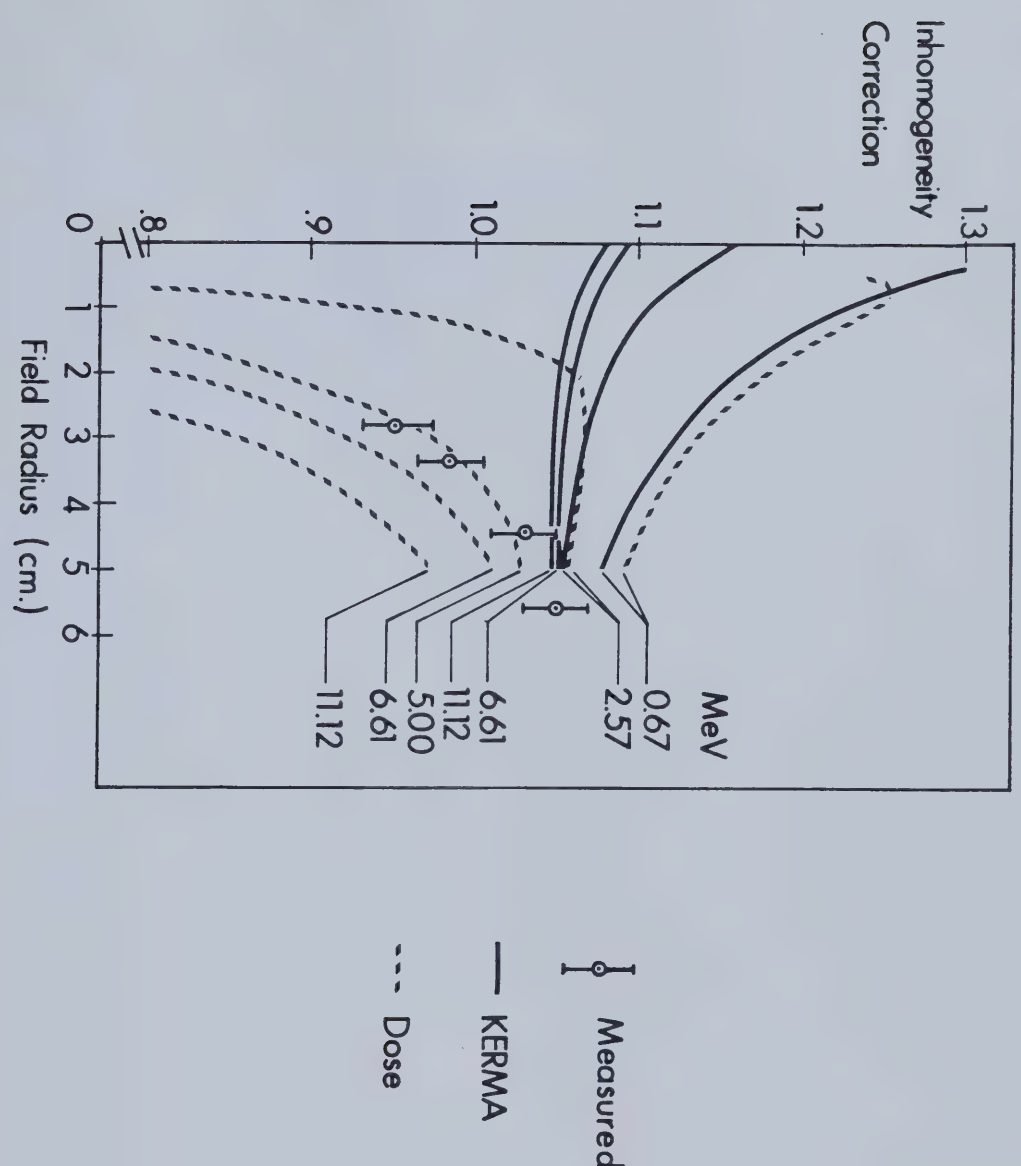

Figure 98. A comparison between dose and KERMA correction factors for the 15 MV spectrum and its spectral components.

7. A Convolution Method Of Calculating Dose

Knowledge finds differences, but
understanding seeks similarities.

7.1. Introduction

Section 3 in Volume 1 indicated that simulating the longitudinal transport of charged particles set-in-motion enabled the dose in the build-up region to be predicted. Section 6 in this Volume illustrated that the lateral transport of charged particles must be included to predict lateral disequilibrium phenomena. Therefore, a dose deposition model for megavoltage x-ray beams is required which explicitly takes into account charged particle transport.

In this section, a method of analysis which is physically sound and internally consistent will be discussed, which allows calculation of 3-dimensional dose distributions in homogeneous or heterogeneous phantoms irradiated with fields of high energy photons when electronic equilibrium is not present. The method is versatile enough to allow for rectangular fields, irregularly-shaped fields and the placement of beam blocks or compensators in the field. The use of measured data as a data base is abandoned and replaced with data generated from first principles by Monte Carlo techniques.

The Monte Carlo method is used to map the spatial distribution of charged particle energy away from a primary photon interaction site. This distribution, called a "primary dose spread array", is convolved spatially with the kinetic energy released (KER) at all the primary interaction sites to yield the primary dose distribution. In a

heterogeneous phantom, the dose spread arrays need to be modified.

Any current method separating primary from scatter dose can be improved with the methodology proposed here. Since convolution is a well-understood mathematical technique, there are conceptual and practical advantages for implementing a convolution framework for the spread of energy due to scattered photons* as well as charged particles set-in-motion.

The proposed method was based on concepts which will not become obsolete as improved computational power becomes available. The fundamental reason for this is the sound physical basis of the Monte Carlo and convolution procedures. Another reason is an inherent flexibility to compromise between speed and accuracy. Therefore, as computers become faster, greater accuracy can be achieved without modifying the algorithm substantially. As well, the present availability of "array processors" is compatible with the array structure of convolution mathematics.

* Dean (86) has used this approach to find where the scatter dose was being absorbed from Cobalt-60 primary photons interacting in one location of a water phantom.

7.2 Primary Dose Spread Arrays

7.2.1 Definition Of A Primary Dose Spread Array

A primary dose spread array* is the 3-dimensional spatial distribution of energy deposited by electrons and positrons which spread from the site of the primary photon interactions. It is generated by tracking the motion of charged particles away from primary interaction sites occurring within a cubic volume element (voxel). These charged particles are followed using the Monte Carlo method in a homogeneous phantom consisting of voxels with the same size, atomic number, and density. The amount of energy deposited at, and in the neighborhood of, the interaction voxel is scored. Figure 99 illustrates the procedure schematically.

7.2.2 The Generation Of Dose Spread Arrays Using The MOCA Monte Carlo Code

The dose spread arrays were generated by a "home-made" Monte Carlo code called MOCA developed from the program Buildup3.for, the Monte Carlo code used to calculate the

* The "dose spread array" is analogous to the "point spread array" used in image processing.

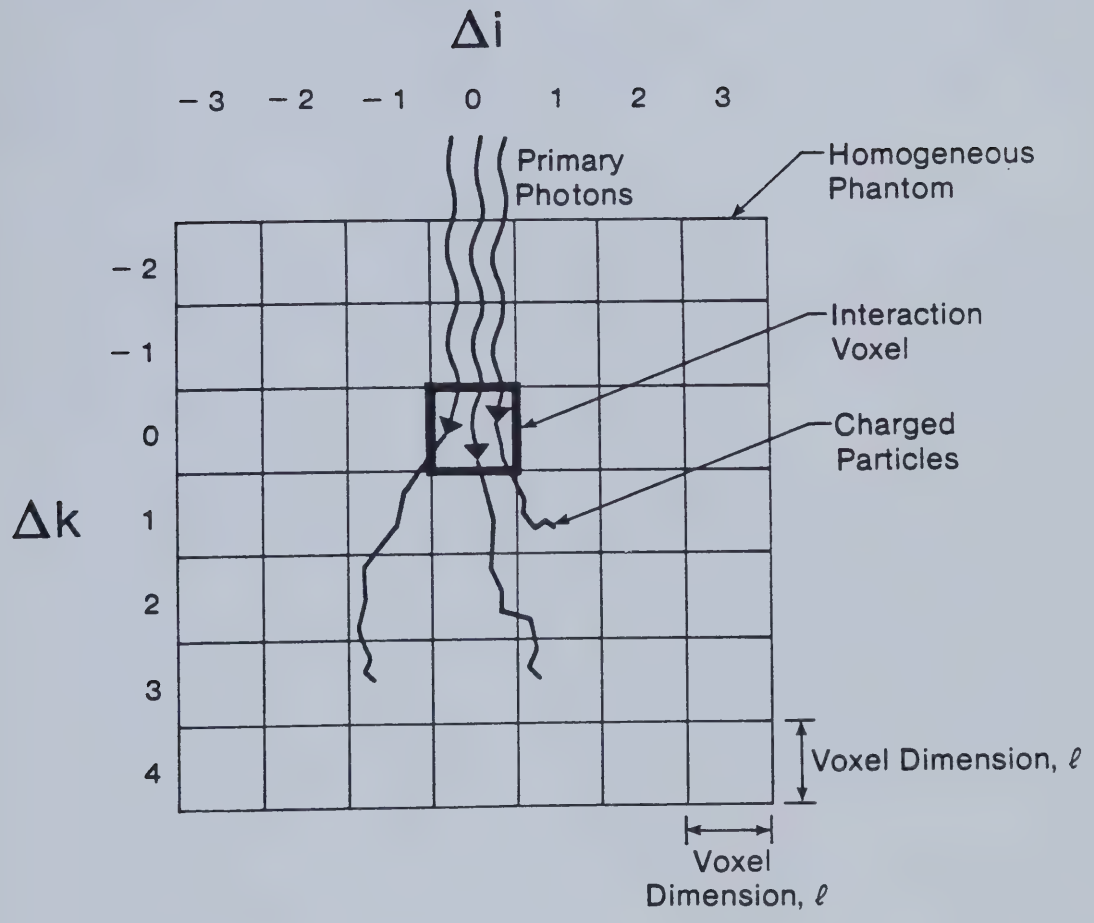

Figure 99. Primary photons interact in the interaction voxel and the charged particles set in motion are followed through the phantom to see where they deposit their kinetic energy.

build-up dose in Section 3 of Volume 1. MOCA takes into account the photoelectric effect, Compton effect and pair production. MOCA produces 0.511 MeV photons when the positron annhilates. Like Buildup3.for, MOCA employs the approximations of continuous slowing down (without generation of secondary "knock-on" electrons) and Gaussian lateral scattering for charged particles. Bremsstrahlung was not included in MOCA. Figures 100 to 102 are flow charts of the program MOCA.

A photon history begins, in MOCA, by initializing its energy, position and direction. The distance the photon travels before it interacts is first determined. The photon (or the scattered photon created by a Compton interaction) is followed until its energy falls below the photon energy cut-off, or it interacts by the photoelectric or pair production effects, or it leaves the phantom. The type of photon interaction is chosen by finding "partial fractions" based on the Compton and pair production attenuation coefficients. Charged particles generated by photon interactions are placed in a "queue" for further processing after the end of the photon history.

MOCA employs a novel technique to determine the kinetic energy acquired by a charged particle following a Compton or a pair production interaction. The Compton interaction cross-section per unit kinetic energy of the recoil electron, $d\sigma/dT$, has a complex dependence on kinetic energy, T. The method provides a way of numerically inverting the differential cross-section with respect to

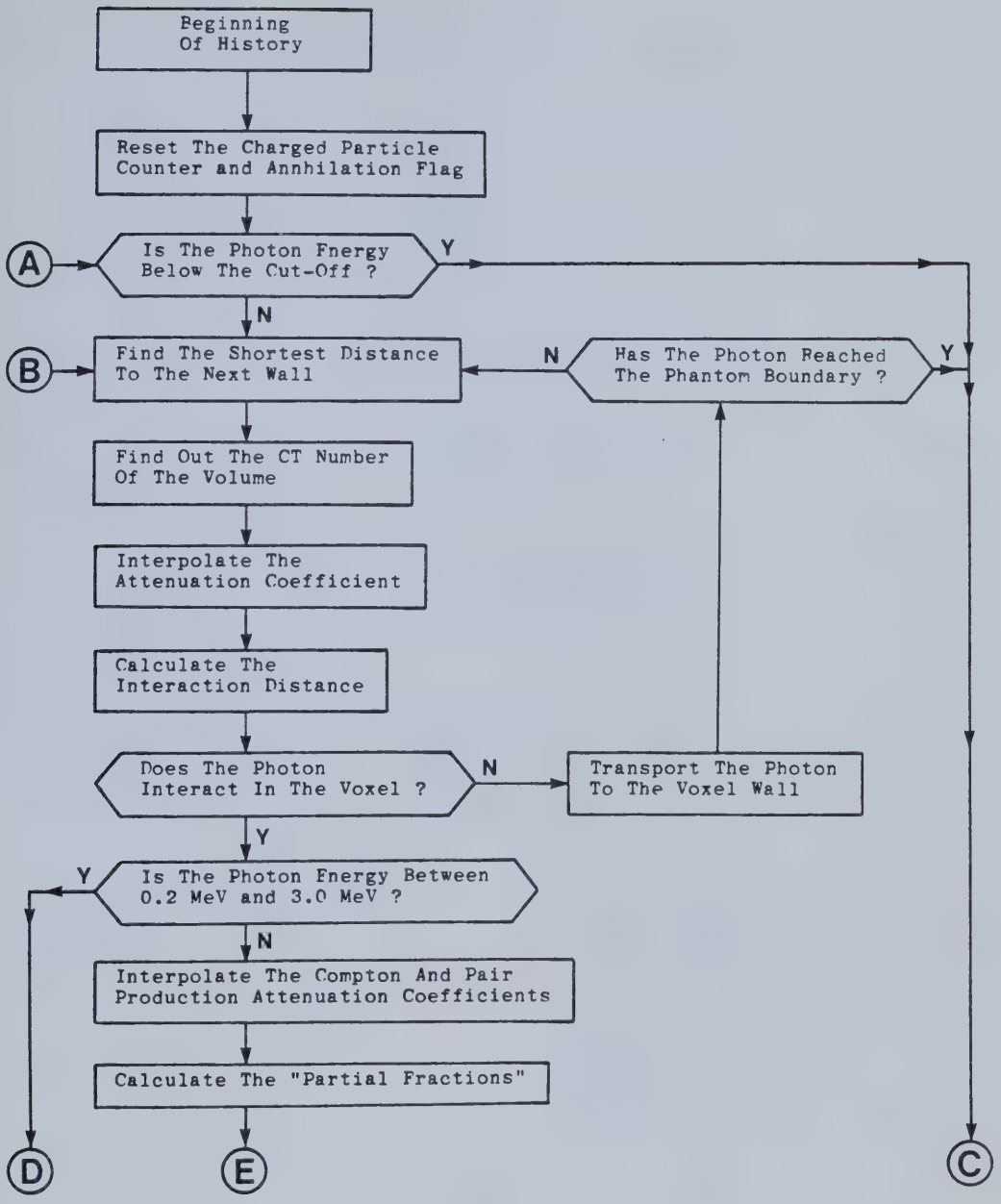

Figure 100. Flow chart for photon transport part of MOCA. A) and B) are from Figure 101. B) can also come from Figure 102. C), D) and E) enter Figure 101.

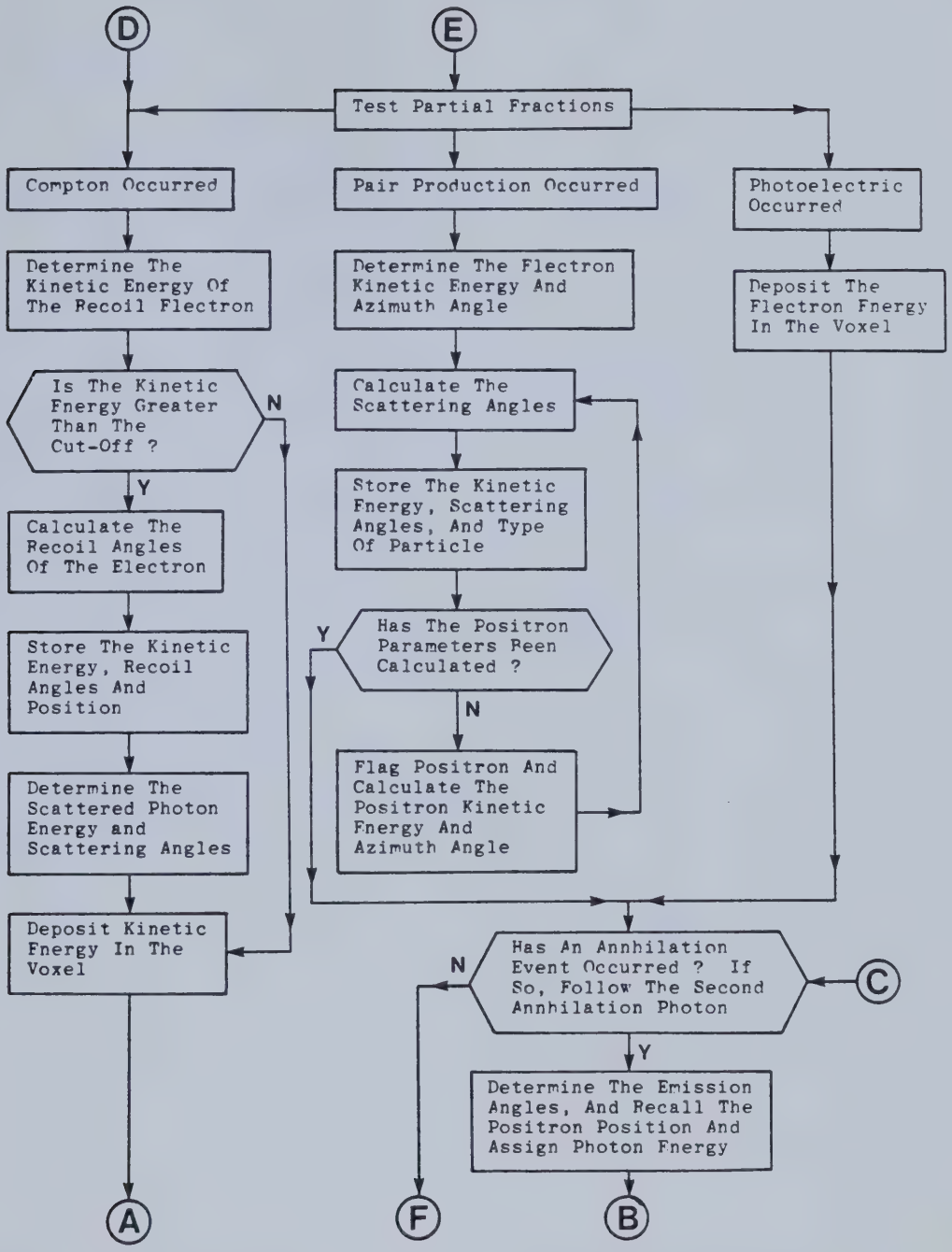

Figure 101. Flow chart for the part of MOCA dealing with the type of photon interaction. C), D) and E) are from Figure 100. A) and B) enter Figure 100. F) enters Figure 102.

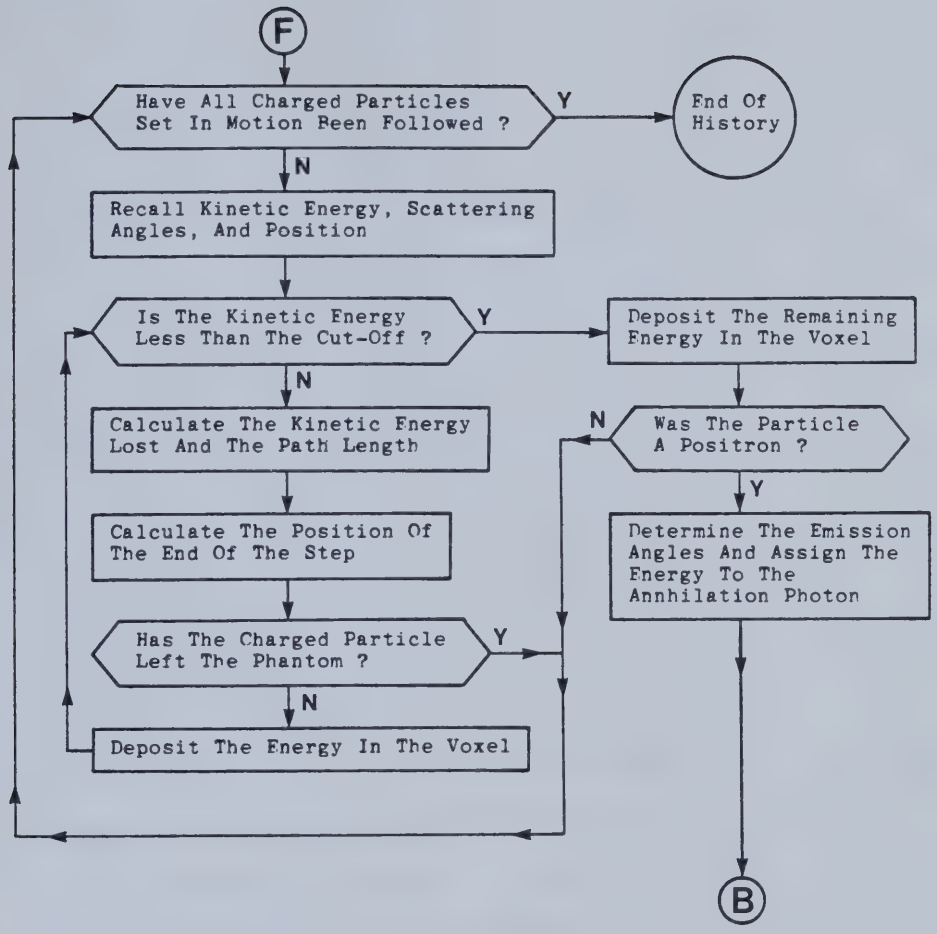

Figure 102. Flow chart for the charged particle transport part of MOCA. F) is from Figure 101. B) enters Figure 100.

kinetic energy.

Figure 103 illustrates the Compton differential cross-section as a function of kinetic energy up to the maximum kinetic energy, Tmax. The total area under the curve is equal to the total Compton cross-section, σ . The curve in Figure 103 is subdivided into N intervals such that the area of each interval has an equal area σ/N. Each interval represents an equiprobable occurrence of interaction. The corresponding kinetic energy of each interval, $T_i(h\nu)$, is found. Since each $T_i(h\nu)$ is equally likely to be the recoil energy of the electron, there can be a one-to-one correspondence with a random number. This is accomplished by normalizing the interval kinetic energy , $T_i(h\nu)$, to the maximum kinetic energy.

Figure 104 illustrates the values of $T(h\nu)/Tmax$ as a function of random number, R, for various values of incident photon energy, $h\nu$(MeV). It can be seen that at higher incident photon energies there is a greater probability of the generation of high energy recoil electrons.

The pair production interaction is treated in the same manner as the Compton interaction except that the maximum kinetic energy, T_A, is now given by Equation 3.1.10. Figure 105 illustrates the values of $T(h\nu)/T_A$ as a function of random number for 3.0 MeV and 10.0 MeV photons. The most probable kinetic energy of a charged particle is around half the maximum energy.

The charged particles generated by a photon are taken from the "queue" at the end of the photon history. Their

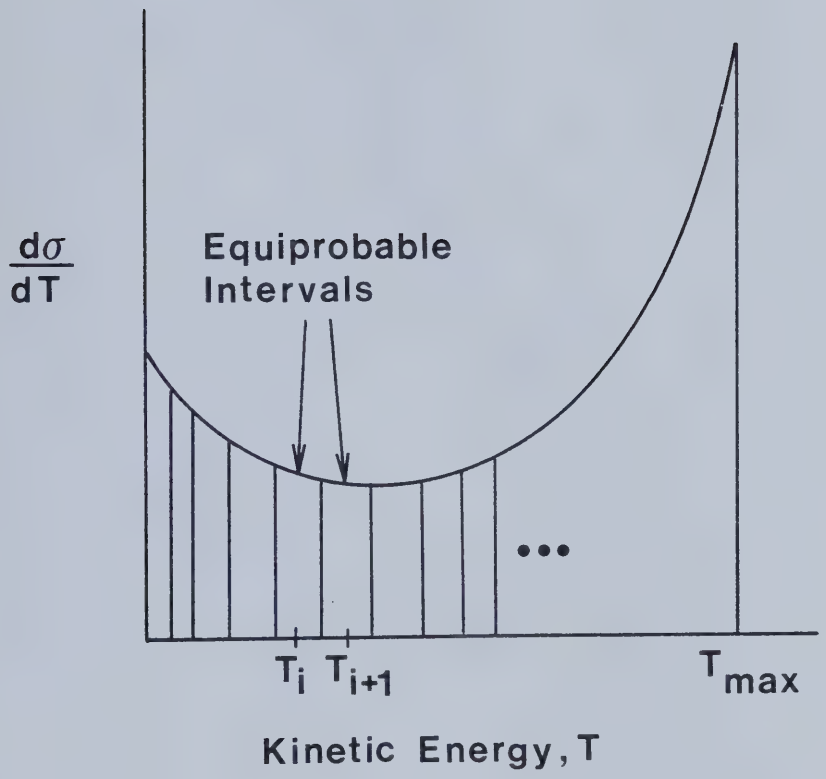

Figure 103. The Compton differential cross-section as a function of kinetic energy. The area under the curve, equal to the total interaction cross-section, is divided up into equiprobable areas.

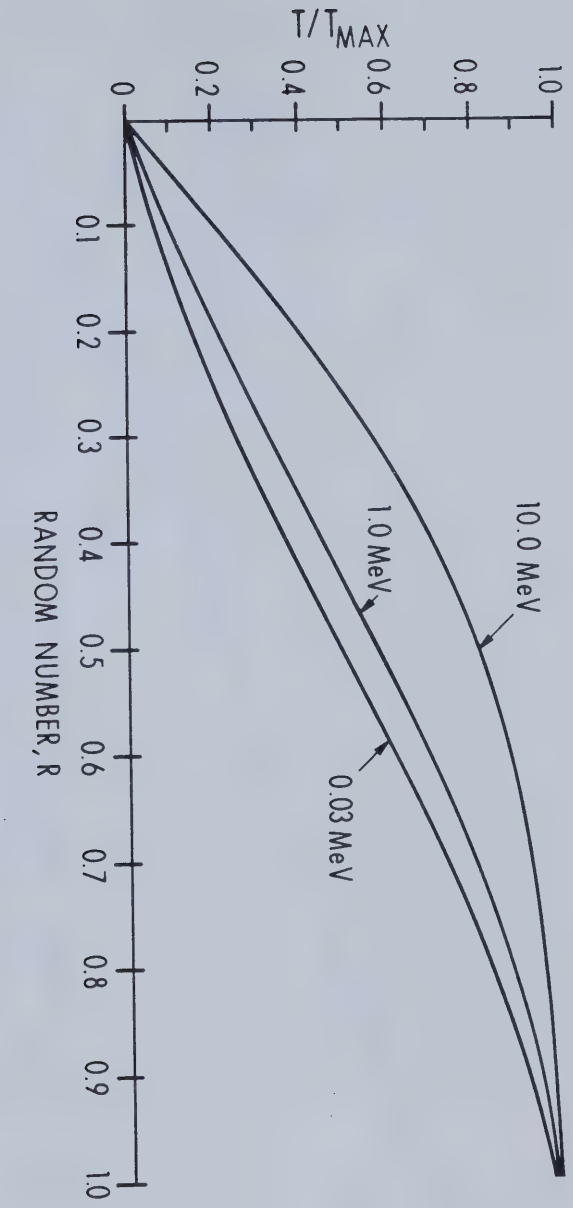

Figure 104. $T(h\nu)/T_{max}$ as a function of random number, R, for various incident photon energies. The Compton recoil electron kinetic energies can be chosen with equally weighted random numbers chosen between 0 and 1.

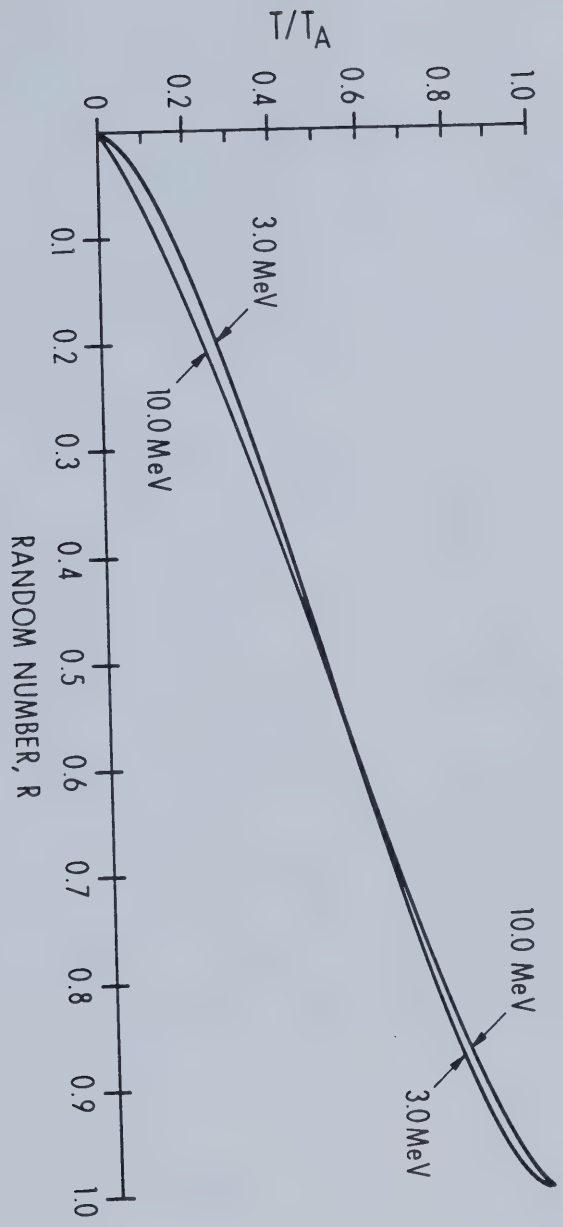

Figure 105. $T(h\nu)/T_A$ as a function of random number, R, for various incident photon energies. The kinetic energy of pair production charged particles can be chosen with equally weighted random numbers chosen between 0 and 1.

kinetic energy, position and direction in which they were set in motion is recalled. The charged particle transport is almost identical to Buildup3.for. The exception is that annhilation photons are produced when a positron reaches the end of its range ("annhilation in flight" is ignored). The annhilation photons are treated as a scattered photon.

Appendix 10 contains a listing of the program MOCA. MOCA was used instead of EGS because MOCA was much simpler than EGS and, therefore, there was much more control over the programming of the geometry to describe the dose spread arrays. Despite its simplicity, MOCA produces almost the same results as EGS. Figures 106 and 107 are a comparison between MOCA and EGS Monte Carlo calculations of the depth-dose from 1.25 MeV and 5 MeV photon beams, respectively. The field size was 10 cm x 10 cm for the MOCA calculation and a field radius of 5.6 cm (the equivalent circular radius for a 10 cm x 10 cm field) for the EGS calculation. Also included in Figure 106 is the measured depth-dose for a Cobalt-60 beam. There is good agreement between the Monte Carlo programs at both energies and with measured data.

7.2.3 Results

Figures 108 and 109 show voxel elements of primary dose spread arrays for a pencil beam of 15 MV x-rays interacting in a homogeneous phantom with cubic voxel dimensions of

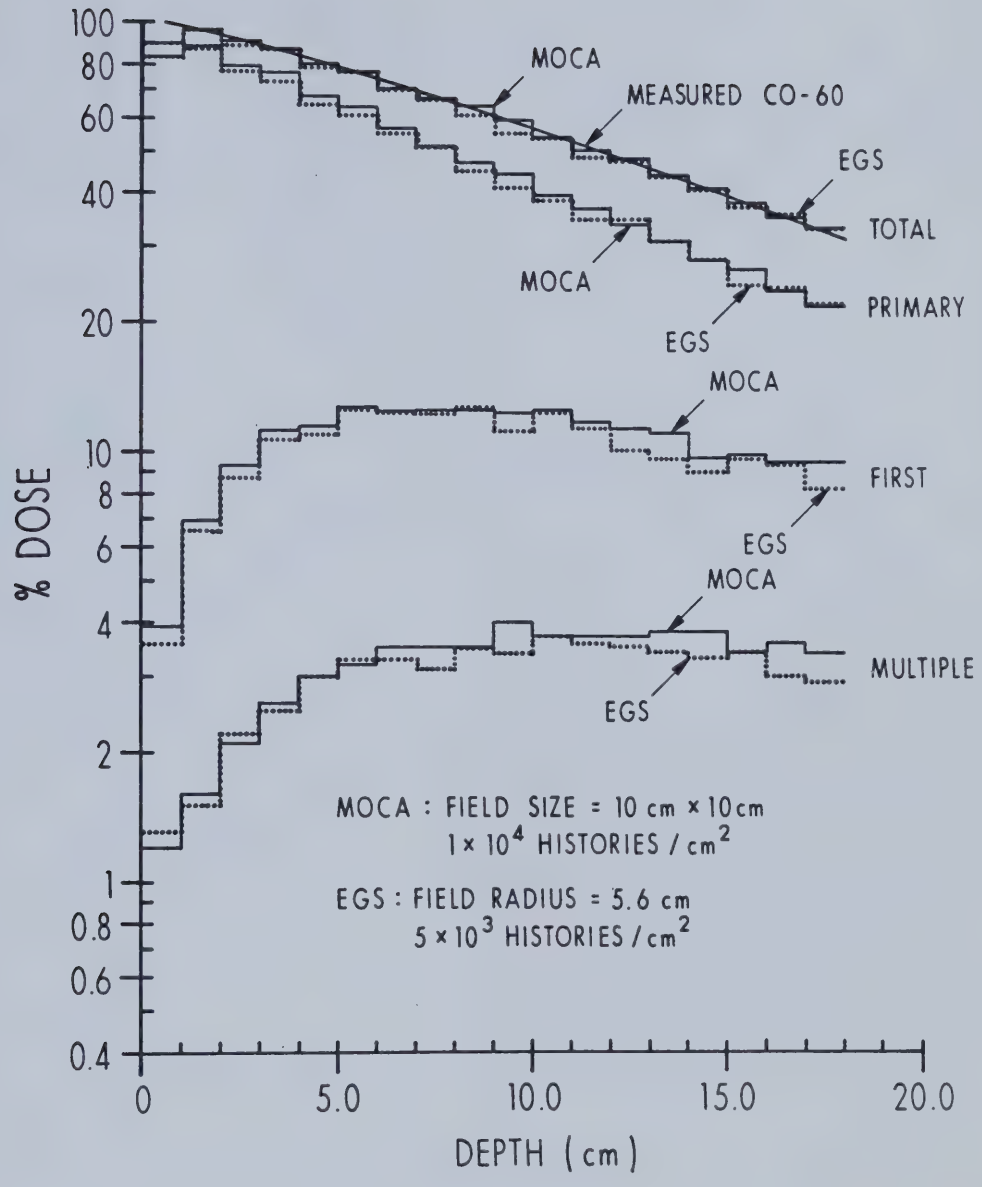

Figure 106. A comparison of components of the percent dose predicted by MOCA and EGS for Cobalt-60 photons (1.25 MeV). The measured total dose is also shown for comparison.

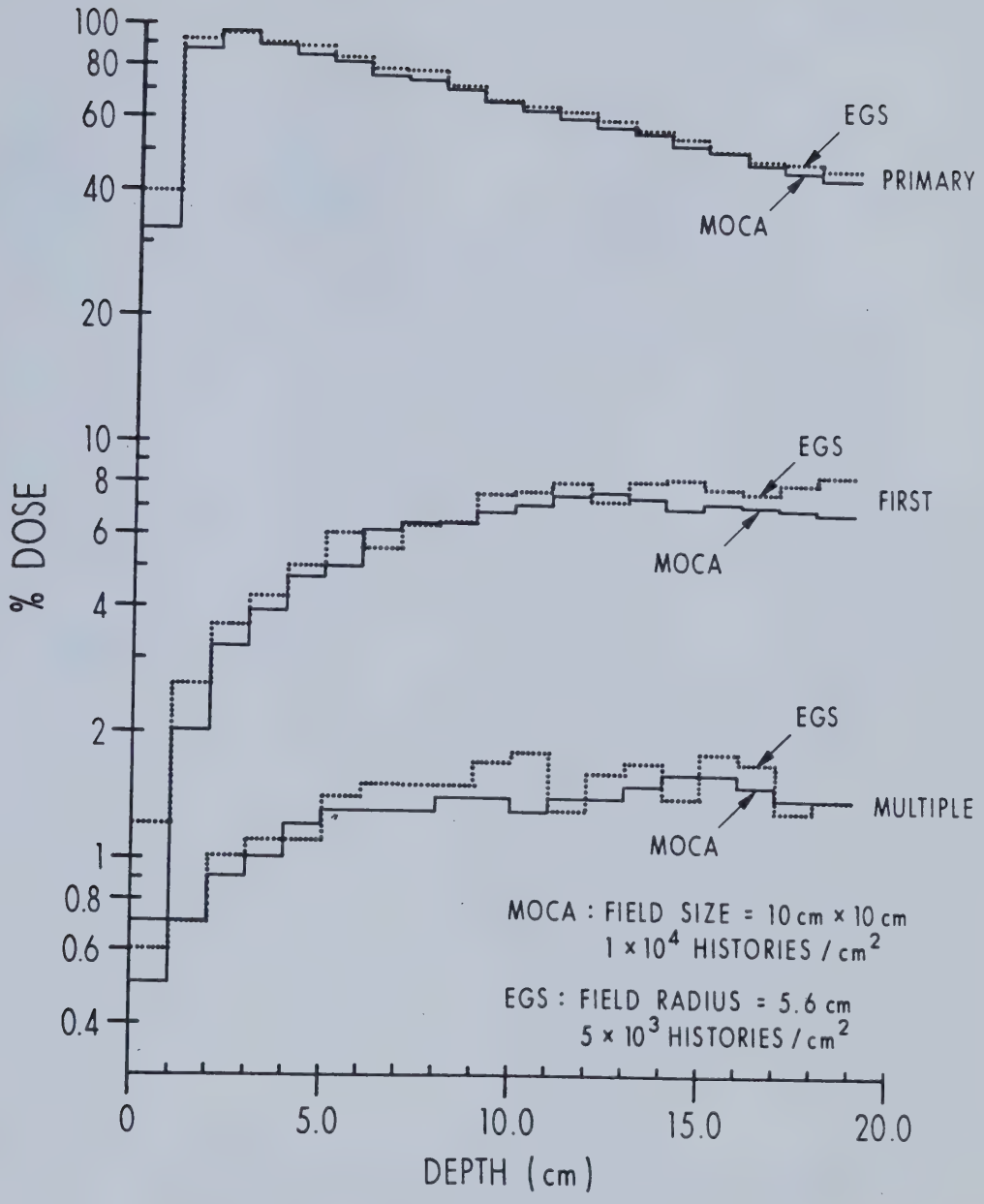

Figure 107. A comparison of components of the percent dose predicted by MOCA and EGS for 5 MeV photons.

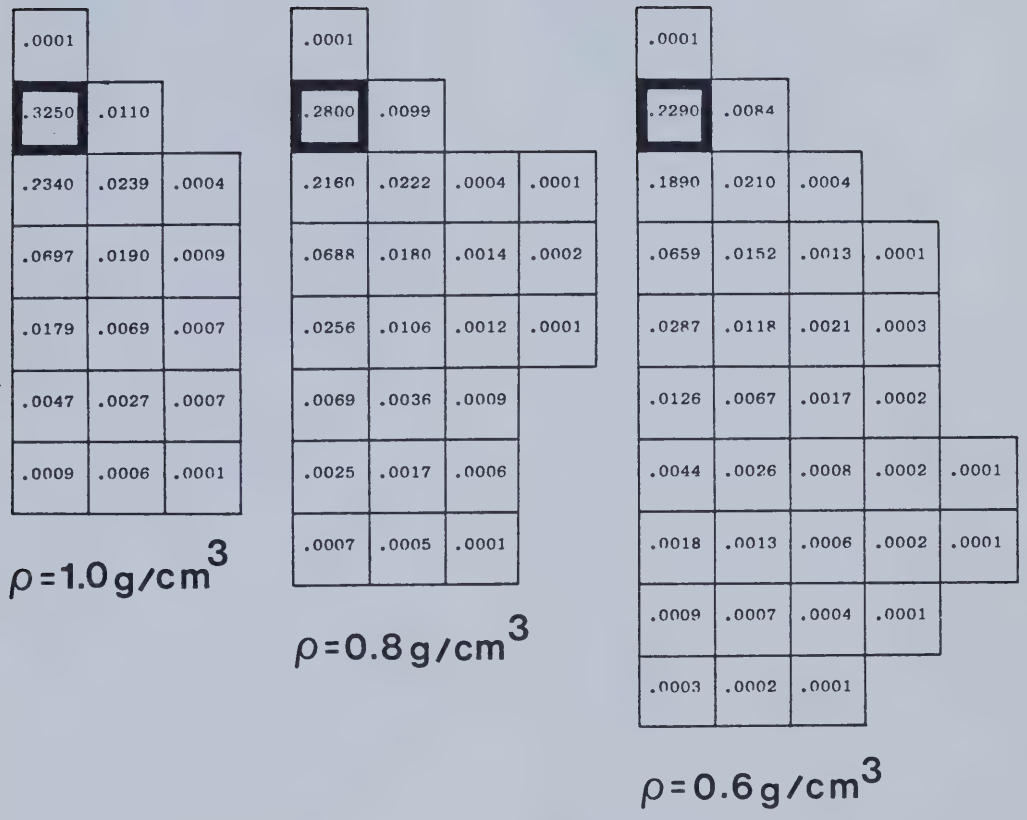

Figure 108. Primary dose spread arrays for 15 MV photons interacting in an interaction voxel (shown with bold boundaries). The voxels are cubic with dimensions of 1.0 cm on each side.

.0001				
.1730	.0065	.0001		
.1440	.0177	.0007		
.0631	.0146	.0010	.0001	
.0275	.0094	.0014	.0003	.0001
.0142	.0070	.0018	.0005	.0002
.0077	.0048	.0017	.0006	.0002
.0041	.0029	.0013	.0004	.0001
.0019	.0015	.0007	.0003	.0001
.0009	.0007	.0004	.0002	.0001
.0005	.0005	.0003	.0002	.0001
.0003	.0003	.0002	.0002	.0001
.0002	.0002	.0001	.0001	
.0001	.0001	.0001		

ρ=0.4g/cm^3

.0001						
.1120	.0051	.0001				
.0908	.0101	.0006	.0001			
.0439	.0104	.0013	.0003			
.0249	.0087	.0018	.0004	.0001		
.0143	.0063	.0015	.0004	.0001		
.0080	.0043	.0012	.0004	.0002	.0001	
.0048	.0031	.0011	.0004	.0002	.0001	
.0031	.0023	.0010	.0005	.0002	.0001	
.0020	.0016	.0009	.0005	.0002	.0001	.0001
.0014	.0012	.0007	.0005	.0002	.0001	.0001
.0010	.0009	.0006	.0004	.0002	.0002	.0001
.0007	.0007	.0005	.0003	.0002	.0001	.0001
.0005	.0005	.0004	.0002	.0002	.0001	.0001
.0003	.0003	.0003	.0002	.0001	.0001	
.0002	.0002	.0002	.0002	.0001	.0001	
.0001	.0001	.0001	.0001	.0001		
.0001	.0001	.0001	.0001	.0001		
.0001	.0001					

ρ=0.2g/cm^3

Figure 109. Primary dose spread arrays for 15 MV photons (see Figure 108).

1.0 cm. The incident photon fluence spectrum obtained using EGS in Section 6 was also used by MOCA. The density of the arrays is from $0.2 g/cm^3$ to $1.0 g/cm^3$ in steps of $0.2 g/cm^3$. The media are assumed to be water-like in chemical composition. The voxels shown in these figures are in the same plane as both the interaction voxel and the primary pencil beam. The beams have the same cross-sectional area as the voxels and are made to interact only in the interaction voxel (bold borders). At least 10^6 charged particles/cm^2 were set in motion by primary photons to generate these arrays. To speed up the convolution process for rectangular fields, the dose spread arrays are produced in a 3-dimensional Cartesian geometry. The dose spread arrays are quadrilaterally symmetric about the primary photon direction, which is designated as the Δk axis. Therefore, an element of a dose spread array can be given by:

$$\begin{aligned} A_p(\rho,\ell,\Delta i,\Delta j,\Delta k) &= A_p(\rho,\ell,-\Delta i,\Delta j,\Delta k) \\ &= A_p(\rho,\ell,\Delta i,-\Delta j,\Delta k) \\ &= A_p(\rho,\ell,-\Delta i,-\Delta j,\Delta k) \end{aligned} \qquad (7.2.1)$$

The dose spread arrays are also symmetric with respect to interchange of the Δi and Δj axis, therefore:

$$A_p(\rho,\ell,\Delta i,\Delta j,\Delta k) = A_p(\rho,\ell,\Delta j,\Delta i,\Delta k) \qquad (7.2.2)$$

Figures 108 and 109 clearly illustrate that the

assumption of local energy deposition at 15 MV is untenable. The value of the dose spread array at the interaction voxel (location 0,0,0) in a 1.0g/cm^3 phantom with a voxel size of 1 cm is 0.325 which indicates 32.5 % of the energy released at the interaction site is deposited there. The value at the same location for a 0.2g/cm^3 phantom with a voxel size of 1 cm is only 0.112. The maximum longitudinal range of charged particles set in motion in a 1.0g/cm^3 phantom is about 4 to 6 cm and in a 0.2g/cm^3 phantom the maximum longitudinal range is about 20 cm! In the lateral direction charged particles can contribute dose about 1 to 3 cm and 5 to 7 cm from the interaction site for 1.0g/cm^3 and 0.2g/cm^3 phantoms, respectively. Figure 110 illustrates the primary dose spread arrays for 6 MV x-rays and a Co-60 (1.25 MeV) photon beam. The spectrum used to determine the 6 MV build-up curves (see Figure 69) was used. The density of the phantoms was 0.5g/cm^3 and the voxel dimension was 1.0 cm. As the energy decreases, more of the primary energy is deposited in the interaction voxel and the longitudinal and lateral range of the charged particles is reduced. At 1.25 MeV in a phantom of density 0.5g/cm^3, the primary energy is deposited within 1.0 cm from the primary interaction site. Therefore, the assumption of local primary energy deposition is more reasonable for Co-60 beams.

The primary dose spread array values indicate the primary energy deposited in each voxel normalized to the collision fraction of the total energy released in the

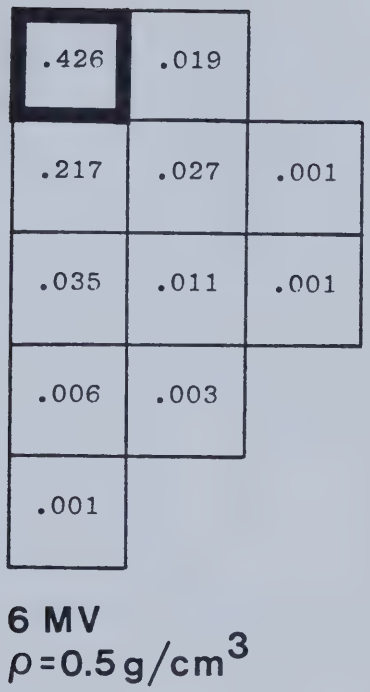

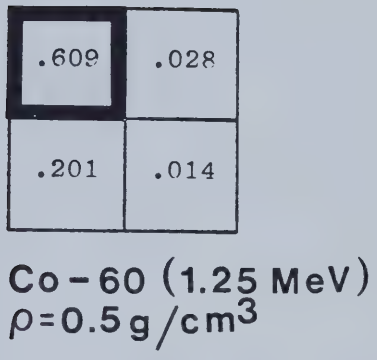

Figure 110. Primary dose spread arrays for 6 MV and Co-60 photons. The voxel dimension is 1.0 cm.

interaction voxel:

$$A_p(\rho,\ell,\Delta i,\Delta j,\Delta k) = \frac{T(\rho,\ell,\Delta i,\Delta j,\Delta k)}{KER(\rho,\ell,0,0,0)} \qquad (7.2.3)$$

Where $Ap(\rho,\ell,\Delta i,\Delta j,\Delta k)$ is the primary dose spread array at a distance $\Delta i,\Delta j,\Delta k$ from the interaction voxel. $T(\rho,\ell,\Delta i,\Delta j,\Delta k)$ is the energy deposited at that site. $KER(\rho,\ell,0,0,0)$ is the total energy of charged particles set in motion at the interaction site that is lost to electron collisions (not bremsstrahlung) in the phantom (87).

Since the phantom is homogeneous, the interaction and dose deposition voxels have the same density. Therefore, the array value is also equal to the dose deposited due to electron collisions in the neighboring voxels per unit kinetic energy released per unit mass, Kc (collision KERMA) (87), at the interaction voxel. If the dose spread arrays are spatially invariant (Section 7.6 will discuss the implications of spatial invariance), Equation 7.2.3 can be expressed as:

$$A_p(\rho,\ell,\Delta i,\Delta j,\Delta k) = \frac{DOSE(\rho,\ell,i+\Delta i,j+\Delta j,k+\Delta k)}{K_c(\rho,\ell,i,j,k)} \qquad (7.2.4)$$

The primary dose spread arrays can be produced for different voxel dimensions and for a variety of water-like phantoms with different densities. Figure 111 illustrates the dose spread arrays with a voxel and beam dimension of 5.0 cm and a density of $0.2 g/cm^3$. The values of the dose

.0001		
.3250	.0111	
.2340	.0240	.0006
.0707	.0184	.0007
.0181	.0075	.0007
.0050	.0028	.0006
.0010	.0006	.0001

$\rho = 0.2\ g/cm^3$

$\ell = 5.0\ cm$

Figure 111. Primary dose spread array for 15 MV photons. The value of $\rho \cdot \ell$ is the same as Figure 108 (left).

spread array elements of Figure 111 are nearly equal to those of Figure 108 (left dose spread array). Therefore, the product of the phantom density, $\rho(g/cm^3)$, and voxel dimension, $\ell(cm)$, is a fundamental measure of the voxel "size" in units of g/cm^2. This is just an extension of O'Connors theorem (71). O'Connors theorem can now be said to be independent of the state of electronic equilibrium. This is expected because, for a material of fixed atomic number, both the stopping power and the angular scattering power are directly proportional to the density (88). This has also been shown experimentally by Young and Kornelson (64,80).

The primary dose spread arrays are stored for various values of voxel size expressed in units of radiological depth, $\rho \cdot \ell$ (from $\rho \cdot \ell = 0.2 g/cm^2$ to $1.0 g/cm^2$ in step sizes of $0.2 g/cm^2$). This allows flexibility in the choice of voxel dimensions for dose computations and hence the spacing of calculation points. For example, a choice of a voxel size of $0.2 g/cm^2$ can be used either for a medium with $\rho = 1.0 g/cm^3$ to establish calculation points spaced at a distance of 0.2 cm or in a medium with $\rho = 0.2 g/cm^3$ for calculation points spaced 1 cm apart. When the desired spatial resolution and density yields a value of $\rho \cdot \ell$ which has not been stored, the dose spread array values need to be interpolated from the stored arrays.

7.3. Scatter Dose Spread Arrays

The Monte Carlo program used to determine the primary dose spread arrays is also used to follow scattered photons and charged particles produced by the scattered photons. The first scattered dose is scored separately from higher order multiple scatter. The dose due to first scatter photons, which is deposited "relatively" close to the primary interaction site, is placed in a truncated first scatter (TFS) dose spread array. The first scatter dose deposited "relatively" far from the primary interaction site is included with multiple scatter in a residual first and multiple scatter (RFMS) dose spread array. Positron annhilation photons are treated as if they were multiple scattered photons. Since, at megavoltage energies, first scattered photons are mainly forward directed, the location of the interaction voxel within the dose spread array has been optimized so that more voxels of the TFS dose spread array are scored "down-stream" of the primary interaction site than "up-stream".

The bulk of first scatter photons have been separated from the multiple scatter photons because of their different spatial distribution and magnitude of contribution to the total dose . Figures 106 and 107 have illustrated the relative contributions of primary, first scatter, and multiple scatter dose for 1.25 MeV and 5.0 MeV photons using EGS and MOCA Monte Carlo programs. The contribution of first scatter photons is almost an order of magnitude lower

than that of primary photons. The contribution of multiple scatter at this field size is less than one half that of first scatter at depths to 20 cm. Separating most of the first scatter from multiple scatter also allows a choice of optimal sizes for each type of dose spread array. Having a high spatial resolution when little dose is being deposited is not an effective use of computation time (89). The size of the TFS dose spread array and the voxel dimension of both the scatter dose spread arrays and the primary dose spread array is selected to compromise speed and accuracy. The more elements in the TFS dose spread array, the slower the convolution calculation. The TFS dose spread array voxel dimension can be made smaller than the RFMS dose spread array, reflecting its proximity and greater importance in contributing to the total dose. The TFS dose spread array is produced and stored for the same $\rho \cdot \ell$ values as the primary dose spread array whereas the RFMS dose spread array is stored for values of $\rho \cdot \ell$ from $1.0 g/cm^2$ to $5.0 g/cm^2$ in steps of $1.0 g/cm^2$. The TFS dose spread array may be truncated without compromising too much accuracy because most first scatter dose is deposited close to the primary interaction site (77). In order to take into account the scatter dose arriving at a field boundary from primary interactions at the opposite boundary, the total lateral size of the RFMS dose spread array must be at least twice that of the largest field in which the dose is to be calculated.

Figures 112 and 113 illustrate examples of the TFS and

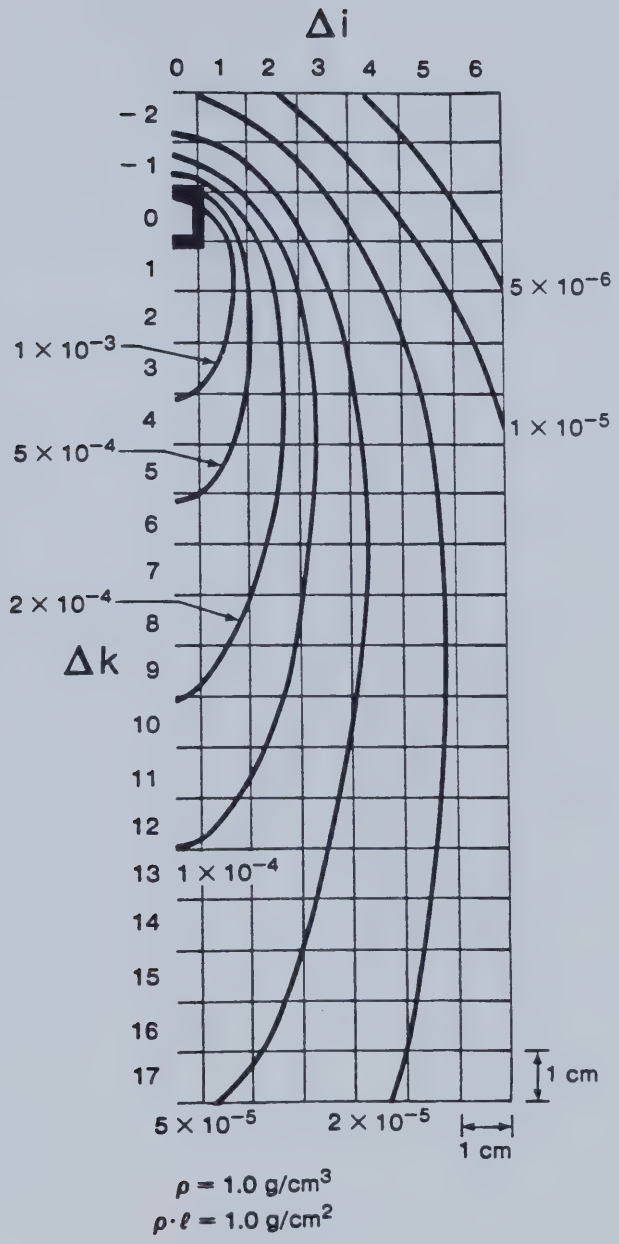

Figure 112. Truncated first scatter (TFS) dose spread array for 15 MV photons.

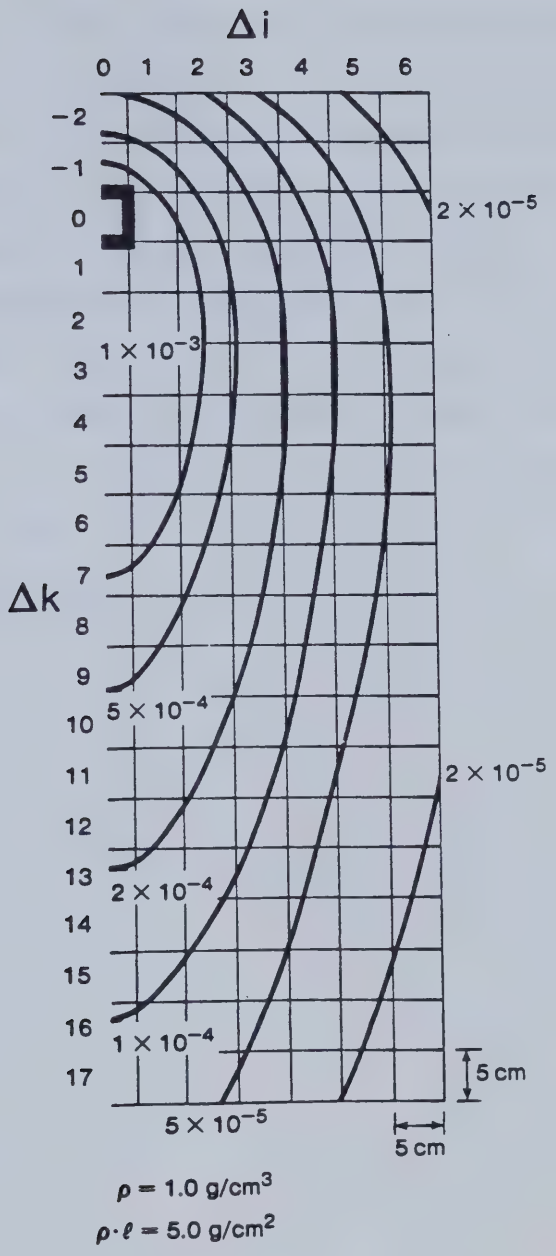

Figure 113. Residual first and multiple scatter (RFMS) dose spread array for 15 MV photons.

RFMS dose spread arrays, respectively. The TFS dose spread array has a $\rho \cdot \ell$ value of $1.0 g/cm^2$ and the RFMS dose spread array $\rho \cdot \ell$ value is $5.0 g/cm^2$. They are displayed as isodose curves. The energy deposited by scattered photons has been normalized to the same value as the primary dose spread array, namely to the collision fraction of the total charged particle energy released by primary photons. Therefore, the dimensionless numbers associated with the isodose lines represent the scatter dose per unit primary collision KERMA. The TFS dose spread array illustrated has a total width of 13 cm and a total height of 15 cm. Any first scatter photon energy not deposited within its boundary is included with the RFMS dose spread array.

7.4 Convolution Dose Calculation In A Homogeneous Phantom

The dose spread arrays can be viewed as the response throughout all the voxels in the phantom to a primary photon "impulse" occurring in one voxel. The dose spread arrays can, therefore, be used as the kernel in a convolution calculation to produce a 3-dimensional dose distribution. The dose contribution, DOSE CONTRIBUTION $(i+\Delta i, j+\Delta j, k+\Delta k)$ to a dose deposition voxel $i+\Delta i, j+\Delta j, k+\Delta k$ due to primary interactions at a voxel i,j,k in a homogeneous water phantom is illustrated in Figure 114 and given by (see Equation 7.2.4): *

$$\text{DOSE CONTRIBUTION } (i+\Delta i, j+\Delta j, k+\Delta k) = A(\rho \cdot \ell = \ell, \Delta i, \Delta j, \Delta k)\, K_c(\rho \cdot \ell = \ell, i, j, k) \qquad (7.4.1)$$

Equation 7.4.1 can be used to generate the absolute dose. However, usually only the relative dose distribution is required. If changes in the beam spectrum (or "hardening") is negliglible, $Kc(\rho \cdot \ell = \ell, i, j, k)$ may be replaced by the relative primary photon fluence:

$$\Phi'(i,j,k) = \frac{\Phi(i,j,k)}{\Phi(0,0,0)} \qquad (7.4.2)$$

* The density, ρ, in the equations of Section 7.4 and in the computer program, Volve.for, is taken to be the gravimetric density.

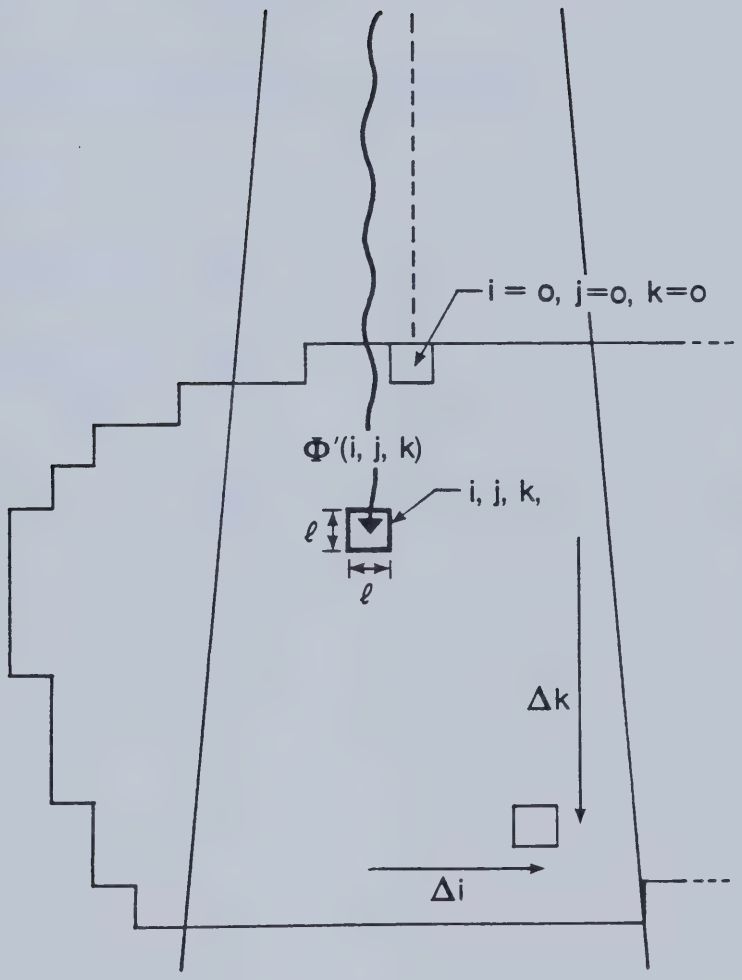

Figure 114. Illustration of the dose contribution at i+Δi, j+Δj, k+Δk due to primary photon interactions at i,j,k from the interaction point of view.

Table 20 Parameters For Determining $\tilde{\mu}$ For 15 MV X-Rays

Energy, $(h\nu_0)_n$ (MeV)	0.67	2.57	6.61	11.12
Fluence Weight, F_n	11	11	11	5
μ_n (cm^{-1})	0.0857	0.0439	0.0267	0.0173
$(\mu_{en}/\rho)_n$ (cm^2/g)	0.0326	0.0241	0.0176	0.0152

The relative fluence, $\Phi'(i,j,k)$, is the primary photon fluence at the interaction voxel normalized to the incident primary fluence at the central axis. For a parallel beam, $\Phi'(i,j,k)$ need only take into account the primary photon attenuation:

$$\Phi'(i,j,k) = \Phi'(i,j,0)e^{-\tilde{\mu}k} \qquad (7.4.3)$$

Where $\tilde{\mu}$ is the KERMA-weighted average attenuation coefficient and is calculated using:

$$\tilde{\mu} = \frac{-1}{k}\ell n\left[\frac{\sum_n F_n e^{-\mu_n k}(\mu_{en}/\rho)_n (h\nu_o)_n}{\sum_n F_n (\mu_{en}/\rho)_n (h\nu_o)_n}\right] \qquad (7.4.4)$$

The summation is over all the spectral components (9), where F_n is the relative weight of the spectral fluence component. The energy of the primary beam is $(h\nu_o)_n$. μ_n is the attenuation coefficient of the spectral component. Table 20 summarizes the parameters for the spectral components. Due to hardening, $\tilde{\mu}$ varies slightly as a function of depth. A constant 0.031 cm^{-1} was used. If the dose at very large depths is required, then the effective attenuation coefficient should be made a variable as a function of depth (i.e. $\tilde{\mu}(z)$). Figure 115 illustrates the value of $\tilde{\mu}$ as a function of depth. The value of $\tilde{\mu}$ agrees well with the 15 MV effective attenuation coefficients found from zero-area TMR data and transmission data (see Figure 116) (90-94). If

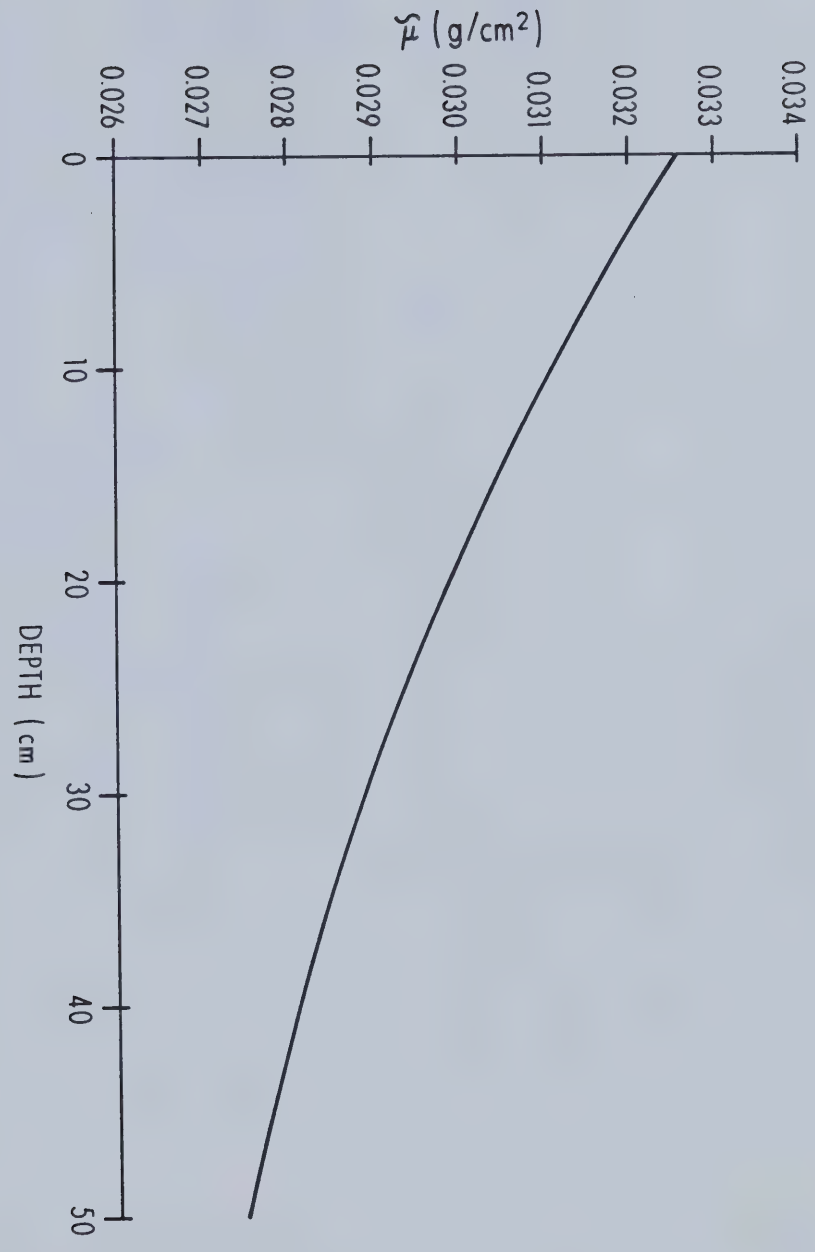

Figure 115. The variation of the effective attenuation coefficient as a function of depth. The parameters used to produce this graph are found in Table 20.

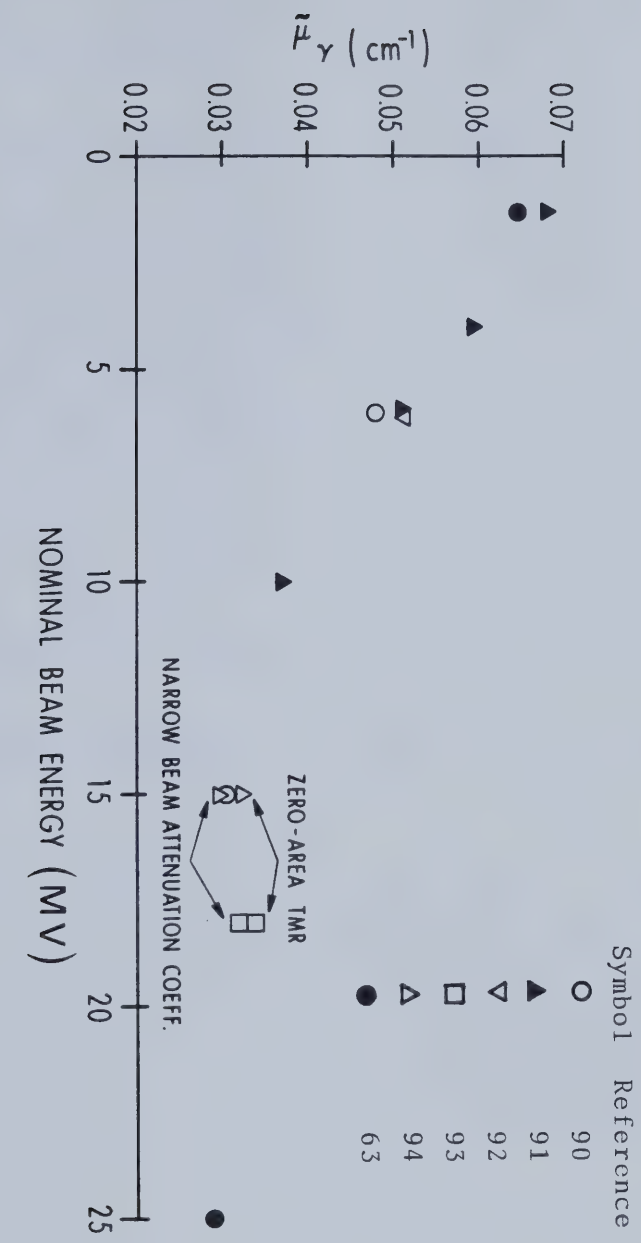

Figure 116. The variation of the measured effective attenuation coefficients as a function of nominal beam energy. This graph was produced from zero-area TMR and narrow beam attenuation experiments cited in the literature.

the beam is diverging, an inverse square reduction of the primary fluence must also be included:

$$\Phi'(i,j,k) = \Phi'(i,j,0)e^{-\tilde{\mu}(D-SSD)}\left(\frac{SSD+d_{max}}{D}\right)^2 \qquad (7.4.5)$$

Where, D, is the distance from the source to the interaction site along the primary ray. $\Phi'(i,j,k)$ can also account for the external contour of the patient (in which case the factor, SSD, in the argument of the exponential in Equation 7.4.5 would not be a constant) and for beam modifying devices such as shielding that alters the relative primary fluence, but does not alter the dose spread arrays. Including the dose spread array, Equation 7.4.1 now becomes:

$$\text{DOSE CONTRIBUTION}(i+\Delta i,j+\Delta j,k+\Delta k) \propto \Phi'(i,j,k)A(\rho\cdot\ell=\ell,\Delta i,\Delta j,\Delta k) \qquad (7.4.6)$$

The convolution of the dose spread arrays with the relative fluence can proceed in two different ways, called the "interaction point of view" and the "dose deposition point of view". In general the calculation may be done by either method, but there are circumstances where one approach is more efficient.

In the interaction point of view, the macroscopic beam is composed of a set of contiguous pencil beams each of which is followed through the phantom to see where the primary interactions occur. The dose spread array contributions throughout the phantom are summed for all such pencil beams. The dose distribution in the interaction

point of view is:

$$DOSE\ (i+\Delta i,j+\Delta j,k+\Delta k) \propto \sum_i \sum_j \sum_k [\Phi'(i,j,k)\ A(\rho\cdot\ell=\ell,\Delta i,\Delta j,\Delta k)] \qquad (7.4.7)$$

Where the i,j,k summation is over all interaction voxels; i.e. those voxels inside the phantom and the field boundary. Depending on the region of interest, the dose outside the beam boundary can also be computed.

Figure 114 illustrates the calculation of dose using the interaction point of view. The relative fluence is calculated for each point along a pencil beam (inside square brackets in Equation 7.4.7) by following the primary pencil beams through the phantom. When a beam blocking device such as a compensator is introduced in the beam, some of the primary pencil beams are affected. The interaction point of view can determine the effect of the changed primary pencil beams on the dose throughout the phantom without recalculating the entire beam. Appendix 11 lists a convolution program, Volve.for, which calculates the dose using the interaction point of view.

The interaction point of view gives the dose throughout a region of interest. Often only the dose at a few voxels is desired. In this case, the dose in these select voxels is calculated using the dose deposition point of view.

In a homogeneous, unbounded phantom there is a geometrical reciprocity between the primary interaction and dose deposition voxels.* Even though the dose spread arrays were produced to describe the transport and absorption of

dose throughout a phantom due to primary interactions at a voxel, they also describe the transport to and absorption at a dose deposition voxel due to an equal magnitude of primary interactions throughout the phantom. This is essentially the same principle as the source-target reciprocity used in health physics to calculate the organ dose due to internal isotopes (95).

Figure 117 illustrates the use of the dose spread arrays from the dose deposition point of view. The dose spread arrays now represent the dose deposited in the dose deposition voxel normalized to the collision KERMA produced in the interaction voxels. The dose deposition point of view calculation sums the dose contribution at the dose deposition voxel due to primary interactions throughout the phantom. The dose at a point I,J,K is given by:

$$DOSE(I,J,K) \propto \sum_{\Delta i}\sum_{\Delta j}\sum_{\Delta k} \Phi'(I-\Delta i, J-\Delta j, K-\Delta k) A(\rho \cdot \ell = \ell, \Delta i, \Delta j, \Delta k) \qquad (7.4.8)$$

If the dose at only a few voxels is required, the dose deposition point of view is far more efficient. For example, the dose deposition point of view should be used when determining the dose along the central axis or along transverse profiles. The dose deposition point of view is mathematically equivalent to taking the convolution using

* This reciprocity only rigorously applies to the RFMS dose spread array when the phantom is infinite.

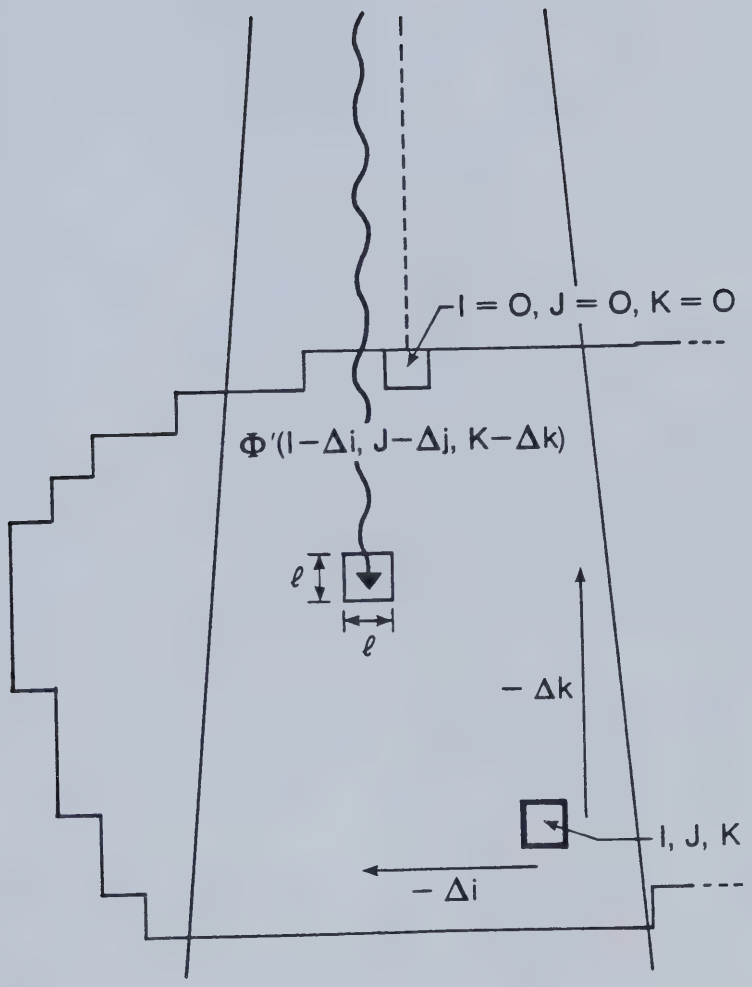

Figure 117. Illustration of the contribution of dose from primary photon interactions at I-Δi, J-Δj, K-Δk arriving at I,J,K using the dose deposition point of view.

the serial product (96). A disadvantage to calculating a large dose distribution using the dose distribution point of view is that a large array for the relative fluence must be pre-calculated and stored before Equation 7.4.8 can be used.

Equations 7.4.6, 7.4.7 and 7.4.8 do not specify which type of dose spread array is being convolved. The same general equations apply to all the dose spread arrays, except the number of terms in the summation and the value of the relative fluence will depend on the voxel dimension of the dose spread array.

The convolution method does not take into account the dose due to contamination. The measured contamination dose was added to the calculated dose. In Volume 1 it was found empirically that the magnitude of the contamination dose depends on five parameters; the 2-dimensional position from the central axis, the radiological depth in the phantom, and the width, a, and length, b, of the field. The amount of contamination is given by:

$$C(x,y,z,a,b) = G(\tilde{\rho}\cdot z)\, c\sqrt{a\cdot b}\; e^{-2x^2/a^2}\; e^{-2y^2/b^2} \qquad (7.4.9)$$

The amount of contamination as a function of radiological depth was found from Figure 63 inside the field and from Figure 31 outside the field. The mean density, along the primary ray, from the surface of the phantom to the calculation point is $\tilde{\rho}$. These graphs have been included in the form of a look-up table, $G(\tilde{\rho}\cdot z)$. The dependence of contamination on field width was found to be linear. The

constant of proportionality, c, was 1.0 %/cm for a 15 MV photon beam. The effective field size is assumed to be the square root of the product of the field dimensions. Equation 7.4.9 assumes a Gaussian dependence of the contamination on the distance from the the central axis.

Figure 118 illustrates the measured and calculated tissue-maximum-ratio (TMR) for a 15 MV beam as a function of depth in a homogeneous water phantom along the beam central axis for field sizes of 6 cm x 6 cm and 20 cm x 20 cm. The calculated TMR curve was obtained by assuming the beam was parallel and had no inverse-square reduction of the fluence with depth, as required for comparison with measured TMR values. The agreement between the measured and calculated dose is better than 1 % beyond a depth of d_{max} and within 10 % in the build-up region. Figure 119 illustrates the percent depth-dose curves for a 6 MV x-ray beam for various field sizes. The agreement is within 1 % beyond d_{max} for 10 cm x 10 cm and 20 cm x 20 cm fields and within 3 % for a 4 cm x 4 cm field.

Figure 120 illustrates dose profiles at d_{max} for field sizes of 10 cm x 10 cm and 30 cm x 30 cm for a 15 MV beam. The fluence profile at the phantom surface was assumed to be uniform inside the beam boundary and zero outside the beam boundary. This assumption appears to be adequate for the 10 cm x 10 cm field, but does not account for the "horns" in the larger field profile. The fall-off in dose near the beam boundaries due to lateral electronic disequilibrium, not geometrical penumbra, is accounted for. Figure 121

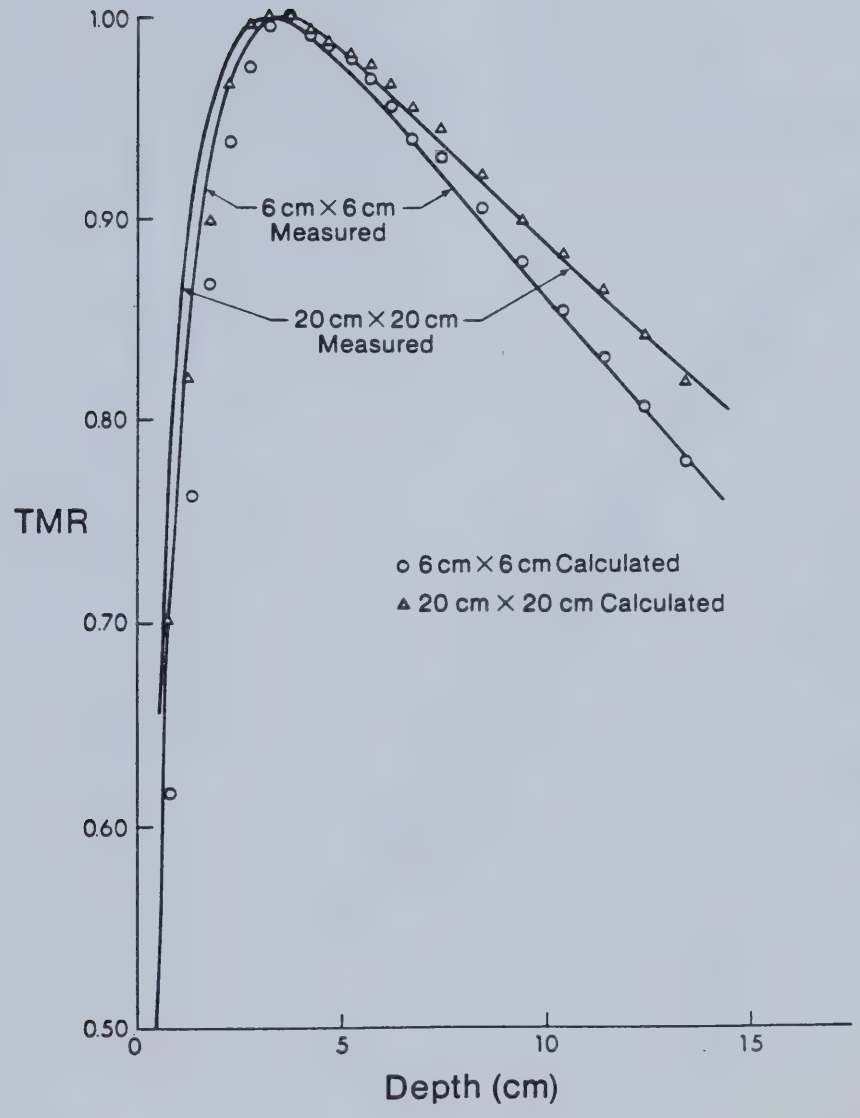

Figure 118. Measured and calculated TMR's for a 15 MV beam as a function of depth along the central axis in a homogeneous water phantom.

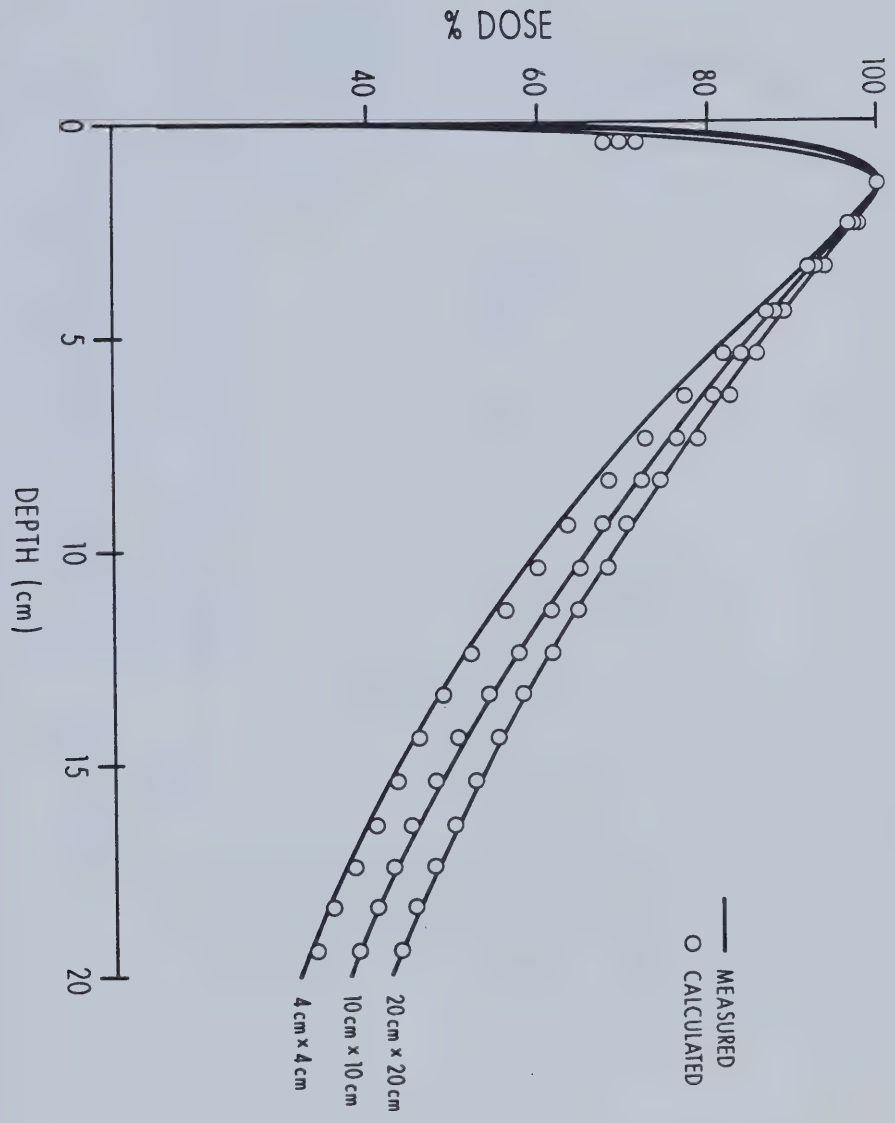

Figure 119. Measured and calculated percent depth-dose data for a 6 MV beam as a function of depth along the central axis in a homogeneous water phantom.

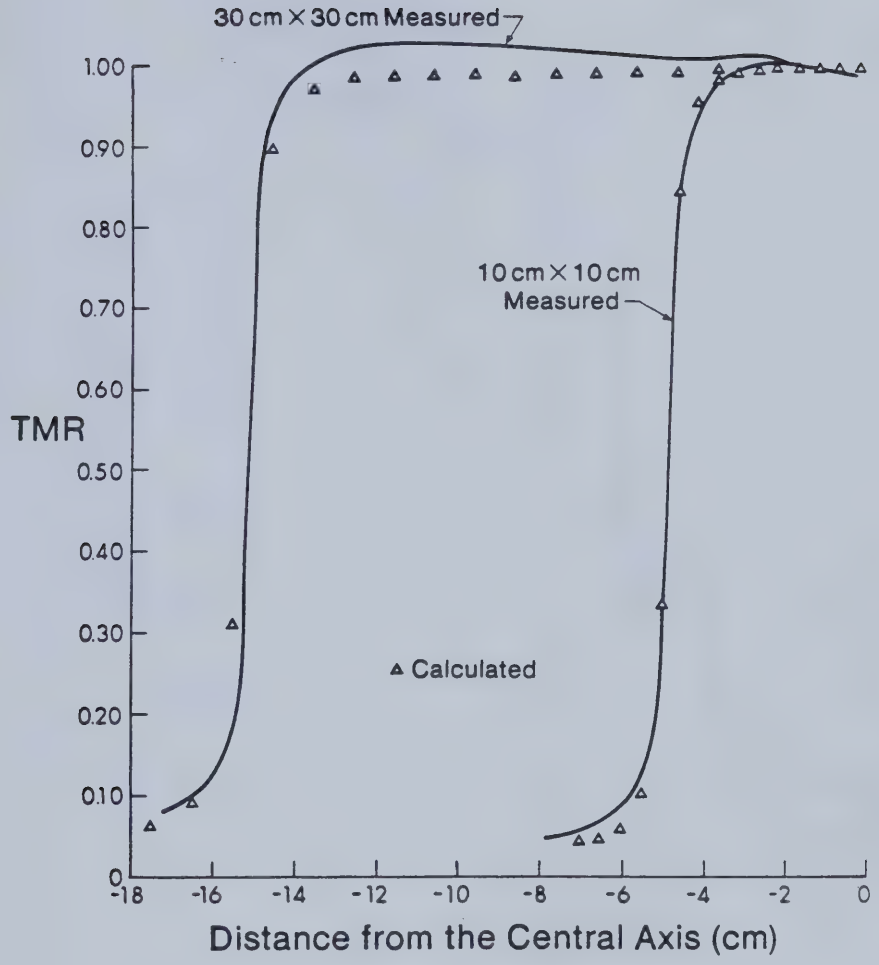

Figure 120. Measured and calculated dose profiles at d_{max} for a 15 MV beam.

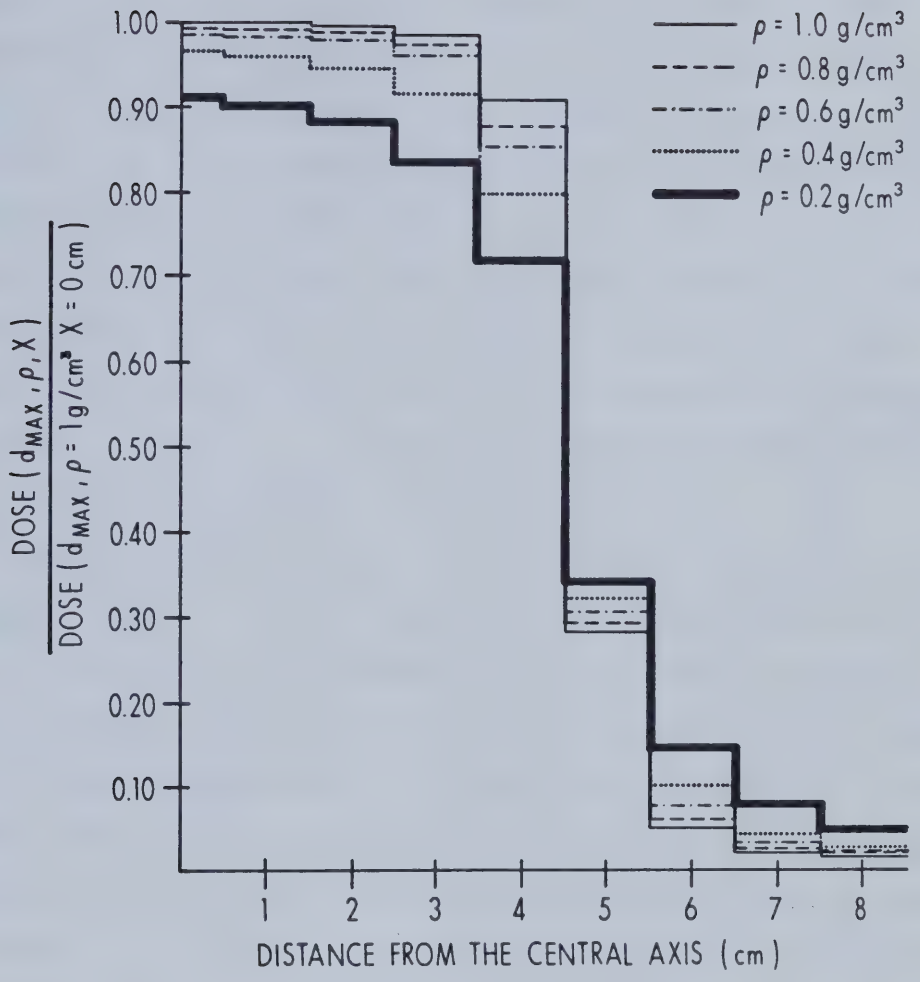

Figure 121. Dose profiles at d_{max} in homogeneous phantoms with various densities. The dose is normalized to the central axis dose in a unit density phantom.

illustrates the dose profiles in homogeneous phantoms with various densities. The dose is normalized to the dose in a unit density phantom at the central axis. The smaller the density, the smaller the dose inside the field. This is especially pronounced near the field boundary. The dose outside the field is greater for smaller densities. This effect has been observed by Kornelsen and Young for 10 MV x-rays (80). It is due to the enhanced range of charged particles in low-density materials. The reduced dose inside the field is mainly due to the charged particles migrating inward from outside the field and the increased dose outside the field is due to an increased number of charged particles "streaming" there from inside the field.

The method can be used to determine the dose in a wedged field. It was assumed that the wedge could be described mathematically as a linear (or "ramp") increase in the primary fluence from one side of the beam to the other. The primary fluence profile is shown in Figure 122 along with the fluence calculated for the 45° and 60° wedges (defined by the angle the isodose lines makes with a line parallel to the phantom surface at some specified depth) supplied by the accelerator manufacturer. The wedge material is steel with an effective attenuation coefficient of 0.284 cm^{-1} (97). The closest fluence profile curve to the linear profile curve is for a 60° wedge. Figure 123 illustrates the calculated isodose curves for a 15 MV beam with a fluence profile as shown in Figure 122 and the measured isodose curve for a 60° wedge. A diverging beam

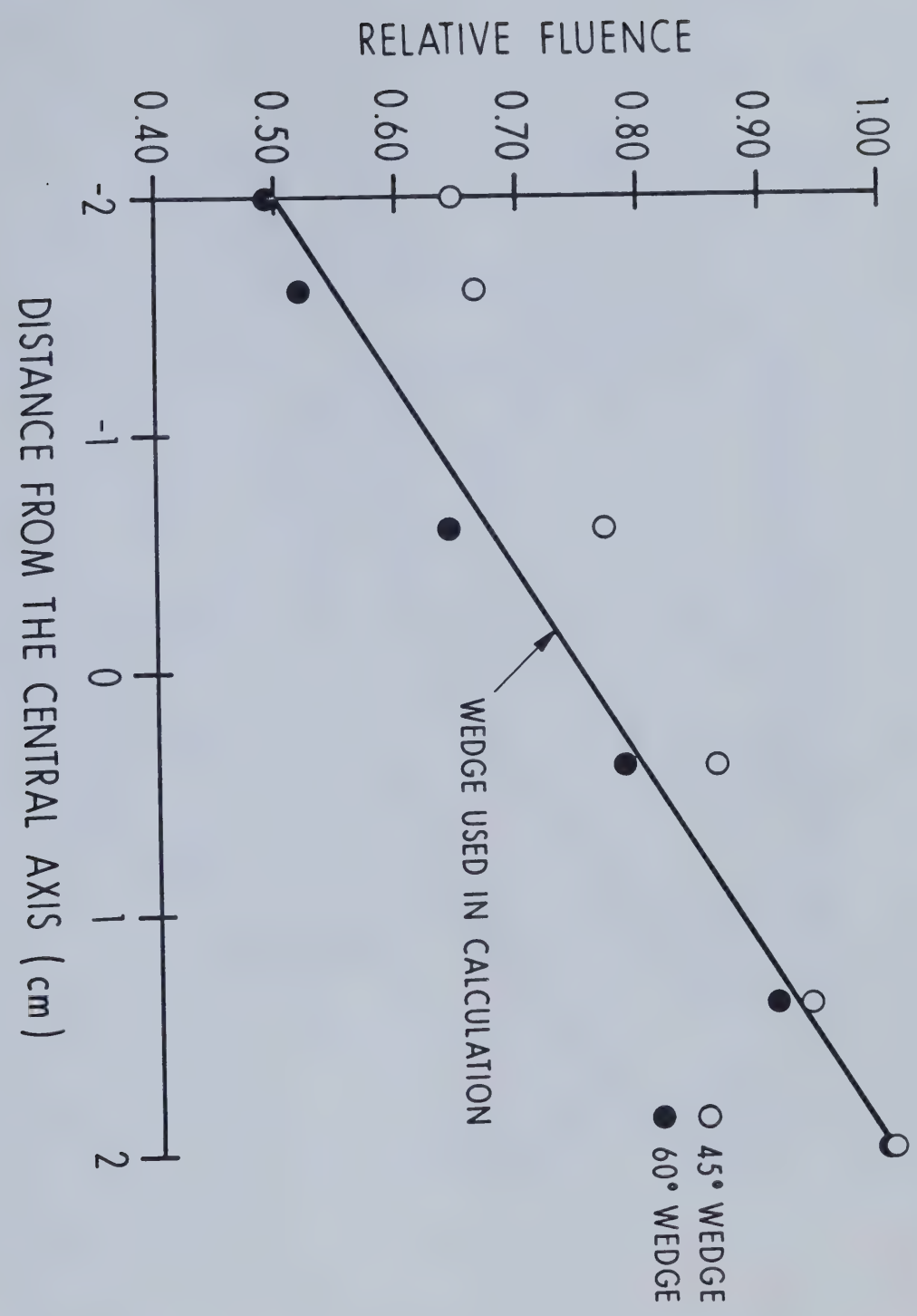

Figure 122. The relative primary fluence profile for 15 MV beam wedges and the fluence profile used to obtain the calculated isodose curve in Figure 123.

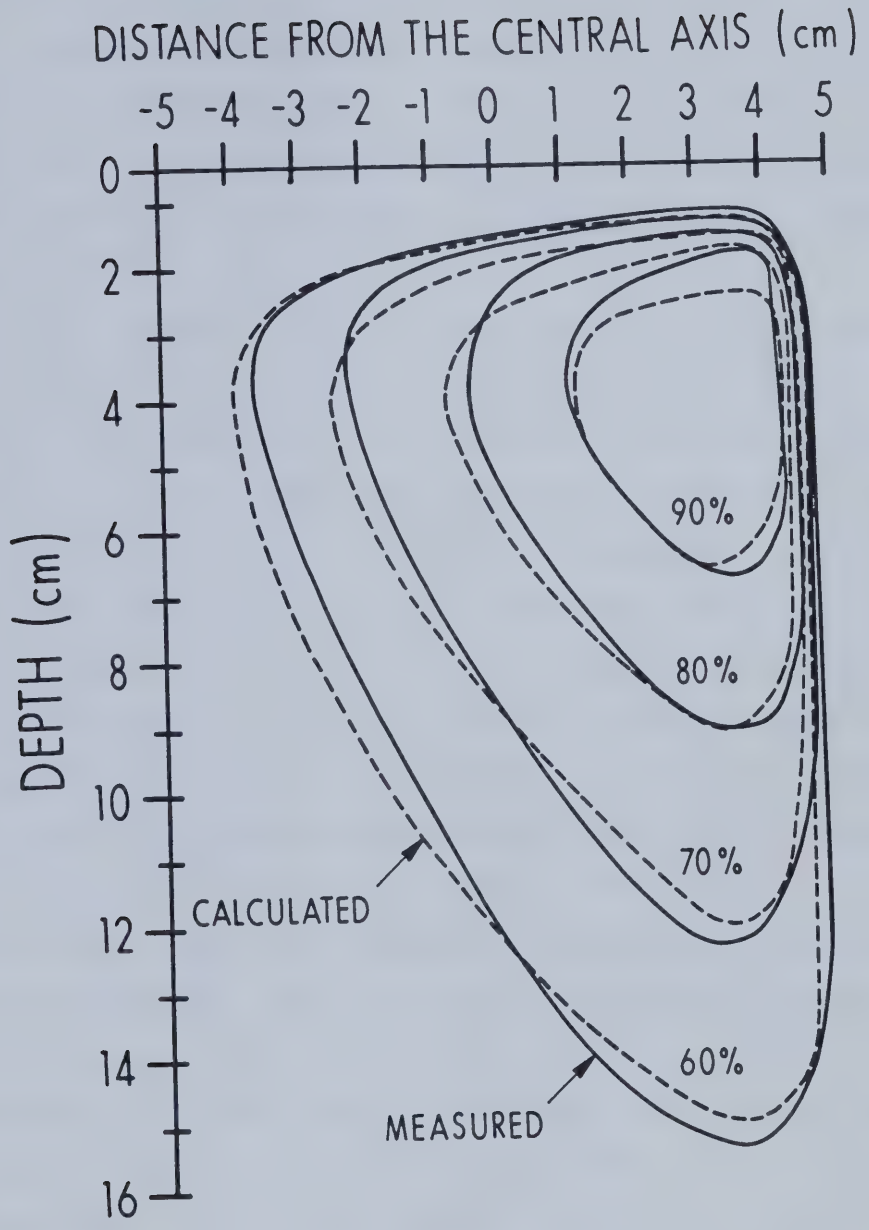

Figure 123. The calculated isodose curve for the fluence profile shown in Figure 122 and the measured isodose curve for a 60^{o} wedge for a 15 MV beam.

was used with a field size of 10 cm x 10 cm defined at the surface of the phantom which was 100 cm from the source. The calculation predicts the characteristic reversal of the slope of the isodose lines in the build-up region. The agreement of the position of the isodose lines is good and might improve by a more closely matched fluence distribution.

The method can also take into account irregularly-shaped fields. Figure 124 illustrates the effect on the dose profile at a depth of 5 cm when a shield is placed in the 15 MV beam. The shield consisted of a bar of cerrobend (lead-tin-bismuth compound) extending completely across the field in a transverse direction to the profile. The width of the bar was 1.5 cm and it had a thickness of 8.5 cm. The primary fluence transmission through the cerrobend was calculated to be 3.1 %. Figure 124 also illustrates a calculation of the profile assuming the primary dose is deposited locally. The measured profile agrees best with the calculation using non-local primary energy deposition. This illustrates that charged particles are streaming into the region under the shield. Also illustrated in Figure 124 is a calculation of the dose using a Clarkson scatter summation technique (98). This involves finding the scatter by summing contributions from the unshielded portion of the field and then adding this to the primary dose under the shield, which is equal to the transmission factor (in this case 0.031) multiplied by the zero-area TMR. This method predicts about one-half of the

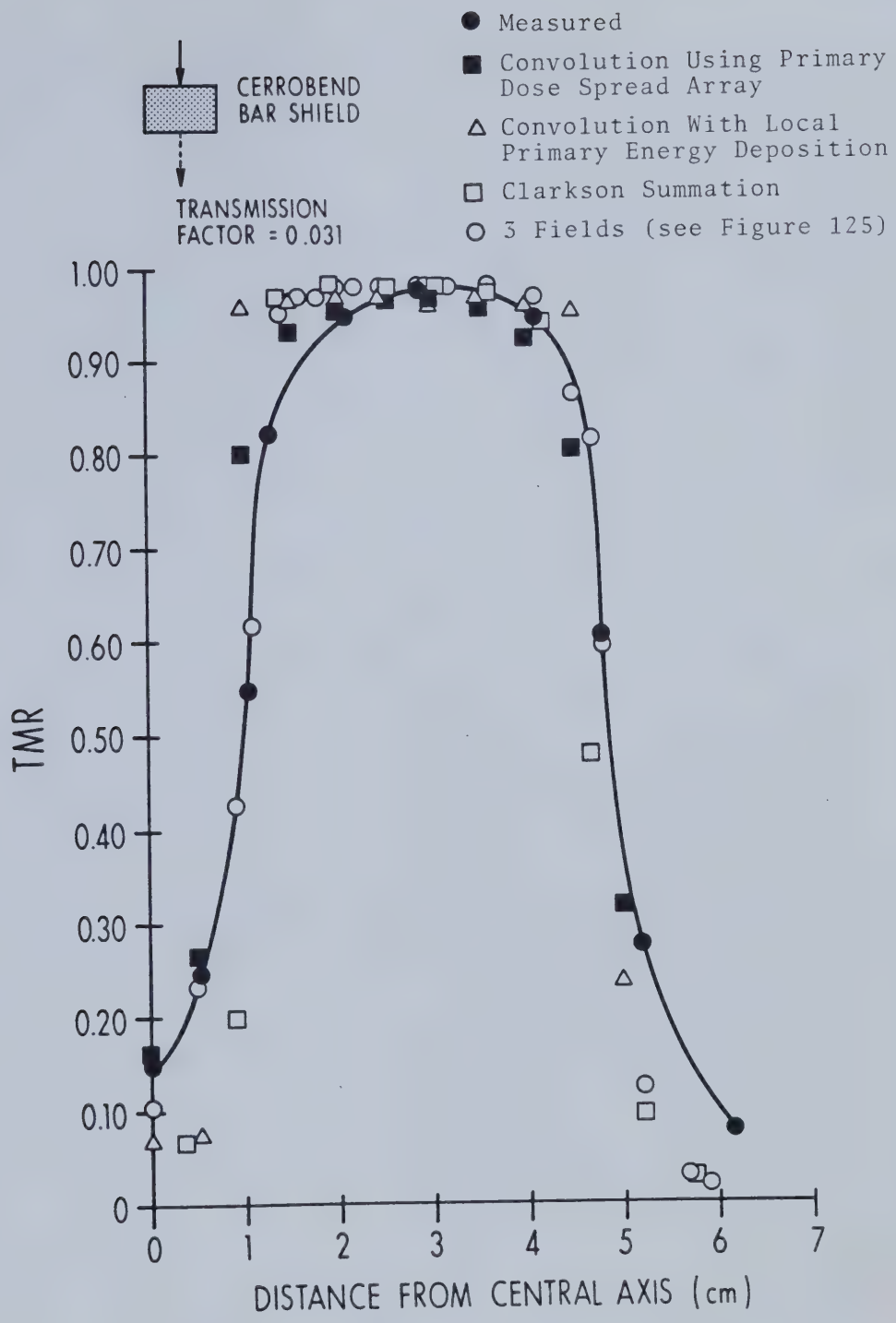

Figure 124. The measured dose profile at a depth of 5 cm when a shield is placed in the 15 MV beam. The relative position of the shield is indicated. Also shown are various calculated dose profiles for this situation.

dose under the shield compared to measured data or the convolution method. This is because this method assumes a total absence of primary dose under the shield being transported from the unshielded portion of the field. This method, which has an underlaying assumption that the primary energy is deposited locally, agrees well with the convolution method in which local primary energy deposition has been assumed here temporarily for comparison (this is achieved by replacing the calculated primary dose spread arrays with an array in which the interaction voxel has a value of 1.0 and all other voxels have values of zero).

The finding in Figure 121 that some of the "penumbra" is due to electronic disequilibrium suggests a simple calculation method for this shield based on measured dose distributions. Figure 125 illustrates that the bar shield can be represented by three fields. The middle field represents the radiation transmission through the shield. The fields have to be tilted so that neighboring field boundaries remain parallel. The relative weight of the shielded field compared to the unshielded field is equal to the transmission factor. Figure 124 also illustrates the calculated dose using this calculation method. It provides better agreement with the measured dose. The shield is acting like a collimator; it is shielding the fluence , but it does not prevent charged particles generated in the unshielded region from being transported to the shielded region.

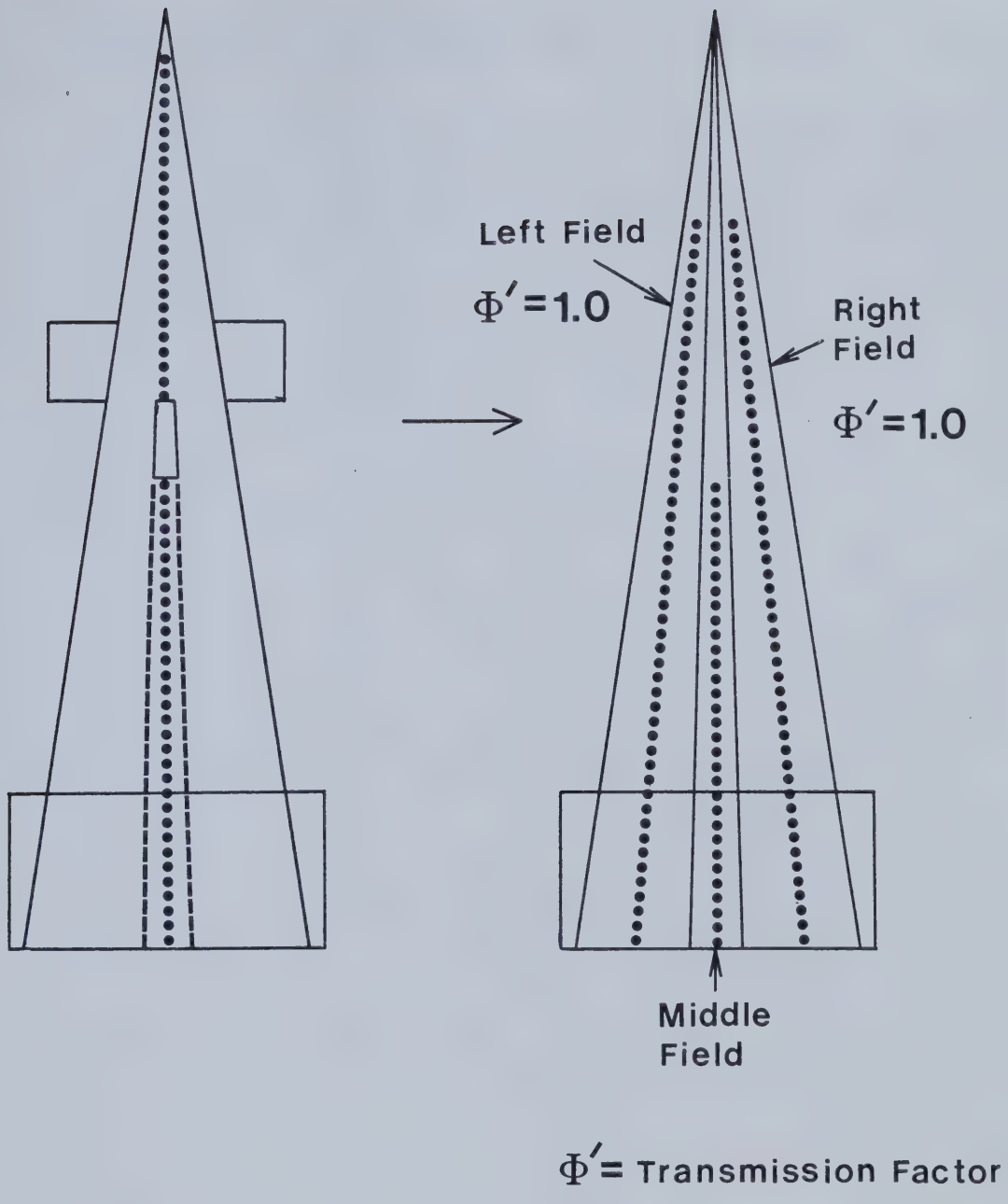

Figure 125. The bar shield represented by three fields. The central axes of the fields are shown with dotted lines. The results of the calculation with this representation is shown in Figure 124.

7.5 Extension to Heterogeneous Media

Charged particle transport through a heterogeneous medium is much more complex. To be rigorous, the primary dose spread arrays would have to be generated for each heterogenous situation that could be encountered. The number of possible combinations is enormous so that an acceptable approximation is necessary to take advantage of data stored in the dose spread arrays generated for homogeneous phantoms of different densities.

Figures 95 and 97 clearly illustrated that in a low-density medium, charged particles migrate a greater distance from the primary interaction site. This must be taken into account when describing the transport of charged particles from a unit density medium such as muscle into a low-density region such as lung. Figures 126 and 127 illustrate a MOCA Monte Carlo generation of the primary, first scatter and multiple scatter dose components for 6 MV x-rays in homogeneous and heterogeneous medium, respectively. The natural logarithm of the percentage of dose normalized to the maximum dose is plotted as a function of depth. The primary component decays approximately exponentially with depth beyond d_{max} in both the unit-density and low-density regions, however, the decay constant is smaller in the low-density medium. The multiple scatter dose has an extended build-up in the unit-density medium. It does not decay exponentially in the low-density medium. Instead, the multiple scatter component first

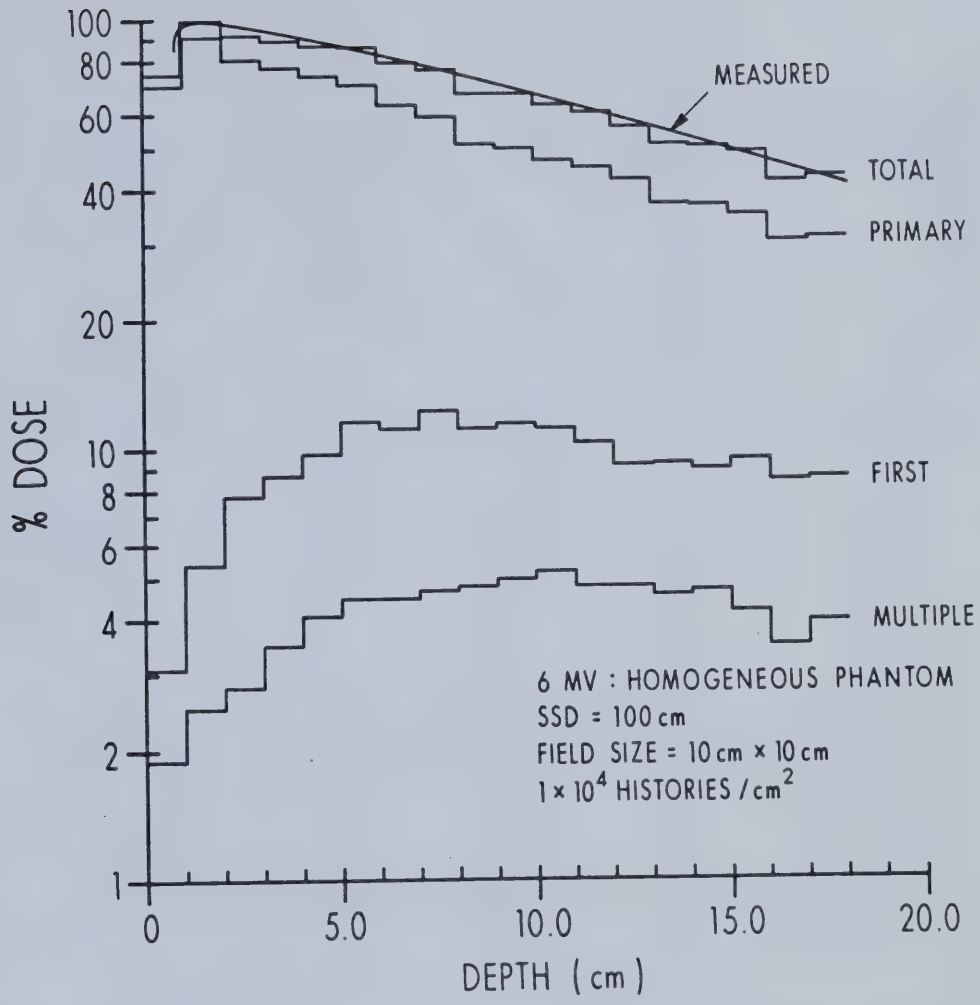

Figure 126. Components of the percent depth dose in a homogeneous water phantom predicted by MOCA for a 6 MV beam. The measured total dose is also shown for comparison.

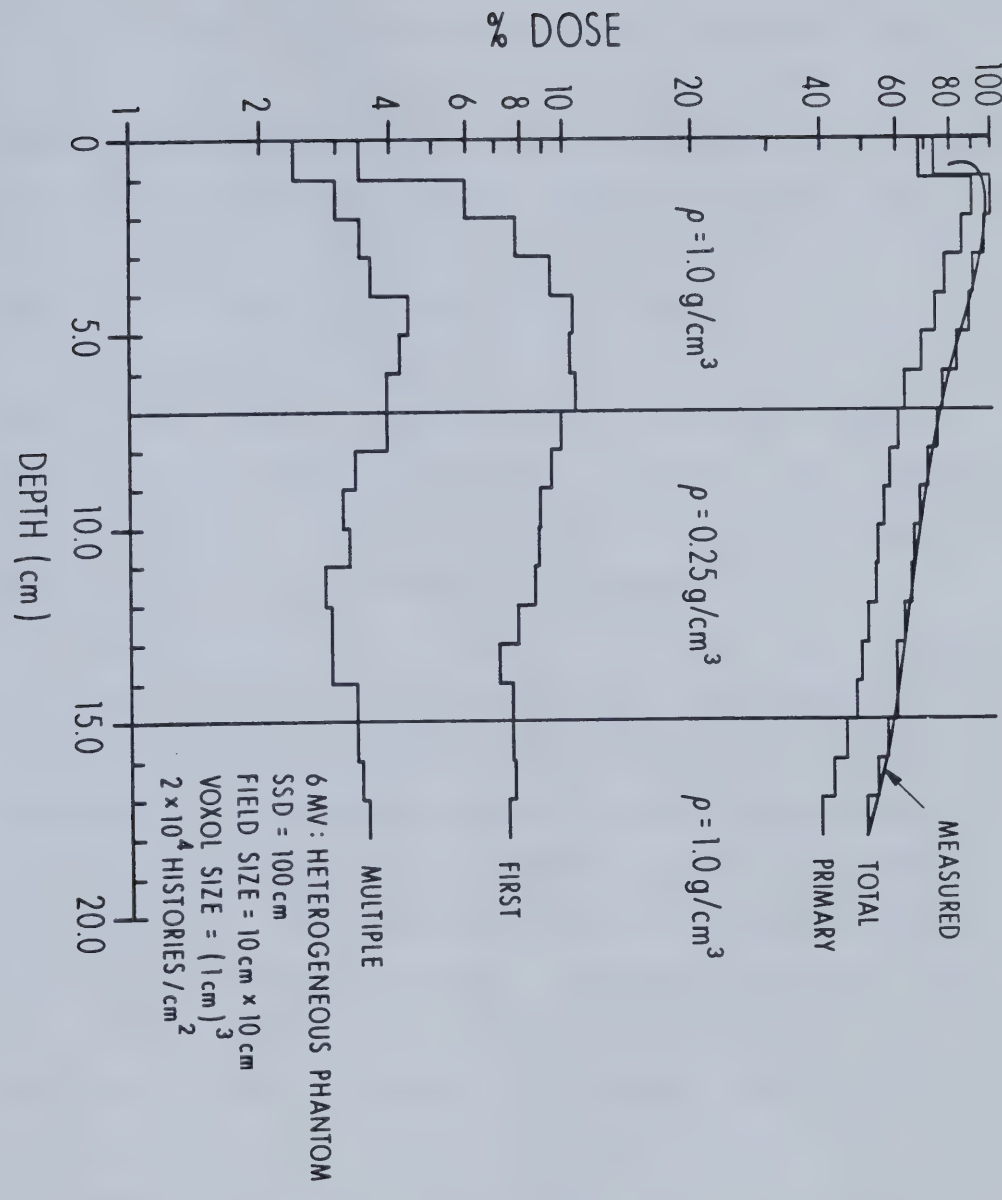

Figure 127. Components of the percent depth dose in a heterogeneous phantom (with water chemical composition) predicted by MOCA for a 6 MV beam. The measured total dose is shown for comparison.

decreases with depth after the first interface (until 10-14 cm beneath the surface) and then increases before the second interface. The first scatter dose has features of both the primary and multiple scatter components. It has a build-up in the unit density material similar to the multiple scatter dose but has an approximate exponential reduction in dose in the low-density material.

The extended build-up in the scatter dose seen in Figures 126 and 127 is reflected by the large longitudinal extent of their dose spread arrays. However, the behavior of the first scatter dose with depth in the heterogeneous medium resembles the primary dose component.

The extension of O'Connors theorem for charged particles set-in-motion suggests that range scaling may be used to approximate charged particle dose spread arrays in heterogeneous phantoms. The dose spread arrays stored for various values of $\rho \cdot \ell$ were, therefore, used. The spatial resolution of the dose calculation, ℓ, is chosen and fixed at the start of the calculation. As shown in Figure 128, the average density, $\tilde{\rho}$, between the interaction and dose deposition sites is found. The array value for the location, $\Delta i, \Delta j, \Delta k$ in a homogeneous phantom with the same $\tilde{\rho} \cdot \ell$ value is found by interpolating between dose spread arrays at fixed $\rho \cdot \ell$ values. Linear interpolation is sufficient because the array values vary relatively slowly as a function of $\rho \cdot \ell$.

There are many algorithms for finding the equivalent homogeneous density "environment" between the interaction and

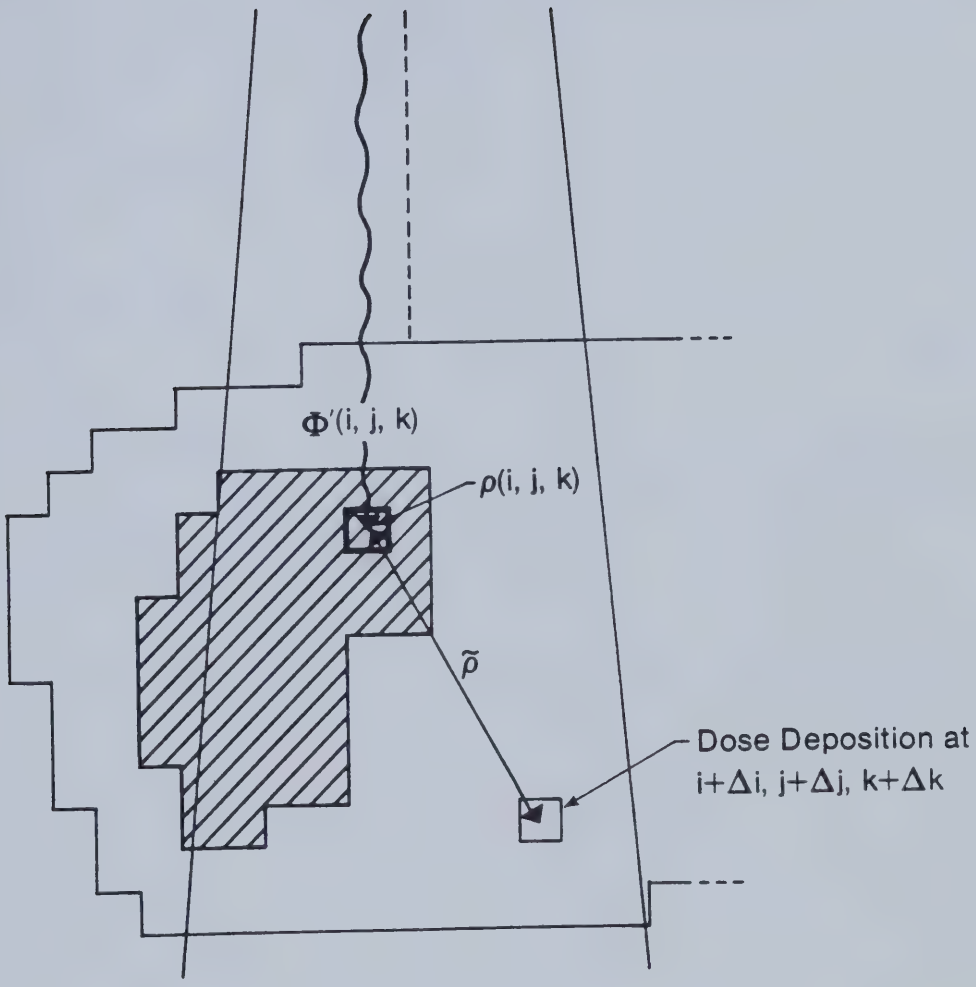

Figure 128. Determination of the average density between the interaction and dose deposition voxels.

dose deposition sites. The simplest, conceptually, is "ray-tracing". Samples of density are taken at evenly spaced intervals between these voxels. Figure 129 illustrates the procedure schematically. Suppose that the number of intervals is N. The number of samples is N+1 (including the beginning and end of the path). The length of each interval in the Cartesian directions is $\delta i, \delta j, \delta k$ where:

$$\delta i = \Delta i/N \tag{7.5.1}$$

$$\delta j = \Delta j/N \tag{7.5.2}$$

$$\delta k = \Delta k/N \tag{7.5.3}$$

The average density is given by:

$$\tilde{\rho} = [f_o \rho(i,j,k) + \sum_{n=1}^{N-1} \rho(i+n\delta i, j+j\delta j, k+n\delta k) + f_N \rho(i+\Delta i, j+\Delta j, k+\Delta k)]/N \tag{7.5.4}$$

The weights of the first and last voxel are f_o and f_N, respectively. These weighting factors are usually set equal to 0.5 because the mean position of charged particles set-in-motion is in the middle of the interaction voxel.

Interpolating to get a dose spread array valid for an average density between the interaction and dose deposition sites, $\tilde{\rho}$, implies that it has been normalized to the total amount of energy released in an interaction voxel of the

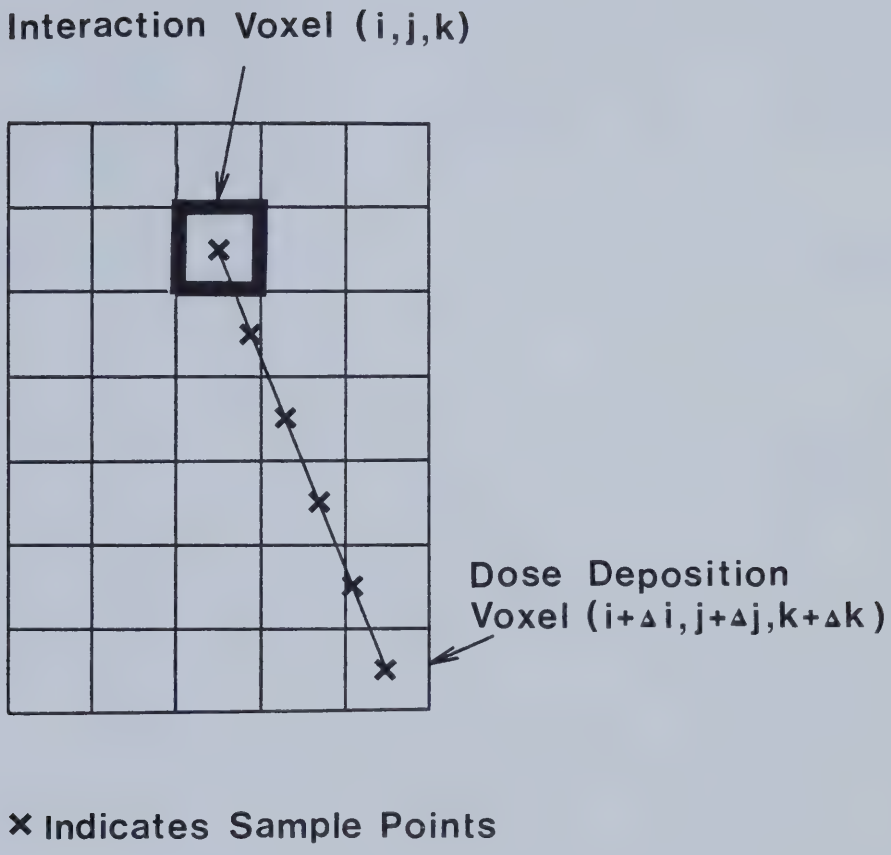

Figure 129. Ray tracing is performed by sampling the density between the interaction and dose deposition voxels.

same density. However, the density of the interaction voxel, ρ (i,j,k), in a heterogeneous phantom, is generally not the same as the average density between the interaction and dose deposition voxel. The primary dose contribution to a dose deposition voxel, due to primary interactions at an interaction voxel of density $\rho(i,j,k)$ when the average density between these voxels is $\tilde{\rho}$, is given by:

$$\text{DOSE CONTRIBUTION}(i+\Delta i,j+\Delta j,k+\Delta k) \propto \Phi'(i,j,k)\,\frac{\rho(i,j,k)}{\tilde{\rho}}\,Ap(\tilde{\rho}\cdot\ell,\Delta i,\Delta j,\Delta k) \qquad (7.5.5)$$

The factor ρ (i,j,k)/ $\tilde{\rho}$ takes into account the different amount of kinetic energy released in the heterogeneous interaction voxel compared to the amount set in motion in the interpolated homogeneous voxel of density, $\tilde{\rho}$. Otherwise, the convolution is carried out in the same manner as in a homogeneous phantom. Therefore, this procedure avoids the need to first compute the dose in water and then calculate an "inhomogeneity correction" separately.

If the phantom is homogeneous, the factor $\rho(i,j,k)/\tilde{\rho}$ in Equation 7.5.5 becomes 1.0 and the equation simplifies to Equation 7.4.6. In any case, Equation 7.5.5 can be simplified to two terms. $\rho(i,j,k)$ depends only on the interaction voxel and $\tilde{\rho}$ depends on the average path density. Therefore, Equation 7.5.5 becomes:

$$\text{DOSE CONTRIBUTION}(i+\Delta i,j+\Delta j,k+\Delta k) \propto \Phi''(i,j,k)\,Ap'(\tilde{\rho}\cdot\ell,\Delta i,\Delta j,\Delta k) \qquad (7.5.6)$$

Where:

$$\Phi''(i,j,k) = \Phi'(i,j,k)\rho(i,j,k)$$

(7.5.7)

$$Ap'(\tilde{\rho}\cdot\ell,\Delta i,\Delta j,\Delta k) = \frac{Ap(\tilde{\rho}\cdot\ell,\Delta i,\Delta j,\Delta k)}{\tilde{\rho}}$$

(7.5.8)

The TFS dose spread array may be range-scaled using the same algorithm. In fact, range scaling the TFS dose spread array gives the exact correction. This is because a first scatter photon interacting at the dose deposition voxel could not have interacted anywhere other than along the path between the primary interaction and dose deposition voxels. Since the primary dose spread array and the TFS dose spread array are stored for the same values of $\rho\cdot\ell$, the primary and TFS dose spread arrays may be combined where they coincide spatially. The TFS dose spread array need only be dealt with separately if it extends beyond the border of the primary dose spread array.

Equations 7.5.5 and 7.5.6 have two implicit assumptions;

1) charged particles only travel on the straight-line path or "ray" between the interaction and dose deposition sites.

2) each portion of the path between the interaction and dose deposition sites has an equal influence in the transportation process.

Both of the above assumptions are, strictly-speaking, untrue. Charged particles interact and scatter almost

continuously so they can travel on any path between the interaction and dose deposition sites with only the constraint that the overall distance travelled is less than the maximum possible pathlength or "range". Charged particle scattering between two points is a highly complex process which cannot be described exactly by an average density. However, the most probable of any path is the direct one between the interaction and dose deposition sites. Therefore, the assumptions should be viewed instead as a first-order approximation to the solution of charged particle transport.

The validity of the approximations were tested by computing primary dose spread arrays directly using the Monte Carlo method for a variety of water-like heterogeneous phantoms to simulate transport across tissue-lung, lung-tissue and air gaps. Figure 130 illustrates, schematically, the phantom and the position of the interaction voxel (the voxel with bold borders) in the phantoms that were tested. Dose spread arrays generated in the heterogeneous phantom from the Monte Carlo method were compared to the calculated dose spread arrays for a heterogeneous phantom using:

$$A^{het}_{p+1st}(\Delta i,\Delta j,\Delta k) = \frac{\rho(i,j,k)}{\tilde{\rho}} A_{p+1st}(\tilde{\rho}\cdot\ell,\Delta i,\Delta j,\Delta k) \qquad (7.5.9)$$

Where $A^{het}_{p+1st}(\tilde{\rho}\cdot\ell,\Delta i,\Delta j,\Delta k)$ is the primary and TFS dose spread arrays combined. Tables A to I in Appendix 12 compare the results of the two calculations. The dose

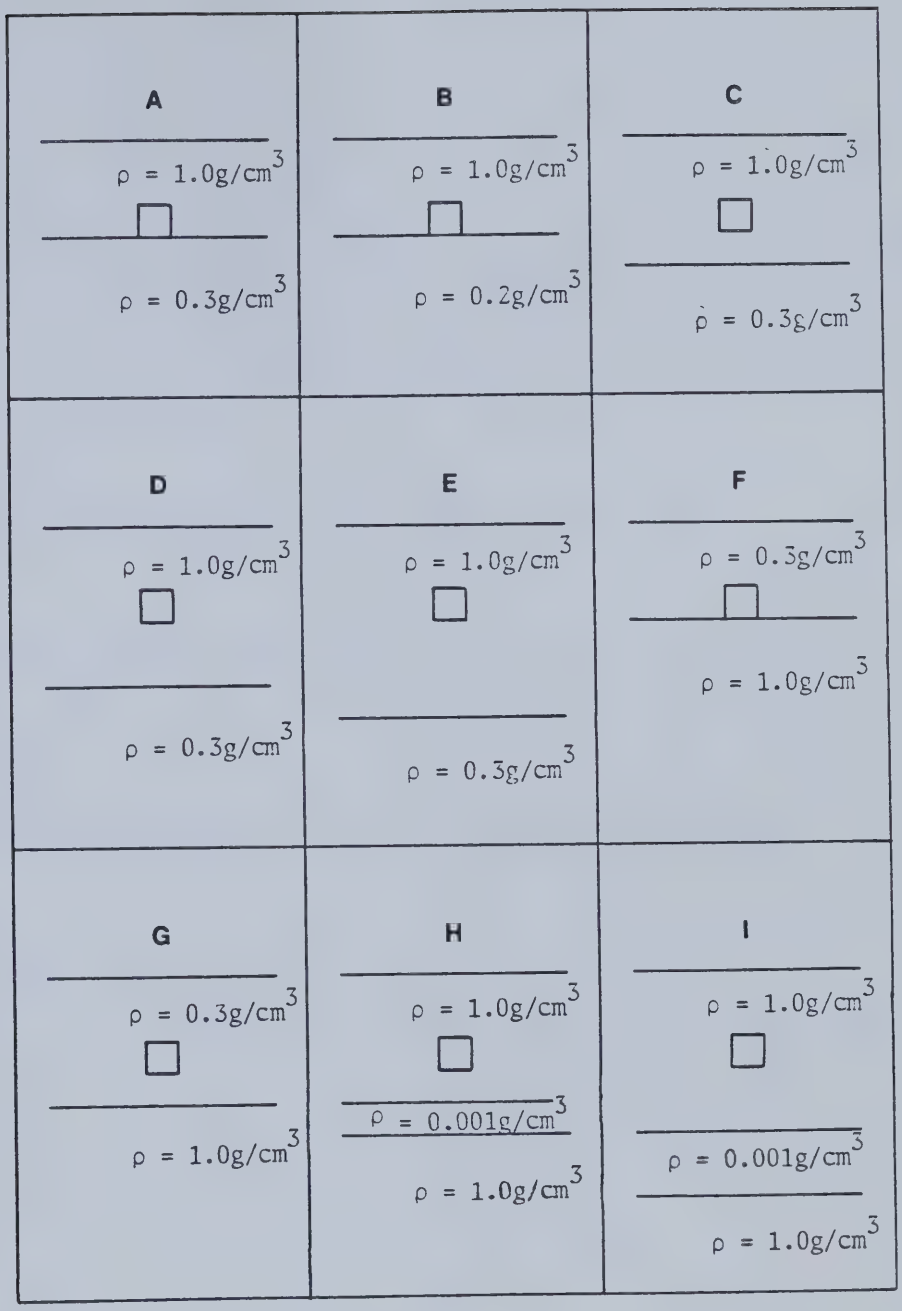

Figure 130. Schematic representation of the slab phantoms tested to verify the approximations used in determining the dose in heterogeneous phantoms. The interaction voxel is shown as a square. The results are found in Appendix 12.

spread arrays are in close agreement with respect to the range and absolute value. The maximum deviation between the two values occurs near the heterogeneity interface. A check was also made to see if the method chosen to find the dose spread arrays in Equation 7.5.9 conserved energy. Equation 7.5.9 gives the amount of dose/unit KERMA being deposited at the dose deposition site, therefore, the sum of energy/unit KERMA is given by:

$$\text{ENERGY SUM} = \sum_{\Delta i \Delta j \Delta k} \sum \sum A^{het}_{p+1st}(\Delta i, \Delta j, \Delta k)\rho(i+\Delta i, j+\Delta j, k+\Delta k) \tag{7.5.10}$$

The value obtained from Equation 7.5.10 was compared to the result from the Monte Carlo calculations using the following:

$$\%\ \text{DEVIATION OF ENERGY SUM} = \frac{\text{MONTE CARLO SUM - CONVOLUTION SUM}}{\text{MONTE CARLO SUM}} \tag{7.5.11}$$

The comparison is shown at the bottom of Tables A to I in Appendix 12. Energy was usually conserved to better than 5 %, except for Situation G, in which the percent deviation was 8 %. The results can be improved by modifying the ray-tracing algorithm. Instead of giving f_o a weight of 0.5 for all rays, some rays are given an f_o weight greater than 0.5. Tables A' to I' in Appendix 12 illustrate the heterogeneous calculation with f_o equal to 0.9 when Δk is positive and Δi and Δj are both 0 and f_o equal to 0.6 when Δk is positive and Δi or Δj (but not both) is ± 1. All other f_o values are still 0.5. Energy is now conserved to better

than 2 % for all values except those in Situation G for which energy was conserved to 5.5 %. The results would probably also improve if the value of f_N was not constant. This has not been tested.

Multiple scatter photons may have interacted anywhere within the phantom, not just between the primary interaction and dose deposition voxels. Therefore, the average "global" density of the phantom is used in Equation 7.5.5 and 7.5.8 instead of the mean density along the path between the interaction and dose deposition voxels. This approximation is further justified because multiple scattering is a minority contributor to the total dose. This approximation avoids calculating the mean density between the interaction and dose deposition voxels of the RFMS dose spread array resulting in a saving of computation time.

Figures 131 and 132 illustrate the TMR correction factor for a 15 MV beam along the central axis for a heterogeneous phantom consisting of horizontal slabs of low-density and unit density material for field sizes of 5 cm x 5 cm and 10 cm x 10 cm. The experimental measurements were the same as those obtained in Section 6. The correction factor is less than 1.0 in cork at 5 cm x 5 cm which indicates that the dose to cork is less than the dose in the homogeneous phantom even though the primary photon fluence is greater. This was shown (in Section 6) to be due to a loss of lateral electronic equilibrium because the distance from the central axis to

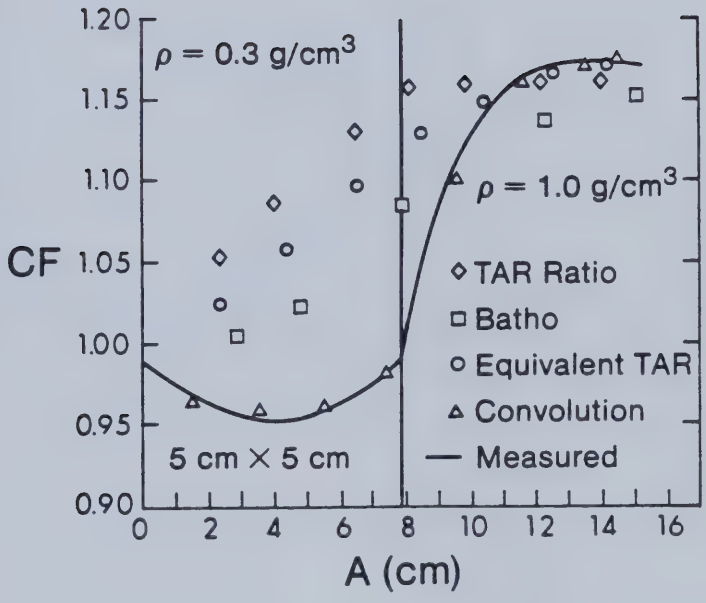

Figure 131. The experimental and measured TMR correction factor for a 15 MV beam. The experimental set-up is shown in Figure 85. The field size is 5 cm x 5 cm.

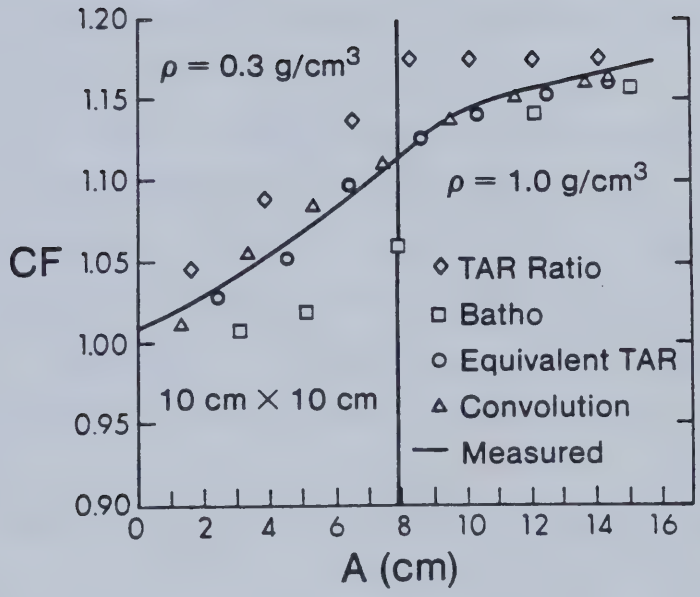

Figure 132. The experimental and measured TMR correction factor for a 15 MV beam. The experimental set-up is shown in Figure 85. The field size is 10 cm x 10 cm.

the field boundary is smaller than the lateral range of charged particles. The dose results of some existing methods are shown for comparison in Figures 131 and 132. The existing methods assume electronic equilibrium and poorly predict the dose in this situation. The convolution calculation predicts not only the correct trend but also predicts the measured correction factor to within 2 %. Lateral equilibrium is established at a field size of 10 cm x 10 cm, and for this situation, the convolution calculation and the equivalent TAR methods both predict the dose adequately.

The choice of weighting of the interaction voxel, f_o, in the ray-tracing algorithm altered the dose in this heterogeneous situation by only a few percent. Therefore, at least for the slab geometries tested, ray-tracing seems to be adequate for determining the average density "environment" between the interaction and dose deposition voxels.

Many dose calculation algorithms, such as the Batho and TAR ratio methods, only correct the dose at the central axis for tissue heterogeneities. Figure 133 illustrates the dose profile at a depth of 9.5 cm inside a $0.30 g/cm^3$ region of a heterogeneous phantom (see inset). The field size is 20 cm x 20 cm. At the central axis, the dose in this heterogeneous phantom is about 5 % greater than the dose in a homogeneous phantom at the same depth. However, the dose in the heterogeneous phantom decreases faster than the dose in a homogeneous phantom at greater distances from the

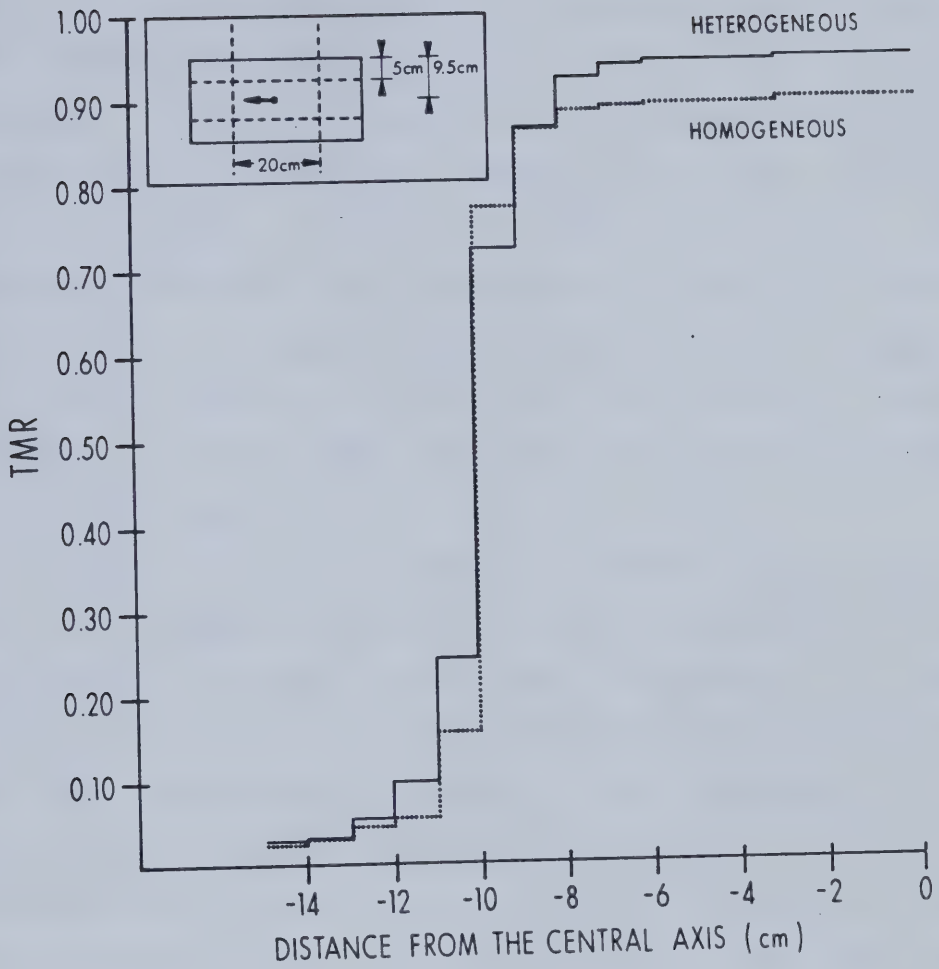

Figure 133. The calculated homogeneous and heterogeneous TMR profile at 9.5 cm depth (A = 4.5 cm) in a 20 cm x 20 cm field.

central axis. Just inside the field boundary, the dose in the heterogeneous phantom is less than the dose in a homogeneous phantom. Outside the field boundary, the dose in the heterogeneous phantom is once again greater than in the homogeneous phantom. The behavior near the field boundary, in the low-density material, can be attributed to charged particles streaming from inside the field (reducing the dose there) to outside the field (increasing the dose there). Therefore, an inhomogeneity correction factor obtained at the central axis cannot be applied throughout the field. Kornelsen and Young (80) have measured similar changes in 10 MV dose profiles in phantoms containing low-density regions.

Traditionally, the effects of a wedged field incident on a heterogeneous phantom on a dose distribution has been performed in two steps. The dose distribution is first calculated for a wedged field incident on a homogeneous phantom. The correction factor is then obtained for a heterogeneous phantom irradiated by an open field. The inhomogeneity correction factors are then multiplied by the dose distribution for the wedged field to obtain the dose distribution. This approach is non-rigorous and has never been tested for its validity. The convolution method is capable of determining the wedged field dose distribution for a heterogeneous phantom in one step.

Figure 134 illustrates that there is good agreement between separating the tasks of determining the wedge dose distribution and the heterogeneous correction and

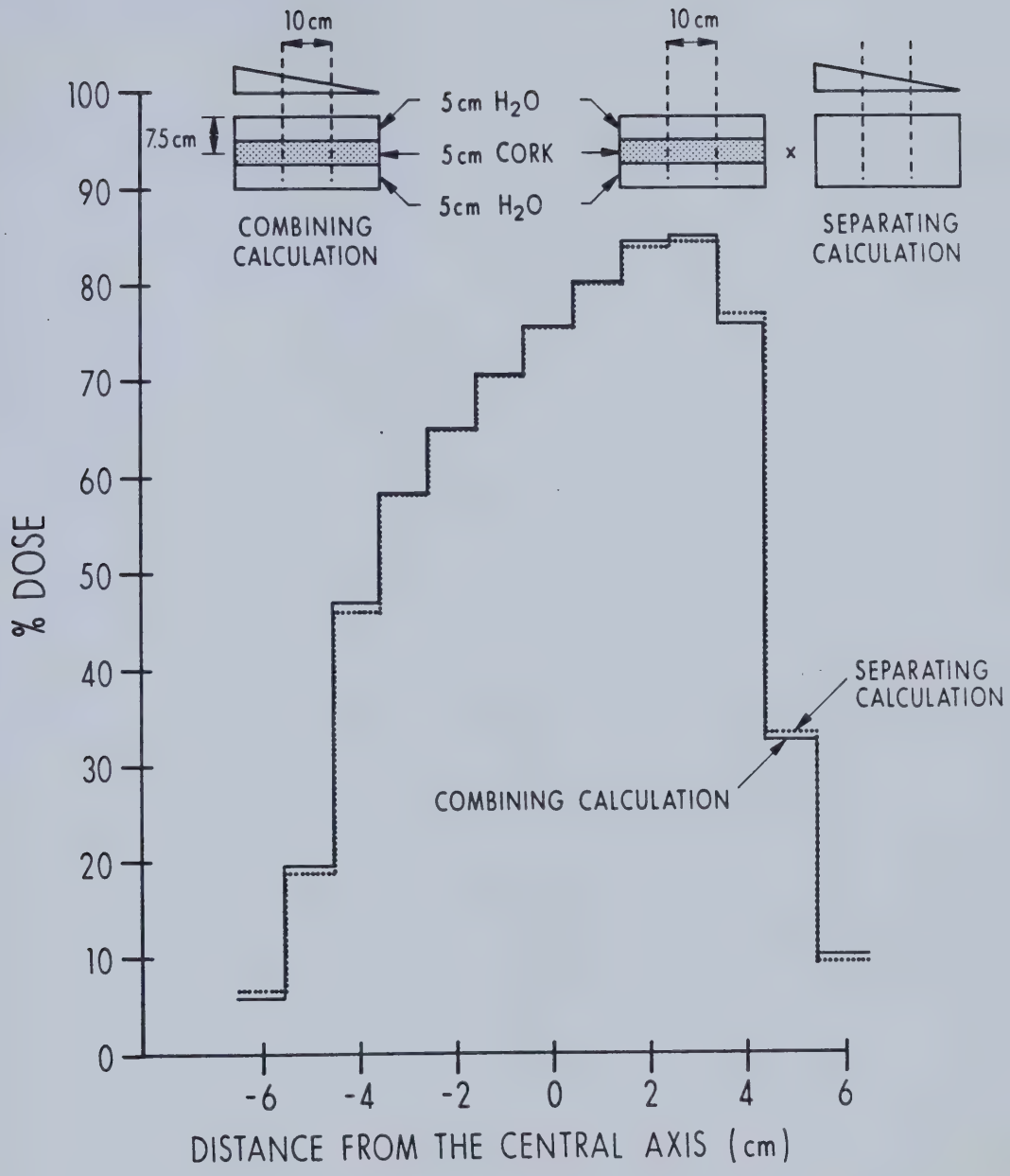

Figure 134. A comparison of separating the task of determining the wedge dose distribution and calculating an inhomogeneity correction factor and performing the calculation in one step. The result in either case is the percent dose profile. The field size is 10 cm x 10 cm. The heterogeneous phantom and wedge are shown schematically.

calculating the wedge and heterogeneous distribution directly in one step.

7.6 The Spatial Invariance Of The Dose Spread Arrays

The dose spread arrays are produced using a very large phantom. The primary dose spread array is finite in extent so the phantom need only have been larger than the maximum range of charged particles set-in-motion. The TFS dose spread array is completely independent of the size of the phantom used in the simulation. The size of the phantom will affect the RFMS dose spread array only. The use of this dose spread array near the edge of the phantom will introduce error. However, since this dose spread array contributes a small fraction to the total dose, this error due to the extent of the phantom, will be insignificant.

The dose spread arrays are not completely spatially invariant in homogeneous phantoms for two other reasons. Beam hardening is due to the preferential removal of low energy photons from the beam. It is possible that the beam will have a "hardened" spectrum near the central axis, due to a greater pathlength of the primary beam through the field flattening filter, as compared to near the beam boundary. In addition, as the beam penetrates the phantom, it contains a greater fraction of higher energy photons. Beam hardening effects were not included in the results described. If it is necessary to include hardening effects for some beams, the convolution can proceed using different dose spread arrays for different locations in the phantom.

Divergent beams have three geometrical characteristics which distinguish them from parallel beams. There is an

inverse square reduction of the primary photons and a linear increase in each field dimension as a function of depth. Another characteristic may have to be taken into account for this method. The dose spread arrays are not invariant for diverging beams. Figure 135 illustrates that a dose spread array should be "tilted" at an angle from the central axis equal to that of the primary beam. For example, the angle of tilt is about 8.5 degrees at a distance of 100 cm from the source at the edge of a 30 cm x 30 cm field. To be rigorous, the subscripts of the dose spread array at $i+\Delta i, j+\Delta j, k+\Delta k$ should be transformed to $i+\Delta i', j+\Delta j', k+\Delta k'$, where:

$$\Delta k' = \frac{(SSD+k)\Delta k + r\Delta r}{D} \qquad (7.6.1)$$

$$\Delta i' = \frac{\Delta i D - i\Delta k'}{SSD+k} \qquad (7.6.2)$$

$$\Delta j' = \frac{\Delta j D - j\Delta k'}{SSD+k} \qquad (7.6.3)$$

Where $r = \sqrt{i^2+j^2}$ and $\Delta r = \sqrt{\Delta i^2 + \Delta j^2}$. If $\Delta i', \Delta j'$, or $\Delta k'$ are not integers, interpolation is necessary. This has not proven to be an important effect when calculating TMR's in the simple phantoms investigated so far. The transformation changes the value of the TMR at the central axis by less than 1 % up to a thickness of 20 cm in a 20 cm X 20 cm field at a distance of 100 cm from the source. However, beam

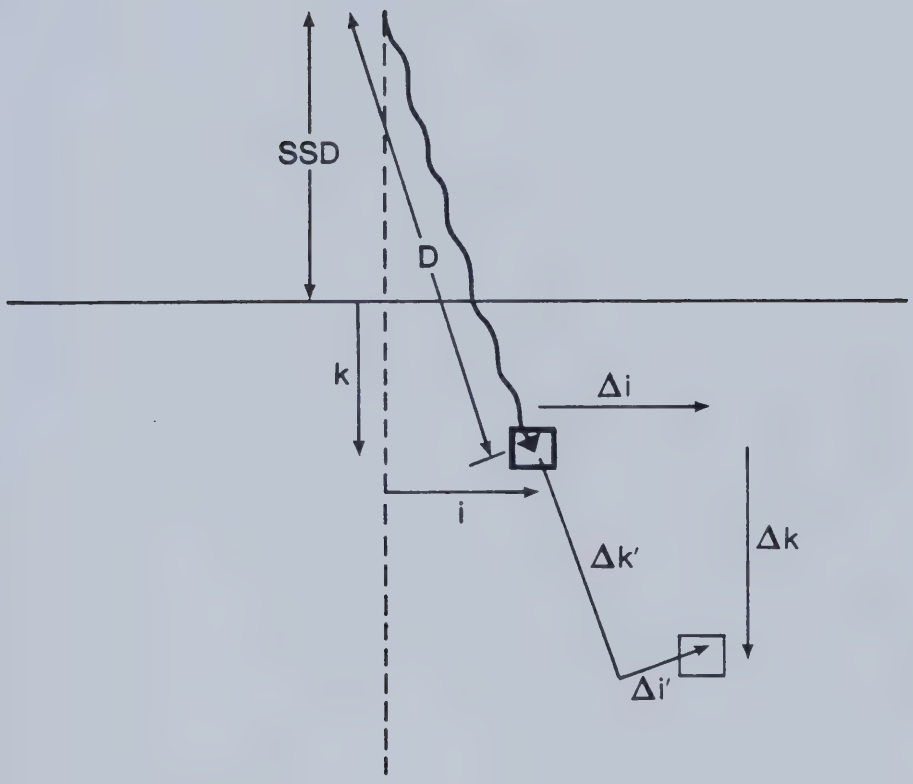

Figure 135. The dose spread array should be tilted to simulate the dose deposition from a divergent primary pencil beam interacting at i,j,k.

divergence will be an important effect when calculating percentage depth-dose for large fields or may be important when calculating dose in phantoms with complex heterogeneities.

7.7 Comparison With Other Methods and Potential Improvements

The convolution method presented has features similar to the equivalent TAR and Δ-Volume methods. Before the similarities are discussed, the characteristics of the method, which are unique, will be summarized.

1) The method explicitly takes into account the transport of charged particles which allows the calculation of dose in the build-up region and in lateral disequilibrium situations such as near beam boundaries or near low-density heterogeneities.

2) The use of experimental measurements as the data base is abandoned. Rather "synthetic measurements" are generated using the Monte Carlo method and validated by comparing the results of calculations with a limited set of experimental measurements.

3) Primary fluence is completely separated from dose deposition.

4) The primary dose, local first scatter dose and multiple scatter dose can be calculated separately. This allows optimization of the calculation resolution for each component to find the best compromise between speed and accuracy.

5) O'Connors theorem is explicitly used because the dose spread arrays are stored for a range of values of phantom

density times voxel dimension.

6) The same algorithm is used to calculate all the dose components.

Figure 136 illustrates a comparison between various dose calculation methods. The Monte Carlo method is the only method with the capabilities of the convolution method. However, it is yet far too slow for routine treatment planning. As computational power becomes less expensive and more available, this may change. Nevertheless, computational hardware improvements will also increase the speed of convolution calculations so that the convolution method will always remain faster than the Monte Carlo method. The convolution method retains the essential features of the Monte Carlo method for this application without the slow calculation time.

A procedure common to all other pencil beam and pixel-by-pixel calculation methods is" ray-tracing". The equivalent TAR method ray-traces to find the density weighted with respect to the amount of scatter originating at a location. The Δ-Volume method ray traces to find the contribution of first (and some second) scatter dose between the calculation point and all other points in the phantom where the primary beam interacts. The dose calculation for the first scatter dose contribution in a homogeneous phantom can be shown to be equivalent to a convolution calculation. This may be shown formally using a continuous 3-dimensional integral representation of first scatter fluence. The first

Algorithms For Making Dose Corrections In Heterogeneous Phantoms

Algorithm	Pathlength	Field Size	Position Of Structure	Shape Of Structure	Electronic Equilibrium
Linear Attenuation Coefficient	Yes	No	No	No	No
Ratio Of TAR's	Yes	Yes	No	No	No
Effective SSD	Yes	Yes	No	No	No
Isodose Shift	Yes	Yes	No	No	No
Batho (Power Law)	Yes	Yes	Yes	No	No
Equivalent TAR	Yes	Yes	Yes	Yes	No
Delta-Volume	Yes	Yes	Yes	Yes	No
Monte Carlo	Yes	Yes	Yes	Yes	Yes
Convolution	Yes	Yes	Yes	Yes	Yes

Figure 136. A comparison of the convolution method with existing dose calculating methods.

scatter photon fluence at a point $\vec{r}$ in a homogeneous phantom, due to primary interactions at a point $\vec{r}'$, is given by:

$$\Phi_{1st}(\vec{r}) = \int_{3D} \Phi p(\vec{r}') \frac{d\sigma}{d\Omega}(\vec{r}-\vec{r}') \frac{\rho(\vec{r}')}{|\vec{r}-\vec{r}'|^2} e^{-\tilde{\mu}|\vec{r}-\vec{r}'|} dV' \tag{7.7.1}$$

Where $\Phi p(\vec{r}')$ is the primary fluence at point $\vec{r}'$ and $\rho(\vec{r}')$ is the density of the primary interaction site. $d\sigma(\vec{r}-\vec{r}')/d\Omega$ is the Compton scattering cross-section in units of cm^2/g. $e^{-\tilde{\mu}|\vec{r}-\vec{r}'|}$ is the attenuation of the first scatter dose between the interaction and dose deposition sites where the vector $\vec{r}-\vec{r}'$ is directed along the path between the interaction and dose deposition sites. Boyer (99) has shown formally that Equation 7.7.1 is a convolution integral. In a formalism used in continuous convolution theory (96) Equation 7.7.1 becomes:

$$\Phi_{1st}(\vec{r}) = \int_{3D} h(\vec{r}')g(\vec{r}-\vec{r}')dV' \tag{7.7.2}$$

Where:

$$h(\vec{r}') = \Phi p(\vec{r}')\rho(\vec{r}') \tag{7.7.3}$$

$$g(\vec{r}-\vec{r}') = \frac{d\sigma}{d\Omega}(\vec{r}-\vec{r}') \frac{e^{-\mu|\vec{r}-\vec{r}'|}}{|\vec{r}-\vec{r}'|^2} \tag{7.7.4}$$

Equation 7.7.2 is just the 3-dimensional continuous analog

of Equation 7.4.8.

In general, the speed of pixel-based calculation methods is much slower than simpler methods. The time depends on the number and type of operations specified by the algorithm and the hardware used to run the program. Currently, the Δ-Volume method requires a significantly longer time than the convolution method when it is running on the same computer (VAX 11/780), presumably under the same operating conditions. The Δ-Volume requires 4.7 hours for a 16 x 16 x 16 dose matrix and 300 hours for a 32 x 32 x 32 matrix (77). The convolution method, by comparison, presently requires 50 min and 8.2 hours, respectively, for the same 3-dimensional distributions. The calculation times for both of these methods can be improved. The slowest part of the pixel-by-pixel methods is ray-tracing. Ray-tracing in the Δ-Volume method is being incorporated into a custom-integrated circuit which is expected to increase its speed by an order of magnitude (77). The convolution method should be particularly well-suited to array processing which should also decrease the calculation by an order of magnitude. The array processor calculation in the interaction point of view will be examined in some detail. The array processor would calculate the following equation for a given $\Delta i, \Delta j, \Delta k$ and relative fluence $\Phi''(i,j,k)$ (from Equation 7.5.7):

$$\Phi''(i,j,k)A'p(\tilde{\rho}\cdot\ell,\Delta i,\Delta j,\Delta k) \qquad (7.7.5)$$

The host computer would calculate $\Phi''(i,j,k)$ and also keep track of where the primary fluence was interacting in the phantom (i.e. the 3-dimensional intersection of the beam and the patient). A flow chart of the host computer calculations is shown in Figure 137. A flow chart of the array processor calculation is shown in Figure 138. The array processor would first calculate the mean density between the interaction site and all the dose deposition sites. The algorithm then specifies a loop for the calculation of Equation 7.7.5. The average density calculation could have been brought within the loop and not stored as an array. However, some of the average density array may be reused for a beam from a different direction also interacting at the same location (i,j,k). Figure 139 illustrates the idea schematically. The Δ-Volume method should also be able to benefit by storing an average density matrix for use with multiple beams. In turn, the convolution method could employ a custom-integrated circuit to calculate the average density array. Both the Δ-Volume and the convolution methods could benefit from an improved ray-tracing algorithm. The algorithm presently employed by both methods is summarized by Equations 7.5.1 to 7.5.4. A more efficient method would be to calculate the density along radial vectors. In the case of the convolution method, in the interaction point of view, the center of the radial vectors would be the interaction site. In this way, the average density, at one point on the radial vector, would use the summation of densities calculated at a point

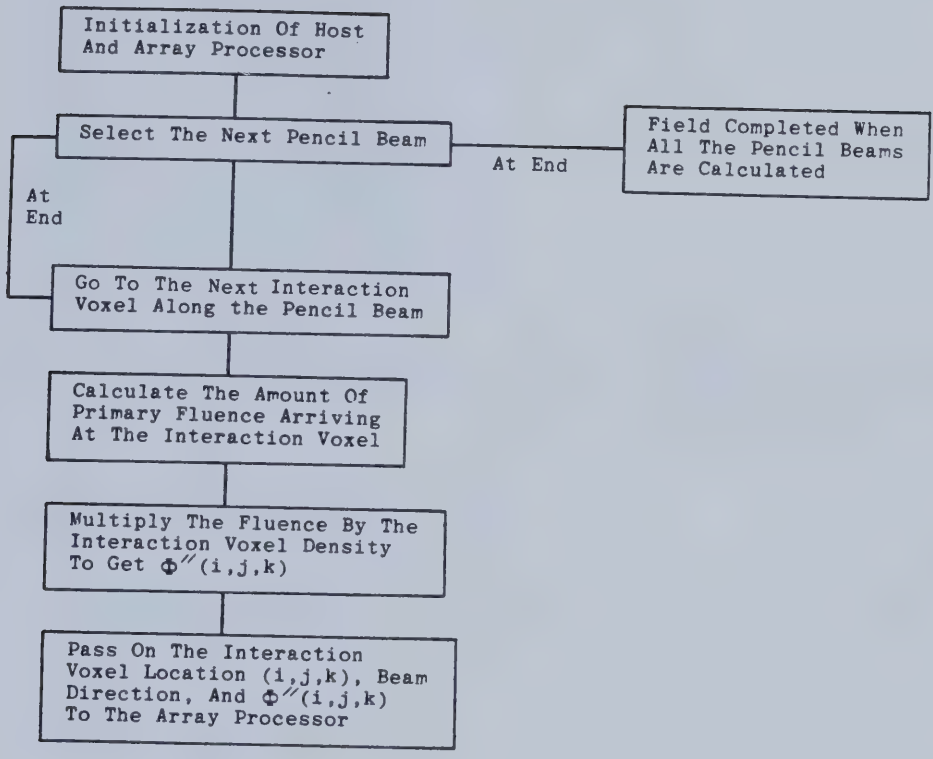

Figure 137. A flow chart of the host computer calculations required if an array processor is used to perform part of the convolution calculations (see Figure 138).

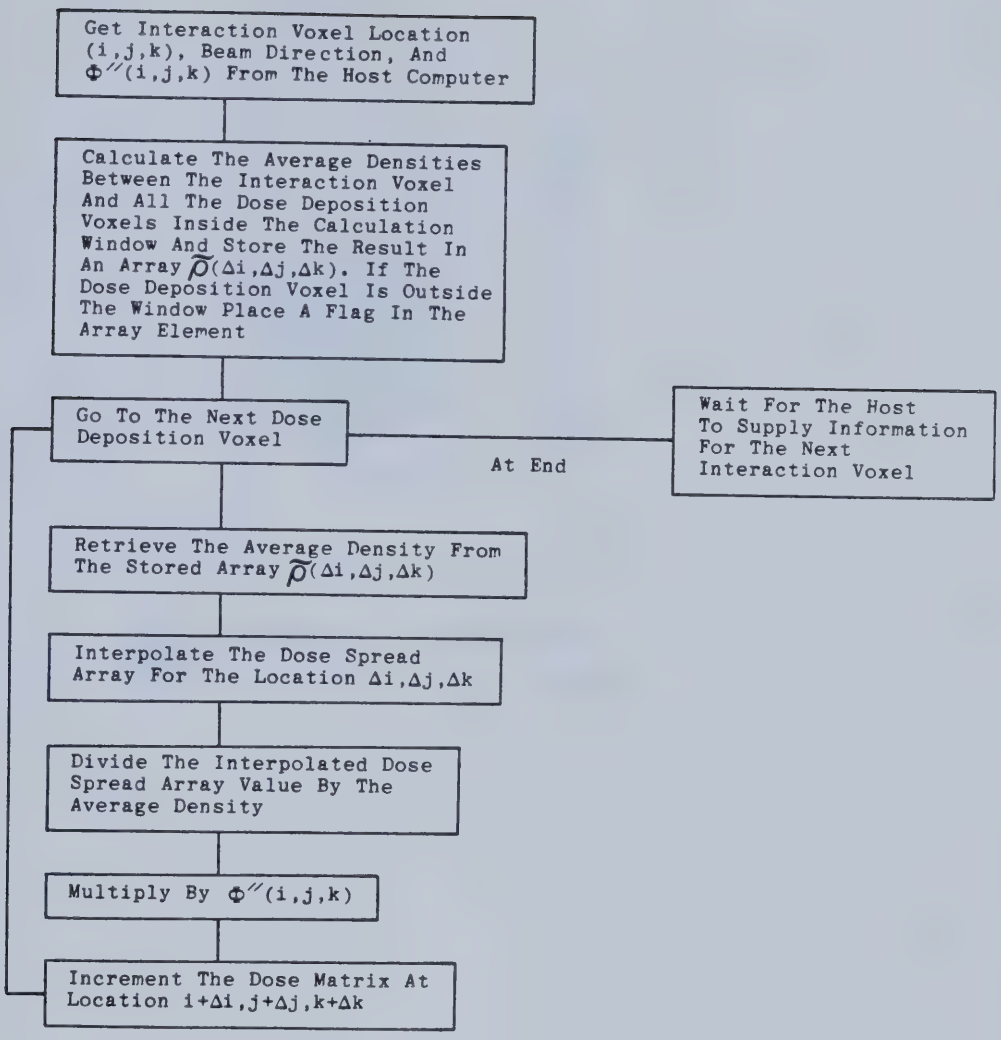

Figure 138. A flow chart of the array processor calculations (see Figure 137).

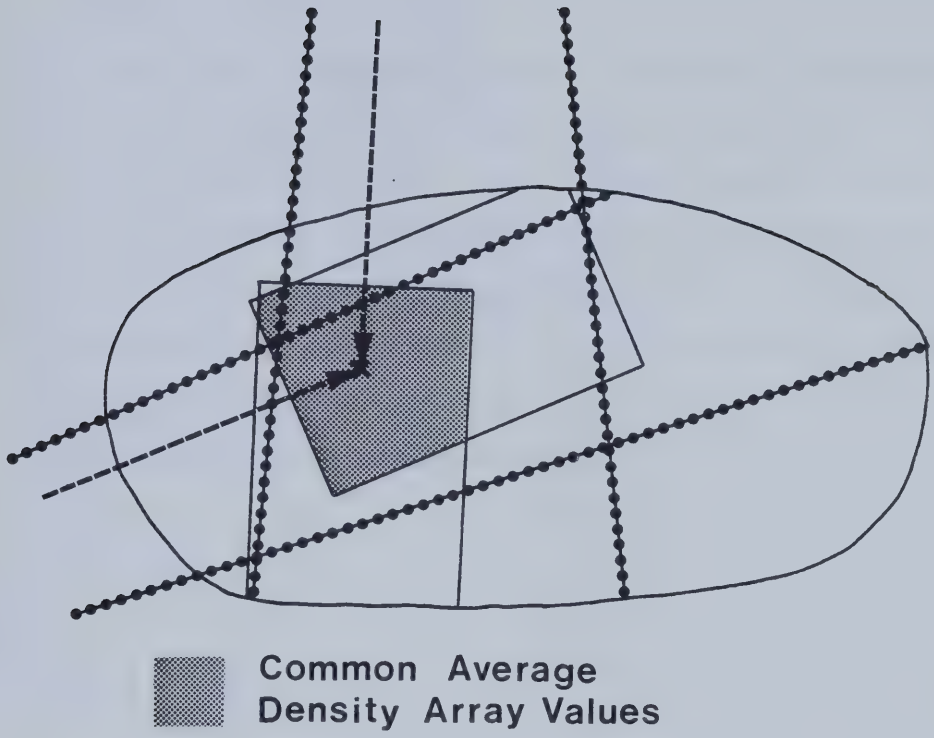

Figure 139. The part of an average density array calculated for one beam, that intersects with the average density array of another beam, may be reused by the second beam.

with a smaller radius. If the dose spread arrays were cubes with 'n' voxels per side, the number of calculations to assemble an average density matrix would be proportional to n^3, with this improved algorithm, compared to the presently used algorithm which is approximately proportional to n^4.

The proponents of the Δ-Volume method (77) have recently adopted a variable grid spacing capability to speed up the calculation. It is philosophically similar to the convolution method in that it calculates the contribution of scatter in a coarser grid resolution from contributions a long distance from the dose point.

7.8 Dose In A Non-Water-Like Heterogeneous Phantom

The present method has been used to calculate the dose in water-like heterogeneities such as lung which have a similar atomic composition. The method could be extended to other media of different atomic composition such as bone.

It is instructive to first examine the situation in a phantom near the junction of two materials with different atomic numbers. Equations 5.2.1 to 5.2.3 can be extended to determine the dose near a heterogeneity due to an atomic number change. Suppose the atomic number in a region of thickness, a, of a phantom is Z_1, and on the other side of the interface is Z_2. The direction of the photon beam is from region 1 to region 2. The dose in region 1 will be given by:

$$DOSE_1(z<a) \propto \left[\frac{\mu_{en}}{\rho}\right]_{Z_1}\left[\frac{\bar{S}}{\rho}\right]_{Z_2}\left(e^{-(\mu_\gamma/\rho)\rho_1 z} - e^{-(\mu_{e^\pm}/\rho)\rho_1 z}\right) \tag{7.8.1}$$

The dose on the other side of the interface will be given by:

$$DOSE_2(z>a) \propto \left[\frac{\mu_{en}}{\rho}\right]_{Z_1}\left[\frac{\bar{S}}{\rho}\right]_{Z_2}\left(e^{-\mu_\gamma/\rho)\rho_1 a} - e^{(\mu_{e^\pm}/\rho)\rho_1 a}\right) x$$

$$x\, e^{(\mu_{e^\pm}/\rho)\rho_2(z-a)} + \left[\frac{\mu_{en}}{\rho}\right]_{Z_2}\left[\frac{\bar{S}}{\rho}\right]_{Z_2}\left(e^{-(\mu_\gamma/\rho)\rho_2(z-a)}\right.$$

$$\left. - e^{-(\mu_{e^\pm}/\rho)\rho_2(z-a)}\right) e^{-(\mu_\gamma/\rho)\rho_1 a} \tag{7.8.2}$$

The first term takes into account the production of charged particles in region 1 that arrive at a depth, z, and the second term takes into account the amount of dose arriving at the same depth, z, from the second region.

The charged particle fluence at the interface will be almost entirely generated in region 1 (except for a small amount of charged particles directed in the backwards direction which has not been included in the above equation). There will be a discontinuity of dose at the interface. The ratio of dose at the interface in region 2 compared to region 1 is equal to:

$$\frac{[\bar{S}/\rho]_{Z_2}}{[\bar{S}/\rho]_{Z_1}} \qquad (7.8.3)$$

This discontinuity has been observed by several authors (63,78,100).

The convolution method may be used to determine the dose in medium with different atomic numbers. The primary dose spread arrays may have to be recalculated for these types of tissue because charged particle scattering is strongly dependent on atomic number (88). The scatter dose spread arrays would not likely be affected because the Compton scattering cross-section per electron is approximately independent of atomic number (9). The density, ρ, would now have to be interpreted as the electron density relative to water (67). As in the simple model described by Equation 7.8.1 and 7.8.2, two additional factors would have to be included when the primary dose is

being calculated:

$$\text{DOSE CONTRIBUTION}(i+\Delta i, j+\Delta j, k+\Delta k) \propto \Phi'(i,j,k) \frac{\rho(i,j,k)}{\tilde{\rho}} \times$$

$$\times \frac{[\frac{\mu_{en}}{\rho}]_{Z(i,j,k)}}{[\frac{\mu_{en}}{\rho}]_{\tilde{Z}}} \frac{[\frac{\bar{S}}{\rho}]_{Z(i+\Delta i, j+\Delta j, k+\Delta k)}}{[\frac{\bar{S}}{\rho}]_{\tilde{Z}}} A_p(\tilde{Z}, \tilde{\rho}\cdot\ell, \Delta i, \Delta j, \Delta k) \qquad (7.8.4)$$

$\tilde{Z}$ is the average effective atomic number between the interaction and dose deposition sites. The first ratio takes into account the relative difference in the amount of energy released in the real interaction voxel of effective atomic number, $Z(i,j,k)$, compared to the amount released in a homogeneous phantom of effective atomic number $\tilde{Z}$. The second ratio takes into account the amount of energy deposited in the real dose deposition voxel of effective atomic number $Z(i+i, j+j, k+k)$ compared to the amount deposited in the homogeneous phantom of effective atomic number $\tilde{Z}$.

8. Discussion and Conclusions Concerning The Convolution Method

> The only justification for our concepts and system of concepts is that they serve to represent the complex of our experiences; beyond this they have no legitimacy.
>
> Albert Einstein
> (The Meaning Of Relativity, 1921)

8.1 Discussion

The dose spread arrays are "synthetic" macroscopic data determined from the microscopic transport of individual particles using the Monte Carlo method. This information cannot be obtained from measurement because a real primary photon beam cannot be "forced" to interact at only one region of the material. This requirement is necessary in order to describe the transport of secondary particles set in motion by primary photon interactions. All the dose spread arrays were generated with the inclusion of charged particle transport. The primary dose spread array is proportional to the energy deposited by charged particles set in motion by primary photons. The scatter dose spread arrays are proportional to the energy deposited by charged particles set in motion by scattered photons. An analytic solution to photon-charged particle transport would be difficult (if not impossible) to obtain (101). For this reason, the Monte Carlo method was used to generate all the dose spread arrays.

The convolution procedure separates the photon - charged particle transport up into physically meaningful components. Primary photon interactions are separated from charged particle and secondary photon transport and energy deposition (101). This division of primary fluence from dose deposition is a more appropriate model of radiation transport than the modification of measured dose distributions in which these two effects are combined. This

does not undermine the importance of obtaining good measurements, since this provides the selection criteria for the photon spectrum used to compute the dose spread arrays.

The spectrum was determined by first finding a tentative "pre-spectrum" which is a measured spectrum obtained from a research accelerator (48). The agreement between the calculated dose and measured dose is a necessary condition for the acceptability of the spectrum, but it is not a sufficient condition. The spectrum may not be unique. Therefore, a better procedure would be to determine the actual spectrum directly by measurement. Transmission measurements, obtained with "good geometry", have been used to obtain spectra (102,103). A problem with spectra determined in this way is that small errors in measurements leads to large errors in the spectral determination. Therefore, the spectrum should be checked by getting the agreement between the measured and calculated dose using this spectrum. If it did not agree then the spectrum should be adjusted to obtain better agreement (although the modification must be kept within the experimental uncertainty).

Transmission measurements are relatively easy to obtain. Using a pre-spectrum based on these measurements, the convolution method could be adopted as the dose calculation method for any accelerator type or energy. What is first required is the dose spread arrays calculated as a function of $\rho \cdot \ell$ and Z for various monoenergetic energies from 0 to 50 MeV (no accelerator with a nominal energy above

50 MV is available). A spectrum would be obtained for energy components for which dose spread arrays have been calculated. The dose spread arrays for the spectrum are obtained using the pre-stored dose spread arrays. The primary attenuation coefficient would then be determined using Equation 7.4.4. The dose distribution would then be calculated for a wide range of field sizes. The calculated dose beyond d_{max} would be compared to the measured dose. If the agreement was not satisfactory, then the spectrum would be modified. The above procedure should be repeated for the new spectrum. Figure 140 is the flow chart of the proposed implementation procedure.

Basing photon dose calculations on the firm mathematical foundation of convolution may allow additional future improvements. In homogeneous phantoms, the dose spread arrays are spatially invariant so that the relative fluence array and dose spread arrays may be Fourier transformed into the spatial frequency domain. The convolution may then proceed much more quickly by multiplying the transformed arrays (99). The dose can then be obtained by taking the inverse Fourier transform of the result. For homogeneous water-like media, this procedure is described mathematically as:

$$DOSE(x,y,z) \propto F^{-1}[F\{\Phi'(i,j,k)\}*F\{A(\rho\cdot\ell=\ell,\Delta i,\Delta j,\Delta k\}] \qquad (8.1)$$

Where F and F^{-1} describe symbolically the 3-dimensional Fourier and inverse Fourier transform, respectively (96).

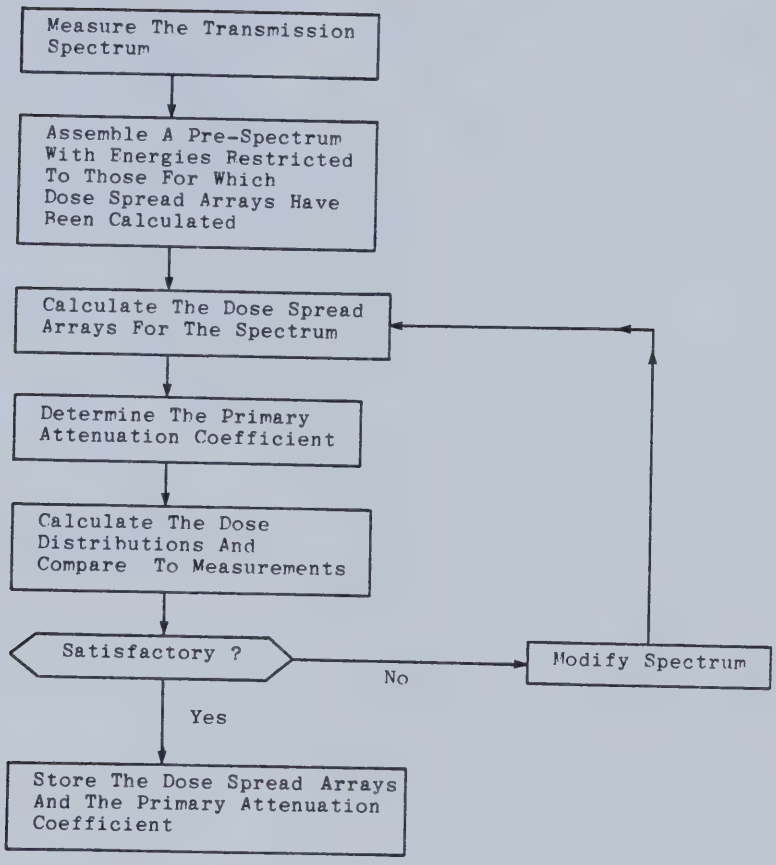

Figure 140. The flow chart of the determination of the correct dose spread array and primary attenuation coefficient based on the transmission spectrum of a linear accelerator.

This procedure is used routinely in image processing applications, and is especially appropriate if an array processor is available.

Deconvolution techniques may be useful in optimizing the delivery of radiation therapy. If one knows the attributes of an optimal dose distribution (eg. uniform dose to the target volume and minimal dose to surrounding tissue), and the beam directions and intensities, the dose spread array can be deconvolved from the ideal dose distribution to obtain the best primary fluence distribution. This information could be used to design modifying devices, such as beam compensators, to approach the ideal relative fluence distribution in homogeneous or heterogeneous media.

8.2. Conclusions

The EGS Monte Carlo modelling in Section 6 confirmed the interpretation in Section 5 that lateral disequilibrium is the reason for reduced dose at the central axis in a low-density medium for small field sizes. This situation is one aspect of a more general phenomenon. Lateral disequilbrium never exists near the field boundary penumbra. It was shown that the penumbra region for high energy linear accelerator beams is due in part to the lateral transport of charged particles. When the field size is small and the phantom has a low-density, the penumbra extends to the central axis. In order to describe the disequilibrium effects, the transport of charged particles have to be included into dose calculations.

A dose calculation method based on convolution was introduced in Section 7 which explicitly took into account charged particle transport. The method was general enough to include the transport of scattered photons. The method relied on the production of "dose spread arrays" to describe the transport of secondary particles from a primary photon interaction voxel to neighboring dose deposition voxels. The values of the elements of the dose spread arrays represent the dose deposited in dose deposition voxels per unit collision KERMA at a primary interaction voxel. The dose spread arrays were obtained from Monte Carlo simulations. The primary dose spread array accounts for the primary dose, the truncated first scatter (TFS) dose spread

array accounts for the first scatter dose deposition close to the primary interaction site, and the residual first and multiple scatter (RFMS) dose spread array accounts for the rest of the first scatter dose and all the multiple scatter dose. The primary dose spread arrays generated in homogeneous water-like phantoms of density, ρ , with voxel dimensions, ℓ , are equivalent to those generated using a phantom density, ρ', with dimensions, ℓ', provided; $\rho \cdot \ell = \rho' \cdot \ell'$. The scaling also applies to the scatter dose spread arrays. This indicates that O'Connors theorem applies to the primary dose even when there is electronic disequilibrium, as well as scatter dose, in a homogeneous phantom.

The dose distribution in 3-dimensions is obtained in a homogeneous phantom by convolving the dose spread array kernel, applicable to the density of the phantom and desired voxel resolution, with the relative fluence. There is a reciprocity between the interaction and dose deposition voxels. The dose spread arrays describe both the transport of dose from an interaction voxel and the arrival of dose at a dose deposition voxel. This allows the convolution to proceed in two ways called the interaction and dose deposition points of view. The method accurately predicts the dose in homogeneous phantoms in situations of electronic disequilibrium including the build-up region and near beam boundaries. The method was shown to provide a unified treatment of dose calculations in that it could account for the changes in dose due to fluence modifying devices such as

beam shields and wedges.

The dose spread arrays, generated for homogeneous phantoms at various values of $\rho \cdot \ell$, are used to describe the transport of dose in heterogeneous phantoms. The average density, $\tilde{\rho}$, between the interaction and dose deposition voxels is determined. The primary and TFS dose spread arrays are interpolated to obtain one appropriate for this average density. The convolution of these arrays in a heterogeneous phantom contains a factor to account for the difference in the amount of interactions between the heterogeneous interaction voxel and the homogeneous interaction voxel with a density equal to the average path density. The RFMS dose spread array in heterogeneous phantoms is scaled using the average phantom density instead of the average path density. The method provided a good prediction of the dose in and near heterogeneous regions.

Although the method is presently only applicable to dose absorption in materials which are water-like in atomic composition, it could be extended to include non-water-like materials. The convolution framework of the method lends itself to Fourier and deconvolution techniques that could improve the calculation speed and optimization of dose.

REFERENCES

(55) Lichter, A.S., Fraas, B.A., van de Geijn, J., Fredrickson, H.A., Glatstein, E., "An Overview of Clinical Requirements and Clinical Utility of Computed Tomography Based Radiotherapy Treatment Planning", in Computed Tomography in Radiation Therapy, Ed., Ling, C.C., Rogers, C.C., Morton, R.J., Raven Press, New York, (1983).

(56) Meyer, J.E., "Computed Tomography in Radiation Therapy Treatment Planning: The Diagnostician", in Computed Tomography in Radiation Therapy, Ed., Ling, C.C., Rogers, C.C., Morton, R.J., Raven Press, New York, (1983).

(57) Geise, R.A., McCullough, E.C., "The Use of CT Scanners in Megavoltage Photon Beam Therapy Planning", Radiology, 124, 133-141, (1977).

(58) Sontag, M.R., Battista, J.J., Bronskill, M.J., Cunningham, J.R., "Implications of Computed Tomography for Inhomogeneity Corrections in Photon Beam Dose Calculations", Radiology, 124, 143-149, (1977).

(59) Battista, J.J., Rider, W.D., Van Dyk, J., "Computed Tomography for Radiotherapy Planning", International Journal of Radiation Oncology, Biology and Physics, 6, 99-107, (1980).

(60) Brooks, R.A., Mitchell, L.G., O'Connor, C.M., Di Chiro, G., "On the Relationship Between Computer Tomography Numbers and Specific Gravity", Physics in Medicine and Biology, Vol. 26, No. 1, 141-147, (1981).

(61) Cassell, K.J., Hobday, P.A., Parker, R.P., "The Implementation of a Generalized Batho Inhomogeneity Correction for Radiotherapy Planning with Direct Use of CT Numbers", Physics in Medicine and Biology, Vol. 26, No. 4, 825-833, (1981).

(62) Reinstein, L.E., McShan, D.L., Land, R.E., Glicksman, A.S., "Three-Dimensional Reconstruction of CT Images for Treatment Planning in Carcinoma of the Lung", in Computed Tomography in Radiation Therapy, Ed., Ling, C.C., Rogers, C.C., Morton, R.J., Raven Press, New York, (1983).

(63) Johns, H.E., Cunningham, J.R., The Physics of Radiology, Fourth Edition, Charles C. Thomas, Springfield, IL., (1983).

REFERENCES (CONT'D)

(64) Young, M.E.J., Kornelsen, R.O., "Dose Corrections for Low-Density Tissue Inhomogeneities and Air Channels for 10-MV X-rays", Medical Physics, Vol. 10, No. 4, 450-455, (1983).

(65) Cunningham, J.R., "Tissue Inhomogeneity Corrections in Photon Beam Treatment Planning", in Progress in Medical Physics, Ed., Orton, C.E., Plenum, New York, (1982).

(66) Batho, H.F., "Lung Corrections in Cobalt-60 Beam Therapy", Journal of the Canadian Association of Radiologists, 15, 79-83, (1964).

(67) Sontag, M.R., Cunningham, J.R., "Corrections to Absorbed Dose Calculations for Tissue Inhomogeneities", Medical Physics, Vol. 4, No. 5, 431-436, (1977).

(68) Lulu, B.A., Bjarngard, B.E., "A Derivation of Batho's Correction Factor for Heterogeneities", Medical Physics, Vol. 9, No. 6, 907-909, (1982).

(69) Lulu, B.A., Bjarngard, B.E., "An Improved Correction Factor for Heterogeneities", Medical Physics, Vol. 9, No. 4, 626 (Abstract), (1982).

(70) Sontag, M.R., Cunningham, J.R., "The Equivalent Tissue-Air-Ratio Method for Making Absorbed Dose Calculations in a Heterogeneous Medium, Radiology, 129, 787-794, (1978).

(71) O'Connor, J.E., "The Variation of Scattered X-rays with Density in an Irradiated Body", Physics in Medicine and Biology, 1, 352-369, (1957).

(72) Tatcher, M., Palti, S., "A Simple Equivalent Tissue-Air-Ratio Method for Calculating Absorbed Dose in a Heterogeneous Medium", Radiology, Vol. 146, No. 2, 527-529, (1983).

(73) Cunningham, J.R., Beaudoin, L., "Calculations for Tissue Inhomogeneities with Experimental Verification", in Proceedings of the XIII International Congress on Radiology, Madrid.

(74) Larson, K.B., Prasad, S.C., "Absorbed Dose Computations for Inhomogeneous Media in Radiation - Treatment Planning Using Differential Scatter-Air-Ratios", in Proceeding of the Second Annual Symposium on Computer Applications in Medical Care, Washington, D.C.

REFERENCES (CONT'D)

(75) Wong, J.W., Henkelman, R.M., "A New Approach to CT Pixel-Based Photon Dose Calculations in Heterogeneous Media", Medical Physics, Vol. 10, No. 2, 199-208, (1983).

(76) Wong, J.W., Henkelman, R.M., Andrew, J.W., Van Dyk, J., Johns, H.E., "Effect of Small Inhomogeneities on Dose in a Cobalt-60 Beam", Medical Physics, Vol. 8, No. 6, 783-791, (1981).

(77) Rosenberger, F., Krippner, K., Stein, D. Jr., Wong, J., "Implementation of the Delta-Volume Dose Calculation Algorithm; in Proceedings of the Eighth International Conference on the use of Computers in Radiation Therapy, Toronto, (1984).

(78) Dutreix, J., Bernard, M., "Dosimetry at Interfaces for High Energy X and Gamma Rays", British Journal of Radiology, 39, 205-210, (1966).

(79) Leung, P.M.K., Seaman, B., Robinson, P., "Low-Density Inhomogeneity Corrections for 22 MV X-ray Therapy", Radiology, 94, 449-451, (1970).

(80) Kornelsen, R.O., Young, M.E.J., "Changes in the Dose-Profile of a 10 MV X-ray Beam Within and Beyond Low-Density Material", Medical Physics, Vol. 9, No. 1, 114-116, (1982).

(81) McGinley, P.H., Sanders, M., "Lung Correction Factors for 45-MV X-ray Therapy", Medical Physics, Vol. 9, No. 5, 738-740, (1982).

(82) Mackie, T.R., Scrimger, J.W., "Modelling the Build-up Region of Megavoltage Photon Beams", Medical Physics, Vol. 9, No. 4, 620 (Abstract),(1982).

(83) Ford, R.L., Nelson, W.R., The EGS Code System: Computer Programs for the Monte Carlo Simulation of Electromagnetic Cascade Showers, Version 3, Stanford Linear Accelerator Report No. 210, Stanford, CA., (1978).

(84) Rogers, D.W.O., "More Realistic Monte Carlo Calculations of Photon Detector Response Functions", Nuclear Instruments and Methods, 199, 531-548, (1982).

(85) Mach, H., Rogers, D.W.O., "A Measurement of Absorbed Dose to Water Per Unit Incident 7-MeV Photon Fluence", Submitted Dec. 1983 to Physics in Medicine and Biology.

(86) Dean, R.D., "A Scattering Kernel for Use in True Three-Dimensional Dose Calculations", Medical Physics, Vol. 7, No. 4, 429 (Abstract), (1980).

REFERENCES (CONT'D)

(87) Attix, F.H., "The Partition of Kerma to Account for Bremsstrahlung", Health Physics, 36, 347-354, (1979).

(88) I.C.R.U. Report 21, Radiation Dosimetry: Electrons with Initial Energies Between 1 and 50 MeV, International Commission on Radiation Units and Measurements, Washington, D.C. (1972).

(89) Bloch, P., Wallace, R., "Computer Generated Scatter Dose Distributions for 6-MV Radiotherapy Photon Beams", Medical Physics, Vol. 6, No. 2, 149-152, (1979).

(90) Barnett, R., "Zero-Area TMR Data Compiled for Cross Cancer Institute, Edmonton, Canada", (Private Communication).

(91) Schell, M.C., Deye, J.A., "Empirical Equation for Tissue-Maximum-Ratios and Scatter-Maximum-Ratios for Indirectly Ionizing Radiotherapy Beams", Medical Physics, Vol. 6, No. 1, 65-67, (1979).

(92) Coffey, C.W. II, Beach, J.L., Thompson, D.J., Mendiondo, M., "X-ray Beam Characteristics of the Varian Clinac 6-100 Linear Accelerator", Medical Physics, Vol. 7, No. 6, 716-722, (1980).

(93) Patterson, M.S., Shragge, P.C., "Characteristics of an 18 MV Photon Beam from a Therac-20 Medical Linear Accelerator", Medical Physics, Vol. 8, No. 3, 312-318, (1981).

(94) Paul, J.M., Koch, F., Khan, F.R., Devi, B.S., "Characteristics of a Mevatron 77 15-MV Photon Beam", Medical Physics, Vol. 10, No. 2, 237-242, (1983).

(95) Cristy, M., "Applying the Reciprocity Dose Principle to Heterogeneous Phantoms: Practical Experience from Monte Carlo Studies", Physics in Medicine and Biology, Vol. 28, No. 11, 1289-1303, (1983).

(96) Bracewell, R., "The Fourier Transform and Its Applications", McGraw-Hill, New York, (1965).

(97) Barnett, R., Tom Baker Cancer Clinic, Calgary, Canada, (Private Communication).

REFERENCES (CONT'D)

(98) Clarkson, J.R., "A Note on Depth Dose in Fields of Irregular Shape", British Journal of Radiology, 14, 265, (1941).

(99) Boyer, A.L., Cancer Therapy and Research Center, San Antonio, TX, (Private Communication).

(100) Webb, S., "The Absorbed Dose in the Vicinity of an Interface Between Two Media Irradiated by a Co-60 Source", British Journal of Radiology, 52, 962-967, (1979).

(101) Roesch, W.C., Radiation Dosimetry, Ed., Attix, F.H., Roesch, W.C., Academic Press, New York, (1968).

(102) Twidell, J.W., "The Determination of X-ray Spectra Using Attenuation Measurements on a Computer Program", Physics in Medicine and Biology, 15, 529-539, (1970).

(103) Huang, P-H., Kase, K., Bjarngard, B.E., "Simulation Studies of 4-MV X-ray Spectral Reconstruction by Numerical Analysis of Transmission Data", Medical Physics, Vol. 9, No. 5, (1982).

Appendices

(Appendices 1 to 9 are in Volume 1)

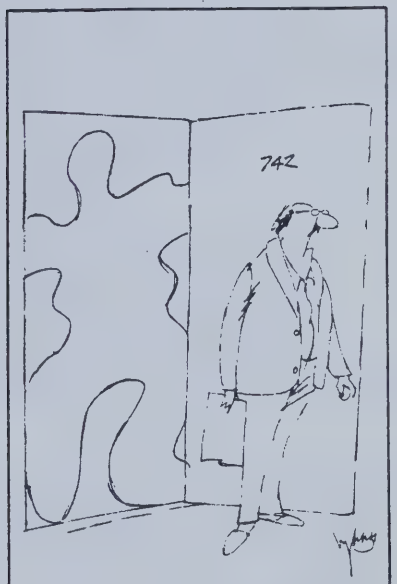

"Agnes, ... do we know an Inhomogeneity?"

Appendix 10. Listing of the MOCA Monte Carlo Code

```
      Program MOCA

c MOnte-CArlo program to generate dose spread arrays.
c The variables are domumented as they occur in the program.

      integer l,ii,nerg,enn(36),intest
      real r,zs,cal,sal,cbeta,sbeta,total
      real stop(179),tha(179),ep,cay
      real eo,e,doset(25,25,25),pl,gaus(100),g
      real z,max,ang,en(36),dose(5,25,25,25)
      integer i,j,m,p,kay,quad(4),chargpart,inquad(4)
      real xnrg(100),mu(100,10),sig(100,10)
      real pi(100,10),que(10),shiftx,shifty

      integer k,nrgint,phantom(25,25,25),multi
      integer charge,ir,vint,annhilflag
      integer order,kinorder(25)
      real nrgx,xs,ys,diml,dimlz
      real lx,ly,lz,short,attentot,dist,attensig
      real attenpi,fraction1,fraction2
      real nrg(35),fac,nrgmax,frac1,frac2
      real tnrg1,tnrg2,compton(35,50),tnrg,arg
      real kinrg(25),kincal(25),kinsal(25)
      real kinsbeta(25),kincbeta(25),kinx(25)
      real kiny(25),kinz(25),kintype(25),rr
      real pairprod(35,50),v,ro,r1,r2,test(4),arr(25)
      real photox,photoy,photoz
      real oldcal,oldsal,oldcbeta,oldsbeta
      real s,th,arg2
      integer n,numspect
      real sum,sqsum,mean(25),stdev(25),sterr(25),maxmean
      real maxsterr,sumpart(4,25)
      real nearx,neary,nearz,near,maxpl,nearo
      integer nearinti,neari,nearintj,nearj,nearintk,neark
      integer history,mark,boundary(7)
      integer oldi,oldj,oldk,smalli,smallj,smallk
      common xs,ys,zs,i,j,k,cbeta,sbeta,cal,sal,diml,dimlz,short

c Gaus.dat stores a table of x's as a function of erf(x). See
c page 163 and 164 in Volume 1 and Appendix 7.

c Dose6.dat is a listing of the dose spread arrays.

c Compton.dat is a look-up table giving the electron kinetic energies
c of equiprobable interactions. See Section 7.2.

c Pairprod.dat is a look-up table giving the electron or positron
c kinetic energies of equiprobable interactions. See Section 7.2.

c Pho15new.dat contains the 15 MV photon spectrum. See Sections 6.
c and 7.2.

c Atten.dat contains the attenuation data, scattering and stopping
c powers as a function of energy (from references 9 and 88).

c Debug.dat can contain information for debugging.

      open(unit=1,status='old',file='gaus.dat')
      open(unit=4,status='new',file='dose6.dat')
      open(unit=6,status='old',file='compton.dat')
```

```
      open(unit=8,status='old',file='pairprod.dat')
      open(unit=11,status='old',file='pho15new.dat')
      open(unit=12,status='old',file='atten.dat')
      open(unit=13,status='new',file='debug.dat')

c The following statements read the look-up tables and initializes.

      multi=1000                !# of incident photons
      intest=3                  !interaction voxel depth indicator
      shiftx=50.0               !x-position to interaction voxel
      shifty=50.0               !y-position to interaction voxel
      dim1=5.0                  !voxel dimension in x and y direction
      dim1z=5.0                 !voxel dimension in the z-direction

c Assign CT-number to the phantom voxels. There is a linear relation
c between density and CT-number (-1000=vacuum, 0=unit density).
c A heterogeneous phantom can be entered.

      do 6 k=1,25
        do 6 j=1,25
          do 6 i=1,25
6           phantom(i,j,k)=-800

c     do 7 k=4,25
c       do 7 j=1,25
c         do 7 i=1,25
c     7             phantom(i,j,k)=0

c     do 8 k=12,25
c       do 8 j=1,25
c         do 8 i=1,25
c     8             phantom(i,j,k)=0

      read(11,345) numspect                     !number of spectral bins
      do 10 i=1,numspect
        read(11,340) xnrg(i),en(i)              !spectrum weighting
10      enn(i)=en(i)/100.0*floatj(multi)        !# histories/bin
      read(11,350) (que(i),i=1,10)              !factor used in pair production
      do 12 l=1,100
12      read(1,422) gaus(l)                     !inverse error function

c 'Nrg' is the energy, 'mu' is the total attenuation coefficient, 'sig' is
c the Compton attenuation coefficient, 'pi' is the pair production
c attenuation coefficient, 'tha' is the scattering power and 'stop' is
c the stopping power.

      do 14 i=1,24
14      read(12,570) nrg(i),mu(i,1),sig(i,1),pi(i,1),tha(i),stop(i)

      do 17 i=17,24
        do 16 k=1,5
16        read (8,550) (pairprod(i,(k-1)*10+m),m=1,10)
17    continue
      do 19 i=1,24
        do 18 k=1,5
18        read (6,550) (compton(i,(k-1)*10+m),m=1,10)
19    continue

      i1=95835                  !random number seed
      cay=0.90                  !fraction of energy remaining after step
      annhilflag=0              !flags the production of annhilation photons
```

```
        charge=0                !number of charged particles to process

        do 200 l=1,numspect     !do for all spectral bins
          do 180 m=1,enn(l)     !do for all photons in the bin

c Initialize the photon's energy,coordinate position and angle
c before transporting.

            xs=ran(i1)*diml+shiftx      !x-position
            ys=ran(i1)*diml+shifty      !y-position

            zs=10.0                     !z-position
            nrgx=xnrg(l)                !photon energy of the current bin
            history=history+1           !photon history counter
            cal=1.0                     !cos(alpha); alpha=zenith angle
            sal=0.0                     !sin(alpha)
            r=6.2832*ran(i1)
            cbeta=cos(r)                !cos(beta); beta=azimuth angle
            sbeta=sin(r)                !sin(beta)
            order=1                     !order of scattering; 1=primary.
                                        !and 2=first scattered photon

c Scattered photons enter at line 20.
c Test to see if the photon's energy is below the photon
c cut-off energy.

20          if (nrgx .lt. 0.03) go to 50        !photon cut-off is 30 keV
            if (order .gt. 4) order=4           !order=4 is multiple scattering

c Photons which didn't interact in the last element
c enter at line 21. Annhilation photons enter here too.

21          continue

c Terminate the primary photon history if it doesn't interact
c in the interaction voxel.

        if (order .eq. 1 .and. zs .lt. 10.0 ) go to 180
        if (order .eq. 1 .and. zs .gt. 15.0 ) go to 180

c Find out the shortest distance to the next wall along
c the photon's path.

        call where

c Find out the C.T. number of the element and the type of
c tissue.

            p=1                 !signifies water

c Interpolate to find out the appropriate attenuation
c coefficient.

            nrgint=1
            do 25 while ( nrgx .gt. nrg(nrgint))
25            nrgint=nrgint+1
            if (nrgint .eq. 1) then
              attentot=mu(1,p)
            else
              fac=(nrgx-nrg(nrgint-1))/(nrg(nrgint)-nrg(nrgint-1))
              attentot=mu(nrgint-1,p)+(mu(nrgint,p)-mu(nrgint-1,p))*fac
```

```
            end if

c Find the interaction distance.

            r=ran(i1)
            if (r .le. 0.0) then
              dist=0.0
            else
              ro=floatj(phantom(i,j,k)+1000)/1000.0
              dist=-alog(r)/attentot/ro
            end if

c Determine if and if so, where, the photon interacts
c in the element. Rejection sampling is used. Short is the
c distance to the voxel wall in the direction of the photon.
c It was determined in Subroutine Where.

            if (short .gt. dist) then

              xs=xs+dist*sal*cbeta       !increment the
              ys=ys+dist*sal*sbeta       !position
              zs=zs+dist*cal             !variables

              i=jifix(xs/diml)+1         !determine the
              j=jifix(ys/diml)+1         !voxel
              k=jifix(zs/dimlz)+1        !location

c Discard the primary photon and choose another primary photon
c if it doesn't interact in the interaction voxel.

              if (order .eq. 1 .and. k .ne. intest) go to 180

c If the photon leaves the phantom, discard it and go on to follow its
c charged particles set in motion.

              if (xs .le. 0.0001 .or. xs .ge. 20.0*diml) go to 50
              if (ys .le. 0.0001 .or. ys .ge. 20.0*diml) go to 50
              if (zs .le. 0.0001 .and. cal .lt. 0.0) go to 50
              if (zs .ge. 20.0*dimlz) go to 50

c Interpolate to get the appropriate Compton and pair
c production attenuation coefficients. The type of
c interaction is determined. 'Fraction1' is the
c fraction of Compton interactions in the total and
c 'fraction2' is the fraction of Compton plus pair
c productions in the total. If the energy is between
c 0.2 and 3.0 MeV a Compton interaction must have occured.

              if (nrgx .gt. 0.2 .and. nrgx .lt. 3.0) go to 30

              attensig=sig(nrgint-1,p)+(sig(nrgint,p)-sig(nrgint-1,p))
         1               *fac
              attenpi=pi(nrgint-1,p)+(pi(nrgint,p)-pi(nrgint-1,p))*fac
              fraction1=attensig/attentot
              fraction2=fraction1+attenpi/attentot

c Determine which interaction occured.

              rr=ran(i1)
              if (rr .lt. fraction1) then
```

```
c A Compton interaction has occured.  The energy
c of the electron is determined.

30              continue

                nrgmax=(2.0*nrgx/.511)*nrgx/(2.0*nrgx/.511+1.0) !Compton edge

                nrgint=1
                do 31 while (nrgx .gt. nrg(nrgint))
31               nrgint=nrgint+1

                frac1=(nrgx-nrg(nrgint-1))/
        1            (nrg(nrgint)-nrg(nrgint-1))
                r=ran(i1)
                ir=jifix(r*50.0)+1
                frac2=50.0*r-floatj(ir-1)

                if (ir .eq. 1) then

                  tnrg=(compton(nrgint-1,1)
        1              +(compton(nrgint,1)-compton(nrgint-1,1))*frac1)
        2              *frac2*nrgmax
                else

                  tnrg1=compton(nrgint-1,ir-1)
        1               +(compton(nrgint-1,ir)-compton(nrgint-1,ir-1))
        2               *frac2
                  tnrg2=compton(nrgint,ir-1)
        1               +(compton(nrgint,ir)-compton(nrgint,ir-1))
        2               *frac2
                  tnrg=(tnrg1+(tnrg2-tnrg1)*frac1)*nrgmax

                end if

c Test to see if the electron is greater than
c the charged particle cut off energy.  If so,
c then calculate and store the scattering
c angles and store the kinetic energy and position.

                r=6.2832*ran(i1)              !azimuth angle in particle coords.

                if (tnrg .gt. 0.1*ro) then

                  charge=charge+1

                  kinrg(charge)=tnrg

                  arg=(nrgmax-tnrg)*(2.0*nrgx/.511+1.0)/tnrg
                  g=atan(sqrt(arg)/(1.0+nrgx/.511))              !zenith angle

c Remember the incident photon's angles in the phantom system.

                  oldcal=cal
                  oldsal=sal
                  oldcbeta=cbeta
                  oldsbeta=sbeta

c Transform from the particle to the phantom coordinate system.

                  call geom(r,g,cal,sal,cbeta,sbeta)
```

```
c The energy, trigonometric information on the
c angle in the phantom coordinate system, the
c position of the electron and the type of particle
c is stored.

                  kinorder(charge)=order
                  kincal(charge)=cal
                  kinsal(charge)=sal
                  kincbeta(charge)=cbeta
                  kinsbeta(charge)=sbeta
                  kinx(charge)=xs
                  kiny(charge)=ys
                  kinz(charge)=zs

c Recall initial photon's angles.

                  cal=oldcal
                  sal=oldsal
                  cbeta=oldcbeta
                  sbeta=oldsbeta

c If the electron is less than the charged particle
c cut off energy, deposit the energy as dose.

               else
                 ro=float(phantom(i,j,k)+1000)/1000.0
                 dose(order,i,j,k)=dose(order,i,j,k)+tnrg/ro
               end if

c The scattered photon is now dealt with.

               order=order+1       !the order of scattering is incresed

c The energy and scattering angles of the scattered
c photon are determined.

               r=r-3.1416          !scattered photon has opposite azimuth angle

               arg2=1-tnrg*0.511/nrgx/(nrgx-tnrg)
               if (arg2 .le. -1.0) then
                 g=-3.1416
               else
                 g=acos(arg2)
               end if

               nrgx=nrgx-tnrg           !determine scattered photon energy

c Transform from the particle to the phantom coordinate system.

               call geom(r,g,cal,sal,cbeta,sbeta)

               go to 20         !scattered photon is followed

             else if (rr .lt. fraction2) then

c The pair production interaction has occured. First the
c energy and scattering angles of the electron are determined.

                  charge=charge+1
                  kintype(charge)=1    !signifies an electron
```

```
                    nrgmax=nrgx-1.022     !available kinetic energy

                    nrgint=1
                    do 41 while (nrgx .gt. nrg(nrgint))
41                    nrgint=nrgint+1
                    frac1=(nrgx-nrg(nrgint-1))/
          1               (nrg(nrgint)-nrg(nrgint-1))
                    r=ran(i1)
                    ir=jifix(r*50.0)+1
                    frac2=50.0*r-floatj(ir-1)
                    if (ir .eq. 1) then
                    tnrg=(pairprod(nrgint-1,1)
          1              +(pairprod(nrgint,1)-pairprod(nrgint-1,1))
          2              *frac1)*frac2*nrgmax
                    else
                    tnrg1=pairprod(nrgint-1,ir-1)
          1               +(pairprod(nrgint-1,ir)
          2               -pairprod(nrgint-1,ir-1))*frac2
                    tnrg2=pairprod(nrgint,ir-1)
          1               +(pairprod(nrgint,ir)
          2               -pairprod(nrgint,ir-1))*frac2
                    tnrg=(tnrg1+(tnrg2-tnrg1)*frac1)*nrgmax
                    end if
                    kinrg(charge)=tnrg

                    r=6.2832*ran(i1)

c This part of the program is done for both the electron
c and positron.  'V' is the ratio of total charged particle
c energy to the energy of the photon.

43                  v=(tnrg+0.511)/nrgx
                    vint=jifix(v*10.0)+1
                    g=que(vint)*alog(nrgx/.511)*.511/nrgx

c Remember the photon's angles in the phantom system

                    oldcal=cal
                    oldsal=sal
                    oldcbeta=cbeta
                    oldsbeta=sbeta

c Transform from the particle to the phantom coordinate system.

                    call geom(r,g,cal,sal,cbeta,sbeta)

c Store the order of scattering, initial charged particle phantom
c angles and position.

                    kinorder(charge)=order
                    kincal(charge)=cal
                    kinsal(charge)=sal
                    kincbeta(charge)=cbeta
                    kinsbeta(charge)=sbeta
                    kinx(charge)=xs
                    kiny(charge)=ys
                    kinz(charge)=zs

c Recall the photon's angles.

                    cal=oldcal
```

```
                    sal=oldsal
                    cbeta=oldcbeta
                    sbeta=oldsbeta

c The energy and scattering angles of the positron
c is determined after those of the electron.

                    if (kintype(charge) .eq. 1) then

                      charge=charge+1
                      kintype(charge)=-1          !signifies a positron
                      tnrg=nrgmax-tnrg
                      kinrg(charge)=tnrg

                      r=r-3.1416          !azimuth angle opposite of electron

                      go to 43            !sent to repeat calculation for positron

                    end if

                  else

c A photoelectric interaction has occurred. All of
c the photon energy is deposited as dose.

                    ro=float(phantom(i,j,k)+1000)/1000.0
                    dose(order,i,j,k)=dose(order,i,j,k)+nrgx/ro

                end if

              else

c An interaction has not occured in the element.
c The photon is transported to the far element
c wall.

                xs=xs+short*sal*cbeta
                ys=ys+short*sal*sbeta
                zs=zs+short*cal

c A test to see if the photon has left the phantom.

                if (xs .le. 0.0001 .or. xs .ge. 20.0*diml) go to 50
                if (ys .le. 0.0001 .or. ys .ge. 20.0*diml) go to 50
                if (zs .le. 0.0001 .and. cal .lt. 0.0) go to 50
                if (zs .ge. 20.0*dimlz) go to 50

                go to 21

              end if

c The photon part of the history is completed at line 50.

50      continue

c The second annhilation photon is set in motion.

        if (annhilflag .eq. 1) then

          annhilflag=0
```

```
            cal=cos(6.2832*r1-3.1416)      !this photon is
            sal=sqrt(1.0-cal*cal)          !in the opposite
            cbeta=cos(6.2832*r2-3.1416)    !direction of the first
            sbeta=sin(6.2832*r2-3.1416)    !annhilation photon.

            xs=photox
            ys=photoy
            zs=photoz

            nrgx=0.511     !photon energy assumed to be 0.511 MeV

            order=4        !treated as a multiple scatter photon

            go to 21

          end if

c The charged particles are transported. First the stored parameters
c are recalled.

          do 120 while (charge .ge. 1)

            e=kinrg(charge)                !kinetic energy

            cal=kincal(charge)             !particle's phantom angles
            sal=kinsal(charge)
            cbeta=kincbeta(charge)
            sbeta=kinsbeta(charge)

            xs=kinx(charge)                !particle's position
            ys=kiny(charge)
            zs=kinz(charge)

            order=kinorder(charge)         !order of scattering

            nrgint=24

            if (order .eq. 1)then
             chargpart=chargpart+1         !number of charged particles
            end if

c The location and distance to the element wall in the particles direction
c is determined.

            call where

            ro=floatj(phantom(i,j,k)+1000)/1000.0

c Do only while the particle's energy is above the cut-off. The cut-off
c depends on the density of the phantom element.

33          do 110 while (e .gt. 0.1*ro)

              call where

c The following statements find the distance to the voxel wall
c in the coordinate directions. The integer voxel locators are also found.

              nearx=abs(xs-floatj(i)*diml)
              nearinti=i+1
              if (nearx .gt. 0.5*diml) then
```

```
                nearx=diml-nearx
                nearinti=i-1
              end if

              neary=abs(ys-floatj(j)*diml)
              nearintj=j+1
              if (neary .gt. 0.5*diml) then
                neary=diml-neary
                nearintj=j-1
              end if

              nearz=abs(zs-floatj(k)*dimlz)
              nearintk=k+1
              if (nearz .gt. 0.5*dimlz) then
                nearz=dimlz-nearz
                nearintk=k-1
              end if

c The nearest voxel is found. The shortest distance to a voxel wall
c in the coordinate directions, 'near', is found.

              near=diml

              if (nearx .lt. near) then
                near=nearx
                neari=nearinti
                nearj=j
                neark=k
              end if

              if (neary .lt. near) then
                near=neary
                neari=i
                nearj=nearintj
                neark=k
              end if

              if (nearz .lt. near) then
                near=nearz
                neari=i
                nearj=j
                neark=nearintk
              end if

c The stopping power, 's' is found using log-linear interpolation.

              do 55 while (e .lt. nrg(nrgint))
55              nrgint=nrgint-1
              frac1=(e-nrg(nrgint))/(nrg(nrgint+1)-nrg(nrgint))
              s=stop(nrgint)+(stop(nrgint+1)-stop(nrgint))*frac1
              s=exp(s)

              ro=floatj(phantom(i,j,k)+1000)/1000.0

              maxpl=e/s/ro                        !maximum path length

              if (maxpl .lt. near) go to 112   !electron can not leave the voxel

c The scattering power, 'th' is found.

              th=tha(nrgint)+(tha(nrgint+1)-tha(nrgint))*frac1
```

```
            th=exp(th)

c 'Ep' is the amount of energy lost in the step. 'Pl' is the pathlength
c of the step.

            ep=(1-cay)*e
            pl=ep/s/ro

c If 'pl' is greater than short, then the pathlength must be shortened
c to 'short' so that the particle does not leave the voxel. If so, the
c new energy lost, 'ep', must be calculated.

            if (pl .gt. short .and. short .gt. 0.0) pl=short
            ep=pl*s*ro

            x=pl*sal*cbeta      !distance travelled during the step
            y=pl*sal*sbeta
            z=pl*cal

            xs=xs+x             !position of the particle at the end of step
            ys=ys+y
            zs=zs+z

            oldi=i      !the voxel location before the step is stored
            oldj=j
            oldk=k

            i=jifix(xs/diml)+1   !voxel location after the step
            j=jifix(ys/diml)+1
            k=jifix(zs/dimlz)+1

            e=e-ep                                          !energy after step

            g=sqrt(th*pl*ro)*gaus(jifix(100.0*ran(i1))+1)  !zenith angle

            r=6.2832*ran(i1)                                !azimuth angle

c Transform from the particle to the phantom coordinate system.

            call geom(r,g,cal,sal,cbeta,sbeta)

c The following statement checks for the edge of the phantom.

            if (xs .le. 0.0001 .or. xs .ge. 20.0*diml) go to 115
            if (ys .le. 0.0001 .or. ys .ge. 20.0*diml) go to 115
            if (zs .le. 0.0001 .and. cal .lt. 0.0) go to 115
            if (zs .ge. 20.0*dimlz) go to 115

c By finding the smallest of the old or new voxel location the correct
c voxel to assign the dose is guaranteed; even if the particle is on
c a voxel wall.

            smalli=jmin0(oldi,i)
            smallj=jmin0(oldj,j)
            smallk=jmin0(oldk,k)

c Assign the energy lost during the step as dose.

            ro=floatj(phantom(smalli,smallj,smallk)+1000)/1000.0
            dose(order,smalli,smallj,smallk)=
        1               dose(order,smalli,smallj,smallk)+ep/ro
```

```
110         continue              !charged particle transport step ends here

c The following checks to see if the nearest voxel is outside the phantom.
c If it is half of the remaining energy will be deposited as dose.

            if (neari .le. 0 .or. neari .ge. 21) then
              e=e/2.0
              go to 112
            end if

            if (nearj .le. 0 .or. nearj .ge. 21) then
              e=e/2.0
              go to 112
            end if

            if (neark .le. 0 .or. neark .ge. 21) then
              e=e/2.0
              go to 112
            end if

c 'Nearo' is the density of the nearest voxel. The remaining energy is
c assigned to the last and nearest voxel such that they both get equal
c energies.

            nearo=floatj(phantom(neari,nearj,neark)+1000)/1000.0
            dose(order,i,j,k)=dose(order,i,j,k)+e/(ro+nearo)
            dose(order,neari,nearj,neark)=
        1       dose(order,neari,nearj,neark)+e/(ro+nearo)
            go to 113

c Statement 112 and its following statement are only done if it is found
c that the particle can not leave the phantom or if the neighboring voxel
c is outside the voxel.

112         ro=floatj(phantom(i,j,k)+1000)/1000.0
            dose(order,i,j,k)=dose(order,i,j,k)+e/ro

113       continue

c The following statements are done if the charged particle was a positron.

          if (kintype(charge) .eq. -1) then

            kintype(charge)=0
            charge=charge-1
            annhilflag=1                !sets flag for the second photon

            r1=ran(i1)
            cal=cos(6.2832*r1)
            sal=sqrt(1.0-cal*cal)
            r2=ran(i1)
            cbeta=cos(6.2832*r2)
            sbeta=sin(6.2832*r2)

            nrgx=0.511

            photox=xs                   !the last position of the
            photoy=ys                   !positron must
            photoz=zs                   !be stored
```

```
            order=4                        !include annhilation photons as
                                           !multiple scatter

            go to 21

          end if

115       continue

          charge=charge-1

120       continue                !end of loop for the charged particle histories

180      continue                 !end of loop for the photon histories

200     continue                  !end of loop for the spectral bins

c The following statements normalize the dose to the maximum
c dose encountered and writes the normalized dose.

        total=0.0
        do 205 k=1,20
          do 205 j=1,20
            do 205 i=1,20
205           total=total+dose(1,i,j,k)          !total primary KERMA

c Print the beam parameters.

        write(4,*) 'Spectrum Multiplier=',multi
        write(4,*) '# Photon Histories=',history
        write(4,*) 'Shiftx=',shiftx
        write(4,*) 'Shifty=',shifty
        write(4,*) 'Primary Interaction Depth Integer=',intest
        write(4,*) 'X-Y Element Size=',dim1
        write(4,*) 'Depth Dimension=',dimlz
        write(4,*) 'Total Primary Dose=',total
        write(4,*) 'Number Of Primary Charged Particles',chargpart

        do 210 k=1,25
          do 210 j=1,25
            do 210 i=1,25
              do 210 q=1,5
                doset(i,j,k)=doset(i,j,k)+dose(q,i,j,k)  !total dose
                                                         !distribution

210     continue

c Two-dimensional primary dose distribution in the plane of the
c primary pencil beam. The dose is normalized to the total primary KERMA.

        write(4,*) 'Coronal Primary Dose Slice'
        do 215 k=1,20
          do 212 i=1,20
212         arr(i)=dose(1,i,11,k)/total
215       write (4,650) (arr(i),i=5,17)

c Three-dimensional total dose distribution normalized to the primary KERMA.

        do 229 k=1,20
          write(4,*)' '
          write(4,580) k
```

```
          do 225 j=1,20
            do 224 i=1,20
224           arr(i)=doset(i,j,k)/total
225         write(4,650) (arr(i),i=5,17)

c Three-dimensional distributions of the primary KERMA
c normalized dose components.

          do 229 q=1,4
            write(4,*) ' '
            if (q .eq. 1)then
              write(4,*) 'Primary Dose'
            else if (q .eq. 2) then
              write(4,*) 'First Scatter Dose'
            else if (q .eq. 3) then
              write(4,*) 'Second Scatter Dose'
            else if (q .eq. 4) then
              write(4,*) 'Multiple Scatter Dose'
            end if
            do 228 j=1,20
              do 227 i=1,20
227             arr(i)=dose(q,i,j,k)/total
228     write(4,650) (arr(i),i=5,17)
229     continue

c Three-dimensional distribution of the primary KERMA
c normalized total scatter dose.

        write(4,*) 'Total Scatter Dose'
        do 245 k=1,20
          write (4,*)' '
          write(4,580) k
          do 245 j=1,20
            do 244 i=1,20
244           arr(i)=(doset(i,j,k)-dose(1,i,j,k))/total
245         write(4,650) (arr(i),i=5,17)

c Three-dimensional distribution of the primary KERMA
c normalized primary plus first scatter dose.

        write(4,*) 'Primary + First'
        do 247 k=1,20
          write (4,*)' '
          write(4,580) k
          do 247 j=1,20
            do 246 i=1,20
246           arr(i)=(dose(1,i,j,k)+dose(2,i,j,k))/total
247         write(4,650) (arr(i),i=5,17)

250     format(' ',i3,2x,f6.2)
340     format(' ',f5.2,2x,f5.2)
345     format(' ',i2)
350     format(' ',10(f4.2,2x))
420     format(' ',e10.4)
422     format(e10.4)
550     format(' ',10(1x,f6.4))
570     format(' ',f5.2,1x,3(f6.4,1x),2(f6.3,1x))
580     format('*****************************k=',i2,'*****************')
650     format(' ',20(1x,e8.3))
655     format(' ',1x,a1,3x,a4,4x,a14,2x,a7,4x,a5,3x,a6,2x,a8)
750     format(' ',i2,2x,f5.3,8x,f4.3,6x,4(4x,f5.3))
```

```
      close(1)
      close(4)
      close(6)
      close(8)
      close(11)
      close(12)

      stop
      end


          subroutine geom(r,g,cal,sal,cbeta,sbeta)

c This subroutine performs the rotational transformations between
c the coordinate system 'attached' to the particle and the system
c 'attached' to the phantom.

          real r,g,cal,sal,cbeta,sbeta
          real ss,cc,oldcal,oldsal,oldcbeta,oldsbeta

c 'G' and 'r' are the sine and cosine respectively in the particle system.
c 'Sal' and 'cal' are the sine and cosine respectively of the zenith
c angle in the phantom system.  'Sbeta' and cbeta are the sine and
c cosine respectively of the azimuth angle in the phantom system.

          if (g .eq. 0.0) go to 400

          oldsal=sal
          oldcal=cal
          oldcbeta=cbeta
          oldsbeta=sbeta

          cal=cal*cos(g)-sal*sin(g)*cos(r)

          if (abs(cal) .ge. 1.0) then
            cal=1.0*sign(1.0,cal)
            sal=0.0
            cbeta=cos(r)
            sbeta=sin(r)
            go to 400
          end if

          sal=sqrt(1.0-cal*cal)

          if (oldsal .eq. 0.0) then
            cbeta=cos(r)
            sbeta=sin(r)
            go to 400
          end if

          ss=sin(g)*sin(r)/sal
          cc=(sin(g)*cos(r)*oldcal+cos(g)*oldsal)/sal

          if (abs(ss) .ge. 1.0) then
           ss=1.0*sign(1.0,ss)
          end if

          if (abs(cc) .ge. 1.0) then
           cc=1.0*sign(1.0,cc)
          end if
```

```
            cbeta=cc*oldcbeta-ss*oldsbeta
            sbeta=ss*oldcbeta+cc*oldsbeta

            if (abs(cbeta) .ge. 1.0) cbeta=1.0*sign(1.0,cbeta)
            if (abs(sbeta) .ge. 1.0) sbeta=1.0*sign(1.0,sbeta)

400         continue

            return
            end


        subroutine where

c This subroutine finds the position and distance to the voxel boundary
c in the particle direction.

        real xs,ys,zs,short,diml,dimlz
        real cbeta,sbeta,cal
        real lx,ly,lz
        integer i,j,k,ib,jb,kb
        common xs,ys,zs,i,j,k,cbeta,sbeta,cal,sal,diml,dimlz,short

c Determine which element the photon is in.

            i=jifix(xs/diml)+1
            j=jifix(ys/diml)+1
            k=jifix(zs/dimlz)+1

c Determine the position of the voxel's walls in the
c direction in which the pazrticle is headed.

            if (sal .eq. 0.0 .or. cbeta .eq. 0.0) then
              lx=999.9*diml
              go to 10
            end if

            if (cbeta .lt. 0.0) then
              if (xs .eq. (floatj(i-1))*diml) then
                lx=(floatj(i-2)*diml-xs)/sal/cbeta
              else
                lx=(floatj(i-1)*diml-xs)/sal/cbeta
              end if
            else
              lx=(floatj(i)*diml-xs)/sal/cbeta
            end if

10          if (sal .eq. 0.0 .or. sbeta .eq. 0.0) then
              ly=999.9*diml
              go to 20
            end if

            if (sbeta .lt. 0.0) then
              if (ys .eq. (floatj(j-1))*diml) then
                ly=(floatj(j-2)*diml-ys)/sal/sbeta
              else
                ly=(floatj(j-1)*diml-ys)/sal/sbeta
              end if
            else
              ly=(floatj(j)*diml-ys)/sal/sbeta
```

```
            end if

20          if (cal .eq. 0.0) then
              lz=999.9*dimlz
              go to 30
            end if

            if (cal .lt. 0.0) then
              if (zs .eq. (floatj(k-1))*dimlz) then
                lz=(floatj(k-2)*dimlz-zs)/cal
              else
                lz=(floatj(k-1)*dimlz-zs)/cal
              end if
            else
              lz=(floatj(k)*dimlz-zs)/cal
            end if

c Determine the distance to the wall that the particle
c in the direction of the particle.
.
30          short=lz
            if (ly .lt. short) short=ly
            if (lx .lt. short) short=lx

        return
        end
```

Appendix 11. Listing of the program Volve.for

```
      Program Volve

c This program convolves the fluence with dose spread arrays to
c yield a dose distribution. It is carried out in "the interaction
c point of view". The primary and truncated first scatter (TFS)
c dose spread arrays are combined. This fine resolution dose spread
c array is is convolved first. Then a lower resolution, residual
c first and multiple scatter dose spread array is convolved. The
c homogeneous and heterogeneous dose distribution is calculated
c separately and a correction factor is determined at the end. The
c dose due to contamination is included. The dose distribution
c can be smoothed. The variables are documented where they occur.
c Lines which have been "commented out" are optional.

      integer albnd,aubnd,blbnd,bubnd,depth,lbndi,ubndi
      integer albnd2,aubnd2,blbnd2,bubnd2,depth2
      integer lbndi2,ubndi2
      integer lbndj,ubndj,lbndk,ubndk
      integer lbndj2,ubndj2,lbndk2,ubndk2
      integer width1,height1,length1
      integer i,j,k,ii,jj,kk,deli,delj,delk
      integer clipwid,cliphei,cliplen,roe,roe2,kprime

      real mu,ro(-25:25,-25:25,50),ro2(-5:5,-5:5,10)
      real invsqr,ssd,dref
      real spray1(5,-6:6,-6:6,-2:12)
      real rfmspray(5,-6:6,-6:6,-2:12)
      real fluxinc,fluxfact
      real avdens,avdens2,avspray
      real dosehet(-25:25,-25:25,50),dosehet2(-5:5,-5:5,0:10)
      real dosehom(-25:25,-25:25,50),dosehom2(-5:5,-5:5,0:10)
      real kerma(50),kerma2(10)
      real oldkerma,cf(-25:25,-25:25,50),kermhet,kermhom
      real arrcf(20),arrhom(20),arrhet(20)
      real f0,f1,f2,c1,c2,row
      real hom(-25:25,-25:25,50),het(-25:25,-25:25,50)
      real contam(0:50,2),avcontam(2),resolv

      common deli,delj,delk,i,j,k,ro,avdens

c Spray.dat contains the primary plus truncated first scatter (TFS)
c dose spread arrays.

c Cf.dat contains the output homogeneous and  heterogeneous dose
c distributions and the correction factor distribution.

c Rfmspray.dat contains the residual first and multiple scatter (RFMS)
c dose spread arrays.

      open(unit=1,status='old',file='spray.dat')
      open(unit=3,status='new',file='cf.dat')
      open(unit=4,status='old',file='rfmspray.dat')

c User requested statements. A slab geometry is modelled by a cubic
c water-like phantom. The beam is parallel.

      ssd=100.0         !source to surface distance
      dref=3.5          !dmax
      resolv=1.0        !specifies voxel size for contamination calculation
```

```
        albnd=-4          !beam half-width in negative x-direction
        aubnd=4           !beam half-width in positve x-direction
        blbnd=-4          !beam half-width in negative y-direction
        bubnd=4           !beam half-width in positive y-direction
        depth=20          !phantom depth

c The calculation windows may be 1,2 or 3-dimensional.

c 3-Dimensional

c       lbndi=albnd       !calculation window in negative x-direction
c       ubndi=aubnd       !calculation window in positive x-direction
c       lbndj=blbnd       !calculation window in negative y-direction
c       ubndj=bubnd       !calculation window in positive y-direction
c       lbndk=1           !lower calculation window in z-direction
c       ubndk=depth       !upper calculation window in z-direction

c 2-Dimensional (in the plane of the central axis)

        lbndi=albnd-1     !calculation window in negative x-direction
        ubndi=aubnd+1     !calculation window in positive x-direction
        lbndj=0           !calculation window in negative y-direction
        ubndj=0           !calculation window in positive y-direction
        lbndk=1           !lower calculation window in z-direction
        ubndk=depth       !upper calculation window in z-direction

c 1-Dimensional (off axis at a specified depth)

c       lbndi=albnd-1     !calculation window in negative x-direction
c       ubndi=aubnd+1     !calculation window in positive x-direction
c       lbndj=0           !calculation window in negative y-direction
c       ubndj=0           !calculation window in positive y-direction
c       lbndk=16          !lower calculation window in z-direction
c       ubndk=16          !upper calculation window in z-direction

c 1-Dimensional (along the central axis)

c       lbndi=0           !calculation window in negative x-direction
c       ubndi=0           !calculation window in positive x-direction
c       lbndj=0           !calculation window in negative y-direction
c       ubndj=0           !calculation window in positive y-direction
c       lbndk=1           !lower calculation window in z-direction
c       ubndk=depth       !upper calculation window in z-direction

c       clipwid=2         !a parameter for delimiting width of dose spread array
c       cliphei=0         !delimits height (delk=negative)
c       cliplen=0         !delimits length (delk=positive)

c Read statements. Read height, length, width, and values of the
c dose spread arrays, and the density array.

        read(1,3000) height1,length1,width1
         do 100 n=1,5
          read(1,*)
          read(4,*)
          do 100 k=-height1,length1
           read(1,*)
           read(1,*)
           read(4,*)
           read(4,*)
           do 100 j=-width1,width1
```

```
            read(1,3010) (spray1(n,i,j,k),i=-width1,width1)
            read(4,3010) (rfmspray(n,i,j,k),i=-width1,width1)
100     continue

        read (4,*)
        read (4,*)
        do 125 n=1,5
         read (4,*)
         read (4,*)
         do 125 k=-1,3
          read (4,*)
          do 125 j=-1,1
           read (4,3010) (rfmspray(n,i,j,k),i=-1,1)
125     continue

c The relative fluence in a homogeneous
c phantom as a function of depth is calculated.

        kerma(1)=1.00
        mu=0.031
        atten=exp(-mu)
        do 150 k=2,depth+1
         kerma(k)=kerma(k-1)*atten
150     continue

c "Contam(depth,region)" is the measured depth dependence of contamination.
c The depth is measured in centimeters. Region=1 is inside the field.
c Region=2 is outside the field. See Volume 1 and Equation 7.4.9 in
c Volume 2.

        contam(0,1)=1.00
        contam(1,1)=0.89
        contam(2,1)=0.50
        contam(3,1)=0.28
        contam(4,1)=0.18
        contam(5,1)=0.12
        contam(6,1)=0.10

        contam(0,2)=1.00
        contam(1,2)=0.94
        contam(2,2)=0.64
        contam(3,2)=0.44
        contam(4,2)=0.37
        contam(5,2)=0.33
        contam(6,2)=0.30

c Beyond dmax the contamination decreases exponentially.

        atten=exp(-0.050)
        do 175 n=1,2
         do 175 k=7,50
          contam(k,n)=contam(k-1,n)*atten
175     continue

c The following statements describe a slab phantom. The central slab can be
c made up of two regions.

        do 200 k=1,15
         do 200 j=-25,25
          do 200 i=-25,25
           ro(i,j,k)=1.0
```

```
200     continue

        do 220 k=16,23
         do 220 j=-25,25
          do 220 i=-25,3
           ro(i,j,k)=0.3
220     continue

        do 230 k=16,23
         do 230 j=-25,25
          do 230 i=4,25
           ro(i,j,k)=0.3
230     continue

        do 240 k=24,50
         do 240 j=-25,25
          do 240 i=-25,25
           ro(i,j,k)=1.0
240     continue

c Convolve for all pencil beams at all depths by summing over all primary
c interaction voxels. "Fluxfact" is the ratio of heterogeneous to homo-
c geneous fluence at a point in a pencil beam.

        do 600 i=albnd-1,aubnd+1          !increment in the x-direction
         ii=jnint(floatj(i)/5.0)          !for RFMS in the x-direction

         do 600 j=blbnd-1,bubnd+1         !increment in the y-direction
          jj=jnint(floatj(j)/5.0)         !for RFMS in the y-direction

c The pencil beams just outside the field can be given a smaller fluence.
c This can account for a geometrical penumbra. 'Fluxinc is the incident
c relative fluence.

c          if (i .eq. albnd-1 .or. i .eq. aubnd+1 .or.
c       1      j .eq. blbnd-1 .or. j .eq. bubnd+1 ) then
c           fluxinc=0.20
c          else
c           fluxinc=1.00
c          end if

c The following can describes a bar shield.

c          if (i .eq. -1 .or. i .eq. 0 .or. i .eq. 1) then
c           fluxinc=0.031
c          end if

           fluxfact=1.00          !fluxfact is the fluence compared to a
                                  !homogeneous phantom

           do 600 k=1,depth       !increment depth (z-direction)
            kk=(k-1)/5+1          !for RFMS in the z-direction

c An inverse square factor can reduce the primary fluence.

c           invsqr=(ssd+dref)**2/
c       1          ((ssd+floatj(k)-.5)**2+
c       2          (floatj(j))**2+(floatj(i))**2)

            invsqr=1.0
```

```
c "Kermhom" and "kermhet" are factors dependent only on the point
c of interaction of the primary fluence.

           kermhom=kerma(k)*invsqr*fluxinc
           kermhet=kermhom*ro(i,j,k)*fluxfact

c Sum over all contributions of the fine resolution dose spread array
c by summing over all dose deposition voxels.

           do 500 deli=-width1+clipwid,width1-clipwid
            do 500 delj=-width1+clipwid,width1-clipwid
             do 500 delk=-height1+cliphei,length1-cliplen

c If the contribution is outside the dose calculation window
c don't bother summing.

              if (i+deli .lt. lbndi) go to 500
              if (i+deli .gt. ubndi) go to 500
              if (j+delj .lt. lbndj) go to 500
              if (j+delj .gt. ubndj) go to 500
              if (k+delk .lt. lbndk) go to 500
              if (k+delk .gt. ubndk) go to 500

c Subroutine "averdens" returns "avdens", the average density
c between the primary interaction and dose deposition voxels.
c "Roe" is an integer identifying a dose spread array obtained for
c a specific density (roe=1 for a physical density of 0.2 g/cm**3,
c roe=2 for 0.4 g/cm**3 ... roe=5 for 1.0 g/cm**3)

              call averdens

c "Avspray" is the dose/KERMA value linearly interpolated between dose
c spread arrays at fixed densities.

              avspray=spray1(roe,deli,delj,delk)+
     1                (spray1(roe+1,deli,delj,delk)-
     2                spray1(roe,deli,delj,delk))*
     3                (5.0*avdens-floatj(roe))

c Second order interpolation can be used if desired.

c             if (avdens .eq. 1.0) then
c              avspray=spray1(5,deli,delj,delk)
c             else
c              if (avdens .ge. 0.6) then
c               f0=spray1(roe-1,deli,delj,delk)
c               f1=spray1(roe,deli,delj,delk)
c               f2=spray1(roe+1,deli,delj,delk)
c              row=(avdens*5.0-floatj(roe))/5.0+0.2
c              else
c               f0=spray1(roe,deli,delj,delk)
c               f1=spray1(roe+1,deli,delj,delk)
c               f2=spray1(roe+2,deli,delj,delk)
c               row=(avdens*5.0-floatj(roe))/5.0
c              end if

c              c1=(row/0.2)*(-3.0*f0+4.0*f1-f2)/2.0
c              c2=(row/0.2)**2*(f0-2.0*f1+f2)/2.0

c              avspray=f0+c1+c2
```

```
c              end if

c "Dosehet" is the heterogeneous dose.

               dosehet(i+deli,j+delj,k+delk)=
     1              dosehet(i+deli,j+delj,k+delk)+
     2              kermhet/avdens*avspray

c "Dosehom" is the homogeneous dose.

               dosehom(i+deli,j+delj,k+delk)=
     1              dosehom(i+deli,j+delj,k+delk)+
     2              kermhom*spray1(5,deli,delj,delk)

500           continue

          fluxfact=fluxfact*exp(mu*(1.0-ro(i,j,k))) !cumulative relative fluence

          avdens2=avdens2+ro(i,j,k)                  !density sum for RFMS

         ro2(ii,jj,kk)=ro2(ii,jj,kk)+ro(i,j,k)   !for RFMS average voxel density

600      continue

c At this point the primary plus truncated first scatter dose spread arrays
c have been convolved. The residual first and multiple scatter (RFMS) dose
c spread array is now convolved.

         albnd2=jnint(floatj(albnd-1)/5.0)        !field boundaries
         aubnd2=jnint(floatj(aubnd+1)/5.0)
         blbnd2=jnint(floatj(blbnd-1)/5.0)
         bubnd2=jnint(floatj(bubnd+1)/5.0)
         depth2=(depth-1)/5.0+1

         lbndi2=jnint(floatj(lbndi)/5.0)-1        !dose calculation window
         ubndi2=jnint(floatj(ubndi)/5.0)+1
         lbndj2=jnint(floatj(lbndj)/5.0)-1
         ubndj2=jnint(floatj(ubndj)/5.0)+1
         lbndk2=0
         ubndk2=(ubndk-1)/5+2

c Calculation of fluence in a homogeneous phantom taking into account
c the coarser resolution.

         kerma2(1)=1.00
         do 700 k=2,depth2+1
          atten=exp(-mu*5.0)
          kerma2(k)=kerma2(k-1)*atten
700      continue

c Calculate the average density in the irradiated portion of the phantom.

         avdens2=avdens2/
         1     ((aubnd-albnd+3)*(bubnd-blbnd+3)*depth)

         roe=jifix(avdens2*5.0)

         roe2=(5.0*avdens2-floatj(roe))

         do 1200 i=albnd2,aubnd2          !increment in x-direction
```

```
          do 1200 j=blbnd2,bubnd2        !increment in y-direction

           fluxinc=1.00

c Calculate the fluence near the field boundary if the geometrical
c penumbra is being taken into account.

c           if (i .eq. aubnd2) then
c            fluxinc=(floatj(jabs(aubnd)+3)
c       1           /5.0-floatj(jabs(i)))*fluxinc
c           else if (i .eq. albnd2) then
c            fluxinc=(floatj(jabs(albnd)+3)
c       1           /5.0-floatj(jabs(i)))*fluxinc
c           end if
c
c           if (j .eq. bubnd2) then
c            fluxinc=(floatj(jabs(bubnd)+3)
c       1           /5.0-floatj(jabs(j)))*fluxinc
c           else if (j .eq. blbnd2) then
c            fluxinc=(floatj(jabs(blbnd)+3)
c       1           /5.0-floatj(jabs(j)))*fluxinc
c           end if

c The following is used with the bar shield.

c           if (i .eq. 0) then
c            fluxinc=0.40
c           end if


c The following is used with a wedge.

c           fluxinc=fluxinc*0.5*floatj(i-albnd2)/
c       1        floatj(aubnd2-albnd2)+0.5*fluxinc

           do 1200 k=1,depth2     !increment depth (z-direction) along
                                  !pencil beam

c Used with the inclusion of inverse square attenuation.

c            invsqr=(ssd+dref)**2/
c       1       .   ((ssd+5.0*floatj(k)-2.5)**2+
c       2           (5.0*floatj(j))**2+(5.0*floatj(i))**2)

            invsqr=1.00

            ro2(i,j,k)=ro2(i,j,k)/125.0          !finish average voxel density

            kermhom=kerma2(k)*invsqr*fluxinc     !homogeneous fluence

            kermhet=kermhom*ro2(i,j,k)      !heterogeneous fluence*voxel density

c Sum over all contributions of the RFMS dose spread array by summing
c over all dose deposition voxels.

            do 1100 deli=-width1,width1
             do 1100 delj=-width1,width1
              do 1100 delk=-height1,length1

               if (i+deli .lt. lbndi2) go to 1100        !inside dose window?
               if (i+deli .gt. ubndi2) go to 1100
```

```
              if (j+delj .lt. lbndj2) go to 1100
              if (j+delj .gt. ubndj2) go to 1100
              if (k+delk .lt. lbndk2) go to 1100
              if (k+delk .gt. ubndk2) go to 1100

c Interpolate the heterogeneous dose spread array.

              avspray=rfmspray(roe,deli,delj,delk)+
             1              (rfmspray(roe+1,deli,delj,delk)-
             2               rfmspray(roe,deli,delj,delk))*roe2

              dosehet2(i+deli,j+delj,k+delk)=            !increment hetero dose
             1       dosehet2(i+deli,j+delj,k+delk)+
             2       kermhet/avdens2*avspray

              dosehom2(i+deli,j+delj,k+delk)=            !increment homo dose
             1       dosehom2(i+deli,j+delj,k+delk)+
             2       kermhom*rfmspray(5,deli,delj,delk)

1100        continue

1200     continue

c Print the primary plus TFS dose before smoothing.

         write(3,*)'Homogeneous Dose Before Smoothing (No Multiple)'
         do 1202 k=lbndk,ubndk
          write(3,*)'******** k=',k,'********'
          do 1201 j=lbndj,ubndj
           do 1201 i=lbndi,ubndi
            arrhom(i)=dosehom(i,j,k)
1201       continue
           write(3,3100)(arrhom(i),i=lbndi,ubndi)
1202     continue

         write(3,*)'Heterogeneous Dose Before Smoothing (No Multiple)'
         do 1204 k=lbndk,ubndk
          write(3,*)'******** k=',k,'********'
          do 1203 j=lbndj,ubndj
           do 1203 i=lbndi,ubndi
            arrhet(i)=dosehet(i,j,k)
1203       continue
           write(3,3100)(arrhet(i),i=lbndi,ubndi)
1204     continue

c "9-point" smoothing.

c        j=0
c        delj=0
c        do 1210 k=lbndk+1,ubndk-1
c          do 1210 i=lbndi+1,ubndi-1
c           do 1210 deli=i-1,i+1
c             do 1210 delk=k-1,k+1
c              het(i,j,k)=het(i,j,k)+dosehet(deli,delj,delk)
c              hom(i,j,k)=hom(i,j,k)+dosehom(deli,delj,delk)
1210     continue

c        do 1220 k=lbndk+1,ubndk-1
c          do 1220 i=lbndi+1,ubndi-1
c            dosehet(i,j,k)=het(i,j,k)/9.0
c            dosehom(i,j,k)=hom(i,j,k)/9.0
```

```
c            het(i,j,k)=0.0
c            hom(i,j,k)=0.0
1220     continue

c Print the primary plus TFS dose after smoothing.

c        write(3,*)'Homogeneous Dose After Smoothing (No Multiple)'
c        do 1250 k=lbndk,ubndk
c         write(3,*)'******** k=',k,'********'
c         do 1250 j=lbndj,ubndj
c          do 1225 i=lbndi,ubndi
c           arrhom(i)=dosehom(i,j,k)
1225       continue
c          write(3,3100)(arrhom(i),i=lbndi,ubndi)
1250     continue

c        write(3,*)'Heterogeneous Dose After Smoothing (No Multiple)'
c        do 1300 k=lbndk,ubndk
c         write(3,*)'******** k=',k,'********'
c         do 1300 j=lbndj,ubndj
c          do 1275 i=lbndi,ubndi
c           arrhet(i)=dosehet(i,j,k)
1275       continue
c          write(3,3100)(arrhet(i),i=lbndi,ubndi)
1300     continue

c Print the phantom and voxel densities used for the RFMS convolution.

c        write(3,*)'Average Phantom Density',avdens2

c        write(3,*)'Average Voxel Density'
c        do 1310 k=lbndk2+1,ubndk2-1
c         write(3,*)'******** k=',k,'********'
c         do 1310 j=lbndj2+1,ubndj2-1
c          do 1305 i=lbndi2+1,ubndi2-1
c           arrhom(i)=ro2(i,j,k)
1305       continue
c          write(3,3100)(arrhom(i),i=lbndi2+1,ubndi2-1)
1310     continue

c Print the RFMS dose distribution.

c        write(3,*)'Homogeneous Multiple Dose'
c        do 1350 k=lbndk2,ubndk2
c         write(3,*)'******** k=',k,'********'
c         do 1350 j=lbndj2,ubndj2
c          do 1325 i=lbndi2,ubndi2
c           arrhom(i)=dosehom2(i,j,k)
1325       continue
c          write(3,3100)(arrhom(i),i=lbndi2,ubndi2)
1350     continue

c        write(3,*)'Heterogeneous Multiple Dose'
c        do 1400 k=lbndk2,ubndk2
c         write(3,*)'******** k=',k,'********'
c         do 1400 j=lbndj2,ubndj2
c          do 1375 i=lbndi2,ubndi2
c           arrhet(i)=dosehet2(i,j,k)
1375       continue
c          write(3,3100)(arrhet(i),i=lbndi2,ubndi2)
1400     continue
```

```
c Add the RFMS dose distribution on to the primary plus RFS dose
c distribution. Calculate the radiological depth for inclusion
c of the contamination dose.

        j=0
        delj=0
        do 1500 k=lbndk,ubndk
          do 1500 i=lbndi,ubndi
           do 1500 deli=i-2,i+2
             do 1500 delk=k-2,k+2
              het(i,j,k)=het(i,j,k)
     1          +dosehet2(jnint(floatj(deli)/5.0)
     2          ,jnint(floatj(delj)/5.0)
     3          ,(delk-1)/5+1)

              hom(i,j,k)=hom(i,j,k)
     1          +dosehom2(jnint(floatj(deli)/5.0)
     2          ,jnint(floatj(delj)/5.0)
     3          ,(delk-1)/5+1)

1500    continue

        do 1575 i=lbndi,ubndi
          avdens=0.0
          do 1575 k=lbndk,ubndk

            dosehet(i,j,k)=het(i,j,k)/25.0+dosehet(i,j,k)
            dosehom(i,j,k)=hom(i,j,k)/25.0+dosehom(i,j,k)

           avdens=avdens+ro(i,j,k)                        !radiological depth

           do 1550 n=1,2

            avcontam(n)=contam(jifix(avdens),n)+          !calculate the
     1                 (contam(jifix(avdens)+1,n)-       !contamintion
     2                  contam(jifix(avdens),n))*        !at the radiological
     3                  (avdens-floatj(jifix(avdens)))   !depth

1550    continue

c Calculate the contamination dose. The contamination dose has a Gaussian
c dependence on position in the field from the central axis, a linear increase
c with field size and a depth dependence found from a look-up table.

           if (i .ge. albnd .or. i .le. aubnd) then

            dosehet(i,j,k)=dosehet(i,j,k)+
     1          avcontam(1)*sqrt(floatj((aubnd-albnd)*
     2          (bubnd-blbnd)))*0.01*resolv

            dosehom(i,j,k)=dosehom(i,j,k)+
     1          contam(k,1)*sqrt(floatj((aubnd-albnd)*
     2          (bubnd-blbnd)))*0.01

           else

            dosehet(i,j,k)=dosehet(i,j,k)+
     1          avcontam(2)*sqrt(floatj((aubnd-albnd)*
     2          (bubnd-blbnd)))*0.01*resolv*
     3          exp(-2.0*floatj(i*i)/(floatj(aubnd-albnd))**2)*
```

```
     4       * exp(-2.0*float(j*j)/(float(bubnd-blbnd))**2)

          dosehom(i,j,k)=dosehom(i,j,k)+
     1        contam(k,2)*sqrt(float((aubnd-albnd)*
     2        (bubnd-blbnd)))*0.01*
     3        exp(-2.0*float(i*i)/(float(aubnd-albnd))**2)*
     4        exp(-2.0*float(j*j)/(float(bubnd-blbnd))**2)

          end if

1575    continue

c Calculate and print the correction factor.

        write(3,*)'Correction Factor'
        do 1800 k=lbndk,ubndk
         write(3,*)'******** k=',k,'********'
         do 1800 j=lbndj,ubndj
          do 1700 i=lbndi,ubndi
           cf(i,j,k)=dosehet(i,j,k)/dosehom(i,j,k)
           arrcf(i)=cf(i,j,k)
           arrhom(i)=dosehom(i,j,k)
           arrhet(i)=dosehet(i,j,k)
1700      continue
          write(3,3100)(arrcf(i),i=lbndi,ubndi)
1800    continue

        write(3,*)'Total Smoothed Homogeneous Dose'
        do 2000 k=lbndk,ubndk
         write(3,*)'******** k=',k,'********'
         do 2000 j=lbndj,ubndj
          do 1900 i=lbndi,ubndi
           arrhom(i)=dosehom(i,j,k)
1900      continue
          write(3,3100)(arrhom(i),i=lbndi,ubndi)
2000    continue

        write(3,*)'Total Smoothed Heterogeneous Dose'
        do 2200 k=lbndk,ubndk
         write(3,*)'******** k=',k,'********'
         do 2200 j=lbndj,ubndj
          do 2100 i=lbndi,ubndi
           arrhet(i)=dosehet(i,j,k)
2100      continue
          write(3,3100)(arrhet(i),i=lbndi,ubndi)
2200    continue

3000    format(' ',3(i2,1x))
3010    format(' ',25(f8.6,1x))
3020    format(25(f4.2,1x))
3060    format(f5.1)
3070    format(' ',f6.3)
3100    format(' ',25(f5.3,1x))

        stop
        end


        subroutine averdens

c An integral differential analyzer algorithm to find the average
```

```
c density along a path between the primary interaction and dose
c deposition voxels. The algorithm samples the density along
c regular increments along the path.

        integer i,j,k,deli,delj,delk,longest

        real ro(-25:25,-25:25,50),avdens,xinc,yinc,zinc
        real scale,denom

        common deli,delj,delk,i,j,k,ro,avdens

        if (deli .eq. 0 .and. delj .eq. 0 .and. delk .eq. 0) then
         avdens=ro(i,j,k)
         go to 200
        end if

c The longest dimension between the interaction and dose deposition
c sites is found.

        longest=jmax0(abs(deli),abs(delj),abs(delk))

c The increments in each direction between the sample points.

        xinc=floatj(deli)/floatj(longest)
        yinc=floatj(delj)/floatj(longest)
        zinc=floatj(delk)/floatj(longest)

c The weight of the interaction voxel in the average density can
c be varied for different dose deposition voxel locations.

        if (deli .eq. 0 .and. delj .eq. 0) then
         f=0.5
        else if(jnint(sqrt(floatj(deli*deli+delj*delj))) .eq. 1)then
         f=0.5
        else if(jnint(sqrt(floatj(deli*deli+delj*delj))) .eq. 2)then
         f=0.5
        else
         f=0.5
        end if

        avdens=0.0

        do 100 n=0,longest
          scale=0.5+f
          if (n .eq. 0) then
           avdens=avdens+ro(i+n*xinc,j+n*yinc,k+jnint(n*zinc))*f
          else if (n .eq. longest) then
           avdens=avdens+ro(i+n*xinc,j+n*yinc,k+jnint(n*zinc))*0.5
          else
           avdens=avdens+ro(i+n*xinc,j+n*yinc,k+jnint(n*zinc))
          end if

100     continue

        avdens=avdens/(floatj(longest-1)+scale)  !divide by the # of sample pts

200     continue

        return
        end
```

Appendix 12. Comparison of Heterogeneous Dose Spread Arrays Calculated by the Convolution Method and by the Monte Carlo Method

Table A

	Δi							
	-3	-2	-1	0	1	2	3	
0	-	-	.012	.329	.012	-	-	
	-	-	.012	.328	.011	-	-	$\rho = 1.0 g/cm^3$
1	-	.001	.034	.306	.034	.001	-	$\rho = 0.3 g/cm^3$
	-	.002	.035	.281	.035	.002	-	
2	-	.003	.032	.137	.032	.003	-	
	.001	.004	.033	.124	.033	.004	.001	
Δk								
3	.001	.004	.024	.067	.024	.004	.001	
	.001	.005	.023	.061	.023	.004	.001	
4	.001	.005	.019	.038	.019	.005	.001	
	.002	.005	.017	.032	.016	.005	.002	
5	.002	.005	.013	.021	.013	.005	.002	
	.002	.005	.012	.018	.012	.005	.002	
6	.001	.004	.008	.012	.008	.004	.001	
	.002	.004	.008	.011	.008	.004	.002	

Upper Number Is Calculated From Homogeneous Dose Spread Arrays.
Lower Number Is From Monte Carlo Simulation Of The Heterogeneous Phantom.

Energy Conserved To -2.8%

Table B

Δk \ Δi	-3	-2	-1	0	1	2	3	
0	-	-	.012	.329	.012	-	-	
	-	-	.012	.327	.012	-	-	ρ = 1.0g/cm^3
1	-	.002	.036	.320	.036	.002	-	ρ = 0.2g/cm^3
	-	.003	.037	.290	.037	.003	-	
2	.001	.003	.038	.159	.038	.003	.001	
	.001	.005	.036	.135	.036	.005	.001	
3	.001	.005	.028	.081	.028	.005	.001	
	.002	.006	.028	.072	.028	.006	.002	
4	.002	.006	.023	.048	.023	.006	.002	
	.002	.006	.020	.041	.020	.006	.002	
5	.002	.005	.016	.029	.016	.005	.002	
	.002	.005	.014	.024	.014	.005	.002	
6	.002	.005	.011	.018	.011	.005	.002	
	.002	.005	.010	.015	.010	.005	.002	

Upper Number Is Calculated From Homogeneous Dose Spread Arrays.
Lower Number Is From Monte Carlo Simulation Of The Heterogeneous Phantom.

Energy Conserved To -1.3%

Table C

Δk \ Δi	-3	-2	-1	0	1	2	3	
0	- -	- -	.012 .012	.329 .329	.012 .011	- -	- -	
1	- -	.001 .001	.025 .025	.239 .239	.025 .025	.001 .001	- -	$\rho = 1.0 g/cm^3$
2	- .001	.002 .003	.023 .021	.086 .074	.023 .021	.002 .003	- .001	$\rho = 0.3 g/cm^3$
3	- .001	.003 .004	.018 .016	.044 .032	.018 .016	.003 .004	- .001	
4	.001 .001	.003 .004	.013 .010	.023 .016	.013 .010	.003 .004	.001 .001	
5	.001 .001	.003 .003	.007 .006	.012 .008	.007 .006	.003 .003	.001 .001	
6	.001 .001	.002 .002	.005 .004	.007 .004	.005 .004	.002 .002	.001 .001	

Upper Number Is Calculated From Homogeneous Dose Spread Arrays.
Lower Number Is From Monte Carlo Simulation Of The Heterogeneous Phantom.

Energy Conserved To -2.1%

Table D

Δk \ Δi	-3	-2	-1	0	1	2	3
0	-	-	.012	.329	.012	-	-
	-	-	.012	.329	.011	-	-
1	-	.001	.025	.239	.025	.001	-
	-	.001	.025	.238	.025	.001	-
2	-	.001	.020	.073	.020	.001	-
	.001	.001	.020	.073	.020	.001	-
3	-	.001	.011	.027	.011	.001	-
	-	.002	.010	.022	.010	.002	-
4	-	.002	.007	.013	.007	.002	-
	-	.002	.005	.009	.005	.002	-
5	-	.001	.004	.007	.004	.001	-
	.001	.001	.003	.004	.003	.001	-
6	.001	.001	.003	.004	.003	.001	-
	.001	.001	.002	.002	.002	.001	.001

Upper Number Is Calculated From Homogeneous Dose Spread Arrays.
Lower Number Is From Monte Carlo Simulation Of The Heterogeneous Phantom.

Energy Conserved To -0.9%

Table E

	Δi							
	-3	-2	-1	0	1	2	3	
0	-	-	.012	.329	.012	-	-	
	-	-	.012	.330	.012	-	-	
1	-	.001	.025	.239	.025	.001	-	
	-	.001	.025	.239	.025	.001	-	
2	-	.001	.020	.073	.020	.001	-	
	-	.001	.020	.073	.020	.001	-	
Δk								
3	-	.001	.008	.020	.008	.001	-	
	-	.001	.008	.020	.008	.001	-	
								$\rho = 1.0 g/cm^3$
4	-	.001	.004	.007	.004	.001	-	$\rho = 0.3 g/cm^3$
	-	.001	.003	.006	.004	.001	-	
5	-	.001	.003	.004	.003	.001	-	
	-	.001	.002	.003	.002	.001	-	
6	-	.001	.002	.002	.002	.001	-	
	-	.001	.001	.002	.001	.001	-	

Upper Number Is Calculated From Homogeneous Dose Spread Arrays.
Lower Number Is From Monte Carlo Simulation Of The Heterogeneous Phantom.

Energy Conserved To -0.2%

Table F

Δk \ Δi	-3	-2	-1	0	1	2	3	
0	-	-	.006	.143	.006	-	-	
	-	-	.006	.145	.006	-	-	$\rho = 0.3 g/cm^3$
1	-	-	.010	.092	.010	-	-	$\rho = 1.0 g/cm^3$
	-	-	.009	.100	.009	-	-	
2	-	.001	.007	.026	.007	.001	-	
	-	-	.007	.029	.007	-	-	
3	-	-	.003	.008	.003	-	-	
	-	-	.003	.009	.003	-	-	
4	-	-	.001	.002	.001	-	-	
	-	-	.001	.002	.001	-	-	
5	-	-	-	.001	-	-	-	
	-	-	-	.001	-	-	-	
6	-	-	-	-	-	-	-	
	-	-	-	-	-	-	-	

Upper Number Is Calculated From Homogeneous Dose Spread Arrays.
Lower Number Is From Monte Carlo Simulation Of The Heterogeneous Phantom.

Energy Conserved To +4.3%

Table G

Δk \ Δi	-3	-2	-1	0	1	2	3
0	-	-	.006	.143	.006	-	-
	-	-	.006	.144	.006	-	-
1	-	.001	.014	.119	.014	.001	-
	-	.001	.014	.118	.014	.001	-
							$\rho = 0.3 g/cm^3$
2	-	.001	.010	.041	.010	.001	-
	-	-	.010	.050	.010	.001	-
							$\rho = 1.0 g/cm^3$
3	-	.001	.006	.013	.006	.001	-
	-	-	.006	.019	.006	.001	-
4	-	.001	.002	.004	.002	.001	-
	-	-	.002	.005	.002	-	-
5	-	-	.001	.001	.001	-	-
	-	-	.001	.002	.001	-	-
6	-	-	-	-	-	-	-
	-	-	-	-	-	-	-

Upper Number Is Calculated From Homogeneous Dose Spread Arrays.
Lower Number Is From Monte Carlo Simulation Of The Heterogeneous Phantom.

Energy Conserved To +7.9%

Table H

Δk \ Δi	-3	-2	-1	0	1	2	3	
0	-	-	.012	.329	.012	-	-	
	-	-	.012	.329	.011	-	-	
1	-	.001	.025	.239	.025	.001	-	
	-	.001	.025	.239	.025	.001	-	$\rho = 1.0 g/cm^3$
2	-	.002	.024	.093	.024	.002	-	
	-	.006	.023	.074	.023	.007	-	$\rho = 0.001 g/cm^3$
3	-	.003	.018	.043	.018	.003	-	$\rho = 1.0 g/cm^3$
	.001	.004	.017	.034	.016	.004	.001	
4	-	.002	.007	.012	.007	.002	-	
	-	.002	.007	.012	.007	.002	-	
5	-	.001	.003	.004	.003	.001	-	
	-	.001	.003	.004	.003	.001	-	
6	-	-	.001	.001	.001	-	-	
	-	-	.001	.001	.001	-	-	

Upper Number Is Calculated From Homogeneous Dose Spread Arrays.
Lower Number Is From Monte Carlo Simulation Of The Heterogeneous Phantom.

Energy Conserved To -1.3%

Table I

Δk \ Δi	-3	-2	-1	0	1	2	3	
0	-	-	.012	.329	.012	-	-	
	-	-	.012	.329	.011	-	-	
1	-	.001	.025	.239	.025	.001	-	
	-	.001	.025	.238	.025	.001	-	
2	-	.002	.024	.093	.024	.002	-	
	.001	.002	.020	.072	.020	.002	-	
								$\rho = 1.0 g/cm^3$
3	.001	.004	.022	.057	.022	.004	.001	
	.003	.005	.016	.033	.016	.005	.004	
								$\rho = 0.001 g/cm^3$
4	.001	.004	.014	.027	.014	.004	.001	
	.001	.004	.012	.019	.012	.004	.001	
5	-	.002	.005	.008	.005	.002	-	$\rho = 1.0 g/cm^3$
	.001	.002	.005	.008	.005	.002	.001	
6	-	.001	.002	.003	.002	.001	-	
	-	.001	.002	.003	.002	.001	-	

Upper Number Is Calculated From Homogeneous Dose Spread Arrays.
Lower Number Is From Monte Carlo Simulation Of The Heterogeneous Phantom.

Energy Conserved To -1.5%

Table A′

Δk \ Δi	-3	-2	-1	0	1	2	3	
0	-	-	.012	.329	.012	-	-	
	-	-	.012	.328	.011	-	-	$\rho = 1.0 g/cm^3$
1	-	.001	.033	.283	.033	.001	-	$\rho = 0.3 g/cm^3$
	-	.002	.035	.281	.035	.002	-	
2	-	.003	.031	.118	.031	.003	-	
	.001	.004	.033	.124	.033	.004	.001	
3	.001	.004	.023	.059	.023	.004	.001	
	.001	.005	.023	.061	.023	.004	.001	
4	.001	.005	.018	.032	.018	.005	.001	
	.002	.005	.017	.032	.016	.005	.002	
5	.002	.005	.013	.018	.013	.005	.002	
	.002	.005	.012	.018	.012	.005	.002	
6	.001	.004	.008	.011	.008	.004	.001	
	.002	.004	.008	.011	.008	.004	.002	

Upper Number Is Calculated From Homogeneous Dose Spread Arrays.
Lower Number Is From Monte Carlo Simulation Of The Heterogeneous Phantom.

Energy Conserved To 0.6%

Table B′

Δk \ Δi	-3	-2	-1	0	1	2	3	
0	- -	- -	.012 .012	.329 .327	.012 .012	- -	- -	ρ = 1.0g/cm^3
1	- -	.002 .003	.035 .037	.290 .290	.035 .037	.002 .003	- -	ρ = 0.2g/cm^3
2	.001 .001	.003 .005	.035 .036	.131 .135	.035 .036	.003 .005	.001 .001	
3	.001 .002	.005 .006	.027 .028	.068 .072	.027 .028	.005 .006	.001 .002	
4	.002 .002	.006 .006	.022 .020	.040 .041	.022 .020	.006 .006	.002 .002	
5	.002 .002	.005 .005	.015 .014	.024 .024	.015 .014	.005 .005	.002 .002	
6	.002 .002	.005 .005	.011 .011	.015 .015	.011 .010	.005 .005	.002 .002	

Upper Number Is Calculated From Homogeneous Dose Spread Arrays.
Lower Number Is From Monte Carlo Simulation Of The Heterogeneous Phantom.

Energy Conserved to 0.3%

Table C′

Δk \ Δi	-3	-2	-1	0	1	2	3	
0	-	-	.012	.329	.012	-	-	
	-	-	.012	.329	.011	-	-	
1	-	.001	.025	.239	.025	.001	-	
	-	.001	.025	.239	.025	.001	-	$\rho = 1.0 g/cm^3$
2	-	.002	.023	.084	.023	.002	-	$\rho = 0.3 g/cm^3$
	.001	.003	.021	.074	.021	.003	.001	
3	-	.003	.018	.041	.018	.003	-	
	.001	.004	.016	.032	.016	.004	.001	
4	.001	.003	.012	.021	.012	.003	.001	
	.001	.004	.010	.016	.010	.004	.001	
5	.001	.003	.007	.010	.007	.003	.001	
	.001	.003	.006	.008	.006	.003	.001	
6	.001	.002	.005	.006	.005	.002	.001	
	.001	.002	.004	.004	.004	.002	.001	

Upper Number Is Calculated From Homogeneous Dose Spread Arrays.
Lower Number Is From Monte Carlo Simulation Of The Heterogeneous Phantom.

Energy Conserved To -1.6%

Table D′

Δk \ Δi	-3	-2	-1	0	1	2	3	
0	-	-	.012	.329	.012	-	-	
	-	-	.012	.329	.011	-	-	
1	-	.001	.025	.239	.025	.001	-	
	-	.001	.025	.238	.025	.001	-	
2	-	.001	.020	.073	.020	.001	-	
	.001	.001	.020	.073	.020	.001	-	$\rho = 1.0 g/cm^3$
3	-	.001	.011	.026	.011	.001	-	$\rho = 0.3 g/cm^3$
	-	.002	.010	.022	.010	.002	-	
4	-	.002	.007	.012	.007	.002	-	
	-	.002	.005	.009	.005	.002	-	
5	-	.001	.004	.006	.004	.001	-	
	.001	.001	.003	.004	.003	.001	-	
6	.001	.001	.003	.003	.003	.001	-	
	.001	.001	.002	.002	.002	.001	.001	

Upper Number Is Calculated From Homogeneous Dose Spread Arrays.
Lower Number Is From Monte Carlo Simulation Of The Heterogeneous Phantom.

Energy Conserved To -0.7%

Table E'

Δk \ Δi	-3	-2	-1	0	1	2	3	
0	- -	- -	.012 .012	.329 .330	.012 .012	- -	- -	
1	- -	.001 .001	.025 .025	.239 .239	.025 .025	.001 .001	- -	
2	- -	.001 .001	.020 .020	.073 .073	.020 .020	.001 .001	- -	
3	- -	.001 .001	.008 .008	.020 .020	.008 .008	.001 .001	- -	$\rho = 1.0 g/cm^3$
4	- -	.001 .001	.004 .003	.007 .006	.004 .004	.001 .001	- -	$\rho = 0.3 g/cm^3$
5	- -	.001 .001	.003 .002	.004 .003	.003 .002	.001 .001	- -	
6	- -	.001 .001	.002 .001	.002 .002	.002 .001	.001 .001	- -	

Upper Number Is Calculated From Homogeneous Dose Spread Arrays.
Lower Number Is From Monte Carlo Simulation Of The Heterogeneous Phantom.

Energy Conserved To -0.2%

Table F′

Δk \ Δi	-3	-2	-1	0	1	2	3	
0	- -	- -	.006 .006	.143 .145	.006 .006	- -	- -	ρ = 0.3g/cm^3
1	- -	- -	.011 .009	.098 .100	.011 .009	- -	- -	ρ = 1.0g/cm^3
2	- -	.001 -	.007 .007	.028 .029	.007 .007	.001 -	- -	
3	- -	- -	.004 .003	.097 .091	.004 .003	- -	- -	
4	- -	- -	.001 .001	.003 .002	.001 .001	- -	- -	
5	- -	- -	- -	.001 .001	- -	- -	- -	
6	- -	- -	- -	- -	- -	- -	- -	

Upper Number Is Calculated From Homogeneous Dose Spread Arrays.
Lower Number Is From Monte Carlo Simulation Of The Heterogeneous Phantom.

Energy Conserved To -1.3%

Table G′

Δk \ Δi	-3	-2	-1	0	1	2	3	
0	- -	- -	.006 .006	.143 .144	.006 .006	- -	- -	
1	- -	.001 .001	.014 .014	.119 .118	.014 .014	.001 .001	- -	$\rho = 0.3 g/cm^3$
2	- -	.001 -	.010 .010	.043 .050	.010 .010	.001 .001	- -	$\rho = 1.0 g/cm^3$
3	- -	.001 -	.006 .006	.014 .019	.006 .006	.001 .001	- -	
4	- -	.001 -	.002 .002	.004 .005	.002 .002	.001 -	- -	
5	- -	- -	.001 .001	.001 .002	.001 .001	- -	- -	
6	- -	- -	- -	- -	- -	- -	- -	

Upper Number Is Calculated From Homogeneous Dose Spread Arrays.
Lower Number Is From Monte Carlo Simulation Of The Heterogeneous Phantom.

Energy Conserved To +5.5%

Table H´

Δk \ Δi	-3	-2	-1	0	1	2	3	
0	-	-	.012	.329	.012	-	-	
	-	-	.012	.329	.011	-	-	
1	-	.001	.025	.239	.025	.001	-	
	-	.001	.025	.239	.025	.001	-	$\rho = 1.0 g/cm^3$
2	-	.002	.024	.089	.024	.002	-	$\rho = 0.001 g/cm^3$
	-	.006	.023	.074	.023	.007	-	
3	-	.003	.017	.040	.017	.003	-	$\rho = 1.0 g/cm^3$
	.001	.004	.017	.034	.016	.004	.001	
4	-	.002	.006	.011	.006	.002	-	
	-	.002	.007	.012	.007	.002	-	
5	-	.001	.003	.004	.003	.001	-	
	-	.001	.003	.004	.003	.001	-	
6	-	-	.001	.001	.001	-	-	
	-	-	.001	.001	.001	-	-	

Upper Number Is Calculated From Homogeneous Dose Spread Arrays.
Lower Number Is From Monte Carlo Simulation Of The Heterogeneous Phantom.

Energy Conserved To -0.6%

Table I

Δk	Δi = -3	-2	-1	0	1	2	3	
0	-	-	.012	.329	.012	-	-	
	-	-	.012	.329	.011	-	-	
1	-	.001	.025	.239	.025	.001	-	
	-	.001	.025	.238	.025	.001	-	
2	-	.002	.024	.093	.024	.002	-	
	.001	.002	.020	.072	.020	.002	-	
								$\rho = 1.0 g/cm^3$
3	.001	.004	.022	.052	.022	.004	.001	
	.003	.005	.016	.033	.016	.005	.004	
								$\rho = 0.001 g/cm^3$
4	.001	.004	.014	.024	.014	.004	.001	
	.001	.004	.012	.019	.012	.004	.001	
5	-	.002	.005	.007	.005	.002	-	$\rho = 1.0 g/cm^3$
	.001	.002	.005	.008	.005	.002	.001	
6	-	.001	.002	.002	.002	.001	-	
	-	.001	.002	.003	.002	.001	-	

Upper Number Is Calculated From Homogeneous Dose Spread Arrays.
Lower Number Is From Monte Carlo Simulation Of The Heterogeneous Phantom.

Energy Conserved To -0.8%

VITA

NAME: Thomas Rockwell Mackie

PLACE OF BIRTH: Eston, Saskatchewan, Canada

YEAR OF BIRTH: 1954

POST-SECONDARY EDUCATION AND DEGREES:

University of Saskatchewan
Saskatoon, Saskatchewan
1974-1978, 1979
B.Sc.(Honors) in Physics 1980

HONOURS AND AWARDS:

Alberta Heritage Foundation for Medical Research Studentship
1981-1984

First Prize, Young Investigators' Symposium
New York, 1983

RELATED WORK EXPERIENCE:

Assistant to Radiation Consultant
University of Saskatchewan
1977

Laboratory Assistant
University of Saskatchewan
1977-1980

Radiation Physicist
Keith Consulting Engineers
1978-1979

Radiation Consultant
1979-1980

Laboratory Assistant
University of Alberta
1980-1984

Summer Research Assistant
Cross Cancer Institute
1981

PUBLICATIONS:

The following was a critique solicited by the Cluff Lake Board of Inquiry chaired by Justice Bayda and delivered to the Inquiry in Regina, Saskatchewan, July 1977:

1. Review of "Appendix C, Radiological Health and Safety", Caplan, H., Mackie, T.R.

The following were published under the auspices of the Atomic Energy Control Board of Canada under the aegis of the Federal-Provincial Task Force on Radioactivity:

1. Mackie, T.R., "Reducing Airborne Radiation in Dwellings using Make-Up Air Ventilation", March 1979.

2. Crilly, R., Mackie, T.R., Haubrich, E.J.J., "A Study of Air Exchange Rates in Dwellings using SF_6 as a Tracer Gas", May 1980.

3. Crilly, R., Mackie, T.R., "Air Make-Up Units for Reducing Radiological Levels", May 1980.

The following article is reprinted in Appendix 9:

1. Mackie, T.R., Scrimger, J.W., "Contamination of a 15 MV Photon Beam by Electrons and Scattered Photons", Radiology, 144, 403-409, July 1982.

The following articles appeared in the proceedings of "The Eighth International Conference on the Use of Computers in Radiation Therapy", July 1984:

1. Mackie, T.R., Scrimger, J.W., "Computing Radiation Dose for High Energy X-rays using a Convolution Method".

2. Battista, J.J., Mackie, T.R., El-Khatib, E., Scrimger, J.W., "Lung Dose Corrections for 6 MV and 15 MV X-rays: Anomolies".

3. Mackie, T.R., Battista, J.J., "A Macroscopic Monte Carlo Method for Electron Beam Dose Calculations: A Proposal".

The following articles have been submitted to the journal, "Medical Physics":

1. Mackie, T.R., Scrimger, J.W., Battista, J.J., "A Convolution Method of Calculating Dose for 15 MV X-rays".

2. Mackie, T.R., El-Khatib, E., Battista, J.J., Scrimger, J.W., Van Dyk, J., Cunningham, J.R., "Lung Dose Corrections for 6 MV and 15 MV X-rays".